



Doctoral Thesis

**SENSITIVITY ANALYSIS
OF THE INITIAL POSTBUCKLING BEHAVIOR
OF ELASTIC STRUCTURES**

submitted in satisfaction of the requirements for the degree of
Doctor of Science in Civil Engineering
of Vienna University of Technology, Faculty of Civil Engineering

Dissertation

**SENSITIVITÄTSANALYSE
DES INITIALEN NACHBEULVERHALTENS ELASTISCHER
STRUKTUREN**

ausgeführt zum Zwecke der Erlangung des akademischen Grades eines
Doktors der technischen Wissenschaften,
eingereicht an der Technischen Universität Wien, Fakultät für Bauingenieurwesen

von

Dipl.-Ing. Gerhard Höfinger
Matrikelnummer 0125076

Fuchsröhrenstraße 39/1/5, 1110 Wien, Österreich

Gutachter: Em.O.Univ.-Prof. Dipl.-Ing. Dr. techn. Dr. h.c.mult. Herbert Mang, Ph. D.
Institut für Mechanik der Werkstoffe und Strukturen,
Technische Universität Wien,
Karlsplatz 13/202, 1040 Wien, Österreich

Gutachter: Ao.Univ. Prof. Dipl.-Ing. Dr.techn. Felix Breiteneker
Institut für Analysis und Scientific Computing
Technische Universität Wien,
Wiedner Hauptstraße 8/101, 1040 Wien, Österreich

Danksagung

Am Beginn dieser Arbeit möchte ich all jenen danken, die mich in der Zeit meines Doktoratsstudiums unterstützt und begleitet haben.

Dank gilt der Österreichischen Akademie der Wissenschaften, die meine Anstellung an der TU Wien als Projektassistent am Institut für Mechanik der Werkstoffe und Strukturen finanziell ermöglichte.

Ich bedanke mich herzlich bei meinem Betreuer, em.O.Univ.-Prof. Dipl.-Ing. Dr.techn. Dr.h.c.mult. Prof. Herbert A. Mang, Ph.D., für seinen unermüdlichen Einsatz für den wissenschaftlichen Erfolg der Arbeitsgruppe Stabilität, die ständige Bereitschaft zur Fragebeantwortung und fachlichen Diskussion und die große Unterstützung, die er mir im Zuge meines Doktoratsstudiums zuteil werden ließ.

Ich danke dem zweiten Begutachter meiner Dissertation, ao.Univ.Prof. Dipl.-Ing. Dr.techn. Felix Breitenecker, für die Bereitschaft, nach der Betreuung meiner Diplomarbeit auch an dieser Stelle mitzuwirken.

Univ.Prof. Dipl.-Ing. Dr.techn. Josef Eberhardsteiner, Dekan der Fakultät für Bauingenieurwesen der TU Wien, danke ich für die freundliche Aufnahme an dieser Fakultät, seine Unterstützung und Beratung.

Spezieller Dank gilt den Damen der Administration des Institutes für Mechanik der Werkstoffe und Strukturen, an deren Seite jede Schlacht im Papierkrieg gewonnen werden konnte.

Danken möchte ich allen Kollegen am Institut für Mechanik der Werkstoffe und Strukturen, die mich, wann immer nötig, unterstützten, allen voran den Mitgliedern meiner Arbeitsgruppe, Xin Jia und Andreas Steinböck.

Ich möchte allen Freunden danken, die jederzeit ein offenes Ohr hatten und sowohl schöne als auch schwierige Momente in den letzten Jahren mit mir teilten. Ich danke meiner Familie, die immer ein starker Rückhalt war, und besonders meinen Eltern, die mich stets ermunterten, meinen Weg bis zum Abschluss des Doktoratsstudiums zu gehen.

Nicht zuletzt danke ich meiner Partnerin Ana, die immer für mich da war, wenn ich sie brauchte.

Abstract

Postbuckling analysis of perfect elastic structures is used to quantify the sensitivity of structures to imperfections. In real structures, as opposed to idealized ones, imperfections are unavoidable. Imperfection-sensitive structures may fail at much lower loads than the buckling load of the corresponding perfect structures. To prevent such failure, the designer should consider the possibility of converting imperfection-sensitive structures into imperfection-insensitive ones by varying suitable design parameters.

Sensitivity analysis of the initial postbuckling behavior provides information about the influence of parametric changes of a structure on its sensitivity to imperfections. Koiter's initial postbuckling analysis, in the framework of the Finite Element Method (FEM), was applied to mathematically describe postbuckling paths and to quantify the degree of imperfection sensitivity of a structure. The consistently linearized eigenvalue problem, representing a generalized eigenvalue problem, was thoroughly analyzed with regard to its usefulness for classification of structures on the basis of their state of stress at buckling. It was used for derivation of a mathematical condition for buckling from a membrane stress state.

Another topic that was investigated in this work is hilltop buckling which is characterized by the coincidence of a bifurcation point and a snap-through point. It was shown that a structure exhibiting hilltop buckling is inherently imperfection sensitive. This was the reason for considering hilltop buckling as the starting point of sensitivity analysis of the initial postbuckling behavior of structures, aimed at the aforementioned conversion of imperfection-sensitive structures into imperfection-insensitive ones.

Another special case is zero-stiffness postbuckling, representing a desirable mode of transition from imperfection sensitivity to imperfection insensitivity. A theoretical investigation of the possibility and predictability of its occurrence was performed.

In order to support the theoretical findings by numerical results, a considerable part of the work leading to this dissertation was the implementation of theoretical results into a computer program based on the FEM. Using finite element routines from the computer code FEAP, an arc-length method for dealing with nonlinear problems, Koiter's postbuckling analysis, and the consistently linearized eigenvalue problem were implemented in MATLAB. Because of limitations of the interface between the two programs, the practical applicability of the program is limited to a few thousand degrees of freedom. Nevertheless, this was sufficient for numerical verification of theoretical results.

The structures investigated in the numerical part of the thesis cover the whole range of the theoretical work: A pin-jointed two-bar system with two degrees

of freedom, exhibiting zero-stiffness postbuckling, was treated analytically, as opposed to the other examples for which the FEM was used. The second example was a *von Mises* truss which is characterized by buckling from a membrane stress state. For this structure, conversion from imperfection sensitivity into imperfection insensitivity does not involve zero-stiffness postbuckling. A shallow cylindrical shell serves as an example of a structure that buckles from a general stress state. A parametrized family of two-hinged arches, subjected to a uniformly distributed load, containing a parabolic arch as a special case, allows numerical verification of special features related to this special case.

Zusammenfassung

Die Nachbeulanalyse perfekter elastischer Strukturen erlaubt deren Identifikation als imperfektionssensitiv bzw. imperfektionsinsensitiv. Perfekte Strukturen stellen Idealisierungen realer Strukturen dar. Imperfektionssensitive Strukturen versagen gegebenenfalls bei deutlich kleineren Belastungen als der Beullast der entsprechenden perfekten Strukturen. Deshalb kann man versuchen, ein ursprünglich imperfektionssensitives System durch Variation geeigneter Parameter in ein imperfektionsinsensitives System überzuführen.

Sensitivitätsanalysen des initialen Nachbeulverhaltens liefern Information über den Einfluss parametrisierter Veränderungen einer Struktur auf das Ausmaß ihrer Imperfektionssensitivität. Die Koiter'sche Nachbeulanalyse, eingebettet in die Finite Elemente Methode (FEM), wurde zur mathematischen Beschreibung des Nachbeulpfades und damit zur Quantifizierung des Grades von Imperfektionssensitivität bzw. -insensitivität verwendet. Das konsistent linearisierte Eigenwertproblem, ein verallgemeinertes Eigenwertproblem, wurde eingehend auf seine Eignung zur Klassifikation von Strukturen in Abhängigkeit von der Art des Spannungszustandes an der Stabilitätsgrenze untersucht. Es wurde auch zur Herleitung einer Bedingung für Beulen, ausgehend von einem Membranspannungszustand, verwendet.

Eingehend analysiert wurde ferner Hilltop buckling, worunter man die Koinzidenz eines Verzweigungs- mit einem Durchschlagspunkt versteht. Es wurde gezeigt, dass Hilltop buckling imperfektionssensitiv ist. Das war auch der Grund dafür, Sensitivitätsanalysen, die auf die Umwandlung von imperfektionssensitiven in imperfektionsinsensitive Strukturen abzielen, mit Hilltop buckling zu beginnen.

Zero-stiffness postbuckling, ein Sonderfall bei dem der gesamte Sekundärpfad auf einem Lastniveau liegt, stellt eine besonders günstige Form des Übergangs von Imperfektionssensitivität zu Imperfektionsinsensitivität dar. Es wurde gezeigt, dass diese besondere Form des Nachbeulpfades einen Membranspannungszustand voraussetzt.

Ein wesentlicher Teil der Arbeit, die zu dieser Dissertation führte, war die algorithmische Übersetzung analytischer Methoden zwecks Integration in ein auf der FEM basiertes Computerprogramm, um damit die theoretischen Resultate numerisch zu untermauern.

Unter Verwendung von Routinen des FEM-Programms FEAP wurde ein Bogenlängenverfahren für nichtlineare Probleme, die Koiter'sche Nachbeulanalyse und das konsistent linearisierte Eigenwertproblem in MATLAB implementiert. Aufgrund von Beschränkungen im Interface zwischen FEAP und MATLAB ist der Einsatz der entwickelten Software auf Probleme mit einigen wenigen tausend Freiheitsgraden beschränkt. Das reicht jedoch aus, um die Ergebnisse der

theoretischen Untersuchungen, etwa anhand des Beispiels einer flachen Zylinderschale, zu verifizieren. Die vier präsentierten Beispiele wurden so gewählt, dass ein möglichst großer Teil der vorgestellten Theorie abgedeckt wird. Das erste Beispiel ist ein aus gelenkig miteinander verbundenen starren Stäben bestehendes System mit zwei Freiheitsgraden, das für eine bestimmte Parameterwahl Zero-stiffness postbuckling aufweist. Die Untersuchung wurde analytisch vorgenommen, im Gegensatz zu den anderen Beispielen, die mittels des erwähnten FEM-Programms gelöst wurden. Die zweite Struktur ist ein durch eine im Scheitel angebrachte, vertikale elastische Feder versteiftes *von Mises* Fachwerk, gekennzeichnet durch einen Membranspannungszustand im Vorbeulbereich. Bei der Transformation dieser ursprünglich imperfektionssensitiven in eine imperfektionsinsensitive Struktur spielt Zero-stiffness postbuckling keine Rolle. Als Beispiel für eine Struktur mit einem allgemeinen Spannungszustand im Vorbeulbereich wurde eine flache Zylinderschale gewählt. Anhand einer parametrisierten Familie von Zweigelenksbögen mit einem Parabelbogen als Spezialfall, wurde die für Verzweigungsbeulen für einen solche Spezialfall hergeleitete mathematische Formel verifiziert.

Contents

1	Introduction	1
2	Stability of elastic structures	4
2.1	Basic definitions	4
2.2	Modes of loss of stability	6
2.3	Imperfection insensitivity	7
2.4	Linear stability problems and linear prebuckling paths	8
3	Koiter's initial postbuckling analysis	10
3.1	Series expansion of the postbuckling path	10
3.2	Symmetry	13
3.3	The coefficients a_1 and a_1^*	15
4	Special modes of buckling and postbuckling	18
4.1	Hilltop buckling	18
4.2	Zero-stiffness postbuckling	22
5	The consistently linearized eigenvalue problem	25
5.1	Definition	25
5.2	Properties of eigenvalues and eigenvectors	26
6	Classification of elastic structures regarding sensitivity analysis of their initial postbuckling behavior	32
6.1	A necessary and sufficient condition for bifurcation buckling from a membrane stress state	33
6.2	Bifurcation buckling from a membrane stress state as a special case in the frame of sensitivity analysis of bifurcation buckling from a general stress state	39
7	Implementation of the theoretical concepts in a computer program	45
7.1	Layout of the computer program	45
7.2	Post-processing	48

7.3	Technical details	49
8	Numerical investigation	55
8.1	Two-bar system	55
8.2	<i>Von Mises</i> truss	59
8.3	Shallow cylindrical shell	65
8.4	Parabolic arch	70
9	Conclusions	74
A	Coefficients in Koiter's initial postbuckling analysis	77
	Bibliography	79

Chapter 1

Introduction

A thorough investigation of the stability of elastic structures does not only involve determination of the stability limit but also consideration of the postbuckling behavior. The reason for this is that the postbuckling behavior of perfect structures has a great influence on the load-bearing capacities of corresponding imperfect structures. In case of pronounced imperfection sensitivity of a perfect structure, the load at which loss of stability of the corresponding real, i.e. imperfect structure occurs may be significantly smaller than the load associated with loss of stability of the perfect structure. A well known example for such a situation is a thin-walled cylinder subjected to axial loads [5].

Sensitivity analysis means to investigate the influence of changes of design parameters on the behavior of a system. In the context of stability analysis, it is performed with the goal to increase the stability limit through variation of suitable design variables. Nevertheless, optimization restricted to the buckling load, i.e. without consideration of the postbuckling path may be unrewarding because it may lead to a concentration of eigenvalues and deterioration of the postbuckling behavior [36]. Optimization of a structure with respect to stability should thus also take the postbuckling behavior into account, as was done e.g. by Bochenek and Kruzelecki [3] and Mróz and Piekarski [23].

The motivation for this work is lack of basic guidelines to design structures such that they are *ab initio* imperfection insensitive. In order to establish such guidelines, the postbuckling behavior of elastic structures must be well understood. Mathematical tools are necessary to find coherences that are not obvious. An

important item of the analysis is the classification of structures with regard to their prebuckling and postbuckling behavior. Special cases of postbuckling behavior should be identified and analyzed.

A method for the analysis of the postbuckling behavior in the vicinity of a bifurcation point was proposed by Koiter [14]. He used asymptotic series expansions at the stability limit. This allows a quantitative assessment of the degree of imperfection sensitivity or insensitivity. Sensitivity analysis of the postbuckling behavior of elastic structures then becomes a sensitivity analysis of the coefficients in Koiter's series expansions. In the work by Mang et al. [21, 29], results from Helnwein's consistently linearized eigenvalue problem [11] were integrated in Koiter's postbuckling analysis. Solutions from the consistently linearized eigenvalue problem, initially proposed by Helnwein [11] and originally intended to estimate the stability limit, carry information that can be used for classification of structures with respect to buckling either from a general or a special stress state. This approach was developed further and applied to special problems by Mang et al. [16, 17, 20] and Steinboeck et al. [30–32]. Godoy [10] and Mróz and Haftka [22] must be mentioned in this context. In their work on sensitivity analysis of the postbuckling behavior, they used different series expansions.

Several publications are restricted to special cases that may occur in the course of sensitivity analysis, such as e.g. zero-stiffness postbuckling, first treated by Tarnai [34], and multiple hilltop buckling, investigated by Ohsaki and Ikeda [24] and Fujii and Noguchi [8].

This dissertation is organized as follows: In Chapter 2, basic definitions are given and the scope of the work is defined. Emphasis is laid on the mathematical description of loss of stability in elastic structures. In Chapter 3, Koiter's postbuckling analysis is reviewed. Chapter 4 is devoted to the treatment of two special modes of loss of stability, the first of which is hilltop buckling. The core of this Chapter is the proof that hilltop buckling is imperfection sensitive. The other special case is zero-stiffness postbuckling. In Chapter 5, the consistently linearized eigenvalue problem is introduced and some of its properties are investigated. Classification of bifurcation buckling on the basis of the stress state from which buckling occurs is the topic of Chapter 6, where results from preceding chapters are used to show how to distinguish between bifurcation buckling

from a general stress state and a membrane stress state. Chapter 7 contains information on the implementation of theoretical concepts into a computer program. Numerical results are presented in Chapter 8. Conclusions from the theoretical investigation and the numerical work are drawn in Chapter 9.

Chapter 2

Stability of elastic structures

2.1 Basic definitions

In this work static, conservative, finite dimensional elastic systems are studied. The deformations need not be small but must not be so large that either nonlinear elasticity or plasticity becomes an issue. Hence, the present work is restricted to geometric nonlinearity. Proportional loading is assumed.

Under these conditions, a potential energy function of the system exists. It is a functional on the load-displacement space:

$$V(\mathbf{u}, \lambda) : \mathbb{R}^N \times \mathbb{R} \rightarrow \mathbb{R}. \quad (2.1)$$

Equilibria of the system are stationary points of the potential energy function. Thus, for the finite-dimensional systems considered herein, a necessary and sufficient condition for equilibrium is the vanishing of the first derivative of $V(\mathbf{u}, \lambda)$, given as

$$\mathbf{G}(\mathbf{u}, \lambda) := V_{,\mathbf{u}}(\mathbf{u}, \lambda) = \mathbf{F}'(\mathbf{u}) - \lambda \mathbf{P}(\mathbf{u}). \quad (2.2)$$

The mechanical interpretation of $\mathbf{G}(\mathbf{u}, \lambda)$ explains its name as out-of-balance force. $\mathbf{F}'(\mathbf{u})$ is the vector of internal forces of the system whereas $\lambda \mathbf{P}(\mathbf{u})$ represents the external forces where the scalar load multiplier λ amplifies the load described by the load vector $\mathbf{P}(\mathbf{u})$. For a suitable choice of coordinates, especially in the frame of the FEM,

$$\mathbf{G}(\mathbf{u}, \lambda) = \mathbf{F}'(\mathbf{u}) - \lambda \bar{\mathbf{P}}. \quad (2.3)$$

The constant load vector $\bar{\mathbf{P}}$ is referred to as reference load.

The equilibrium solutions form curves in the load-displacement space which can be locally parametrized as $(\mathbf{u}(\lambda), \lambda)$ up to singular points. Employing the implicit function theorem allows calculation of a tangent to these curves:

$$\mathbf{u}_{,\lambda}(\lambda) = (\mathbf{G}_{,\mathbf{u}})^{-1} \cdot \mathbf{G}_{,\lambda} \quad (2.4)$$

With the nomenclature used in engineering, this reads as

$$\mathbf{K}_T(\mathbf{u}) \cdot \frac{d\mathbf{u}}{d\lambda} = \bar{\mathbf{P}} \quad (2.5)$$

where

$$\mathbf{K}_T(\mathbf{u}) := (\mathbf{F}'(\mathbf{u}))_{,\mathbf{u}} = \mathbf{G}_{,\mathbf{u}} \quad (2.6)$$

is called tangent stiffness matrix. Alternatively, the differential form of (2.5) may be used:

$$\mathbf{K}_T(\mathbf{u}) \cdot d\mathbf{u} = d\lambda \bar{\mathbf{P}}. \quad (2.7)$$

The implicit function theorem guarantees unique solutions only as long as \mathbf{K}_T is regular. With the help of (2.4), *equilibrium paths* (connected one-dimensional sets of solutions of (2.3)) can be constructed. The solution path that contains the unloaded state, i.e. the solution $(\lambda = 0, \mathbf{u} = \mathbf{0})$, is called primary path and denoted as $\tilde{\mathbf{u}}(\lambda)$. A solution $(\mathbf{u}_0, \lambda_0)$ is called stable if it is a strong local minimum of the potential energy function. As a consequence, $\mathbf{K}_T(\mathbf{u}_0)$ has only strictly positive eigenvalues. If λ is increased from zero, then, for a specific value $\lambda = \lambda_S$, referred to as the *critical load*, the equilibrium $(\mathbf{u}_S := \tilde{\mathbf{u}}(\lambda_S), \lambda_S)$ is just still stable or just no longer stable.

The tangent stiffness matrix for nonlinear problems can be decomposed as [38]

$$\mathbf{K}_T = \mathbf{K}_0 + \mathbf{K}_\sigma + \mathbf{K}_L \quad (2.8)$$

where \mathbf{K}_0 is the small-displacement stiffness matrix. For linear problems, \mathbf{K}_0 is the stiffness matrix. \mathbf{K}_σ is the initial stress matrix, depending on the current stress level, and \mathbf{K}_L is the initial displacement matrix, containing terms that are linear and quadratic in \mathbf{u} .

In the following, a notation introduced in [29] will be used:

$$\tilde{\mathbf{K}}_T(\lambda) := \mathbf{K}_T(\tilde{\mathbf{u}}(\lambda)). \quad (2.9)$$

This locally defines a matrix curve along the primary path. $\tilde{\mathbf{K}}_T(\lambda)$ indicates equilibrium states on the primary path whereas $\mathbf{K}_T(\mathbf{u})$ refers to configurations which, in general, represent out-of-balance states.

2.2 Modes of loss of stability

In the context of this work, loss of stability occurs in the form of *snap-through* or of *bifurcation buckling*. Both modes of loss of stability are characterized by the singularity of the tangent stiffness matrix $\tilde{\mathbf{K}}_T$. In both cases, at least one of its eigenvalues equals zero. The corresponding eigenvector is denoted as \mathbf{v}_1 :

$$\tilde{\mathbf{K}}_T \cdot \mathbf{v}_1 = \mathbf{0}. \quad (2.10)$$

If $\tilde{\mathbf{K}}_T$ is singular, the implicit function theorem states that (2.4) does not allow calculation of a unique local parametrization by λ . There are basically three reasons why a unique solution of this form does not exist. The first one is snap-through, characterized by a limit point on the load-displacement path. The load along the primary path has a local maximum. At such a point, in a load-controlled setting, the structure would dynamically snap to an equilibrium solution which may have much larger displacements for the same load level. In terms of the implicit function theorem, the equilibrium path has a unique tangent but cannot be explicitly described by a function that depends on λ as an independent variable. Thus, the extended system

$$\left(\tilde{\mathbf{K}}_T \mid \bar{\mathbf{P}} \right) \quad (2.11)$$

has full rank, which implies

$$\mathbf{v}_1^T \cdot \bar{\mathbf{P}} \neq 0. \quad (2.12)$$

The second reason is the existence of two or more tangents to equilibrium paths at a point, i.e. a *bifurcation point*. At bifurcation points, two or more equilibrium paths intersect. A path that intersects the primary path is called *secondary path*. In this work, only simple bifurcation points are considered, i.e. we restrict

ourselves to structures for which exactly two equilibrium paths intersect at a bifurcation point. Two tangents exist at the bifurcation point. Thus, (2.11) does not have full rank which, together with a defect of $\widetilde{\mathbf{K}}_T$ of 1, implies

$$\mathbf{v}_1^T \cdot \bar{\mathbf{P}} = 0. \quad (2.13)$$

The third reason, mentioned just for the sake of completeness, is the technically irrelevant case of an isolated solution, which means that the solution is not part of an equilibrium path. Such a solution cannot be obtained by the techniques generally used in the context of the nonlinear FEM where equilibrium paths are determined incrementally.

The coincidence of a snap-through point and a bifurcation point is called *hilltop buckling*. The stiffness matrix has a defect of at least two. The eigenspace associated with the eigenvalue zero, containing the snap-through mode and the bifurcation buckling mode, is at least of dimension two.

On the basis of the preceding considerations, stability limits can be summarized as follows:

For snap-through,

$$d\lambda = 0, \quad \widetilde{\mathbf{K}}_T \cdot d\mathbf{u} = \mathbf{0}, \quad d\mathbf{u}^T \cdot \bar{\mathbf{P}} \neq 0. \quad (2.14)$$

For bifurcation of equilibrium,

$$d\lambda \neq 0, \quad \widetilde{\mathbf{K}}_T \cdot d\mathbf{u} \neq \mathbf{0}, \quad \mathbf{v}_1^T \cdot \bar{\mathbf{P}} = 0, \quad \widetilde{\mathbf{K}}_T \cdot \mathbf{v}_1 = \mathbf{0}. \quad (2.15)$$

For hilltop buckling,

$$d\lambda = 0, \quad \widetilde{\mathbf{K}}_T \cdot d\mathbf{u} = \mathbf{0}, \quad \mathbf{v}_1^T \cdot \bar{\mathbf{P}} = 0, \quad \widetilde{\mathbf{K}}_T \cdot \mathbf{v}_1 = \mathbf{0}. \quad (2.16)$$

2.3 Imperfection insensitivity

The difference in the load level with respect to the one referring to the stability limit can be written as

$$\Delta\lambda(\kappa, \eta) = \lambda_1(\kappa)\eta + \lambda_2(\kappa)\eta^2 + \lambda_3(\kappa)\eta^3 + \lambda_4(\kappa)\eta^4 + O(\eta^5) \quad (2.17)$$

where η denotes an independent path parameter describing the secondary path and κ represents a design parameter of the structure. In Chapter 3, a method for calculation of the coefficients of (2.17) will be presented. A criterion for imperfection insensitivity using the coefficients of (2.17) is given by (see [31])

$$\exists k \in \{2, 4, 6, \dots\} : \quad \lambda_k > 0, \quad \lambda_i = 0 \quad \forall i \in \mathbb{N} \text{ with } i < k. \quad (2.18)$$

In most cases, this simply reduces to $\lambda_1 = 0$, $\lambda_2 > 0$. Following Bochenek [2], a condition for stability at the bifurcation point and, thus, for imperfection insensitivity is given as

$$\lambda_{,\varphi}(\varphi) \text{sign}(\varphi) \geq 0, \quad \forall \varphi \in [\varphi_1, \varphi_2], \quad (2.19)$$

where $\lambda(\varphi)$ denotes the load level along the secondary path as a function of a degree of freedom φ of the system under consideration and $[\varphi_1, \varphi_2]$ stands for an interval containing the configuration at incipient buckling.

The two definitions of imperfection insensitivity agree with the exception of *zero-stiffness postbuckling* which is a special case that will be discussed in Section 4.2

2.4 Linear stability problems and linear prebuckling paths

Taking into account that for a given structure either the stability problem or the primary path or both can be linear or nonlinear, four combinations are possible. We talk of a linear stability problem if (2.8) degenerates to

$$\tilde{\mathbf{K}}_T(\lambda) = \mathbf{K}_0 + \lambda \mathbf{K}_1 \quad (2.20)$$

where \mathbf{K}_0 and \mathbf{K}_1 are constant matrices. This is the case if \mathbf{K}_L vanishes and $\mathbf{K}_\sigma = \lambda \mathbf{K}_1$ [38]. Consequently, computation of the buckling load λ_S is simplified because the condition for loss of stability, i.e. $\det(\tilde{\mathbf{K}}_T) = 0$, is just a polynomial equation in λ . A stiffness matrix as in (2.20) is obtained e.g. for in-plane loaded plates with linear prebuckling paths [38]. The reasonable assumption of stability

in the unloaded state, $\lambda = 0$, requires that \mathbf{K}_0 is positive definite. A linear prebuckling path is at hand if

$$\tilde{\mathbf{u}}_{,\lambda}(\lambda) = \mathbf{k}, \quad \tilde{\mathbf{u}}_{,\lambda\lambda}(\lambda) = \mathbf{0} \quad (2.21)$$

where \mathbf{k} is a constant vector. Then, (2.5) becomes

$$\tilde{\mathbf{K}}_T \cdot \mathbf{k} = \bar{\mathbf{P}}. \quad (2.22)$$

Differentiation along the primary path yields

$$\tilde{\mathbf{K}}_{T,\lambda} \cdot \mathbf{k} = \mathbf{0}. \quad (2.23)$$

This shows that $\tilde{\mathbf{K}}_{T,\lambda}$ is singular in this case, requiring special treatment (see Chapter 5).

Steinboeck et al. [30] have shown that linear prebuckling paths and linear stability problems are not mutually conditional.

Chapter 3

Koiter's initial postbuckling analysis

The main tool for assessment of the postbuckling behavior, used in this work, is Koiter's initial postbuckling analysis. In his pioneering work, Koiter [14] introduced a method to find series expansions for the load and the displacement along the secondary path.

3.1 Series expansion of the postbuckling path

The basic idea consists of describing the secondary path in the load-displacement space in terms of the load $\lambda(\eta)$ and the displacement offset $\nu(\eta)$ from the primary path, where η denotes an independent path parameter. Thus, point B on the secondary path is characterized by its load $\lambda(\eta_B) = \lambda_B$ and its displacement $\tilde{\mathbf{u}}(\lambda(\eta_B)) + \nu(\eta_B)$. This is illustrated in Figure 3.1. $\lambda(\eta)$ and $\nu(\eta)$ are replaced by their respective Taylor series expansions,

$$\nu(\eta) = \nu_1\eta + \nu_2\eta^2 + \nu_3\eta^3 + \nu_4\eta^4 + O(\eta^5), \quad (3.1)$$

$$\lambda(\eta) = \lambda_S + \lambda_1\eta + \lambda_2\eta^2 + \lambda_3\eta^3 + \lambda_4\eta^4 + O(\eta^5), \quad (3.2)$$

from which the coefficients are calculated successively, employing the equilibrium equations. Equilibrium along the secondary path is expressed as

$$\tilde{\mathbf{G}}(\eta) := \mathbf{G}(\tilde{\mathbf{u}}(\lambda(\eta)) + \nu(\eta), \lambda(\eta)) \equiv \mathbf{0}. \quad (3.3)$$

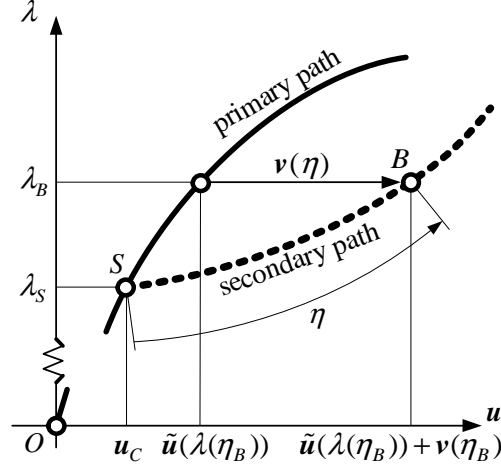


Figure 3.1: Parametrization of the secondary path for Koiter's initial postbuckling analysis.

Inserting (3.1) and (3.2) into the Taylor series of (3.3) and ordering terms according to the power order of η gives

$$\tilde{\mathbf{G}}(\eta) = \mathbf{G}_1\eta + \mathbf{G}_2\eta^2 + \mathbf{G}_3\eta^3 + \mathbf{G}_4\eta^4 + O(\eta^5) \equiv \mathbf{0}. \quad (3.4)$$

Under the assumption of sufficient smoothness of $\tilde{\mathbf{G}}(\eta)$, a necessary and sufficient condition for its vanishing is the vanishing of each coefficient of its series expansion in terms of η , at the bifurcation point S . This gives a set of equations allowing sequential calculation of the coefficients \mathbf{v}_i and λ_i . Exemplarily, the first three equations are given here:

$$\mathbf{G}_1 = \tilde{\mathbf{K}}_T \cdot \mathbf{v}_1 = \mathbf{0}, \quad (3.5)$$

$$\mathbf{G}_2 = \tilde{\mathbf{K}}_T \cdot \mathbf{v}_2 + \lambda_1 \tilde{\mathbf{K}}_{T,\lambda} \cdot \mathbf{v}_1 + \frac{1}{2} \mathbf{K}_{T,u} : \mathbf{v}_1 \otimes \mathbf{v}_1 = \mathbf{0}, \quad (3.6)$$

$$\begin{aligned} \mathbf{G}_3 = & \tilde{\mathbf{K}}_T \cdot \mathbf{v}_3 + \lambda_2 \tilde{\mathbf{K}}_{T,\lambda} \cdot \mathbf{v}_1 \\ & + \lambda_1 \tilde{\mathbf{K}}_{T,\lambda} \cdot \mathbf{v}_2 + \frac{1}{2} \lambda_1^2 \tilde{\mathbf{K}}_{T,\lambda\lambda} \cdot \mathbf{v}_1 + \mathbf{K}_{T,u} : \mathbf{v}_1 \otimes \mathbf{v}_2 \\ & + \frac{1}{2} \lambda_1 \mathbf{K}_{T,u\lambda} : \mathbf{v}_1 \otimes \mathbf{v}_1 + \frac{1}{6} \mathbf{K}_{T,uuu} : \mathbf{v}_1 \otimes \mathbf{v}_1 \otimes \mathbf{v}_1 = \mathbf{0}. \end{aligned} \quad (3.7)$$

Differentiation of \mathbf{K}_T and $\mathbf{K}_{T,u}$ with respect to λ is to be understood as the directional derivative in the direction of the tangent to the primary path. A more

detailed explanation of this notation together with expressions for the coefficients up to sixth order can be found in [21].

Equation (3.5) allows calculation of \mathbf{v}_1 , as the bifurcation point is characterized by the singularity of the tangent stiffness matrix. This relation determines \mathbf{v}_1 only up to a constant factor.

$$\|\mathbf{v}_1\|_2 = 1 \quad (3.8)$$

or

$$\mathbf{v}_1^T \cdot \widetilde{\mathbf{K}}_{T,\lambda} \cdot \mathbf{v}_1 = -1 \quad (3.9)$$

represent constraint equations that render \mathbf{v}_1 unique. Premultiplication of (3.6) with \mathbf{v}_1^T enables calculation of λ_1 :

$$\lambda_1 = -\frac{1}{2} \frac{\mathbf{v}_1^T \cdot \mathbf{K}_{T,\mathbf{u}} : \mathbf{v}_1 \otimes \mathbf{v}_1}{\mathbf{v}_1^T \cdot \widetilde{\mathbf{K}}_{T,\lambda} \cdot \mathbf{v}_1}. \quad (3.10)$$

Once λ_1 is known, (3.6) provides \mathbf{v}_2 :

$$\widetilde{\mathbf{K}}_T \cdot \mathbf{v}_2 = -\widetilde{\mathbf{K}}_{T,\lambda} \cdot \mathbf{v}_1 \lambda_1 - \frac{1}{2} \mathbf{K}_{T,\mathbf{u}} : \mathbf{v}_1 \otimes \mathbf{v}_1. \quad (3.11)$$

This singular equation does not have a unique solution, but the existence of a solution is guaranteed by the fact that the right-hand side is orthogonal to \mathbf{v}_1 as a consequence of (3.10). In order to make \mathbf{v}_2 and the coefficients of higher order, to which analogous considerations apply, unique,

$$\mathbf{v}_1 \perp \mathbf{v}_k, \quad j = 2, 3, \dots \quad (3.12)$$

has proved to be a reasonable choice for additional constraints [6].

Proceeding in the same manner, λ_2 is obtained from (3.7) as

$$\begin{aligned} \lambda_2 = & -\frac{1}{\mathbf{v}_1^T \widetilde{\mathbf{K}}_{T,\lambda} \mathbf{v}_1} \left(\frac{1}{2} \lambda_1^2 \mathbf{v}_1^T \cdot \widetilde{\mathbf{K}}_{T,\lambda\lambda} \cdot \mathbf{v}_1 \right. \\ & + \lambda_1 \left(\mathbf{v}_1^T \cdot \widetilde{\mathbf{K}}_{T,\lambda} \cdot \mathbf{v}_2 + \frac{1}{2} \mathbf{v}_1^T \mathbf{K}_{T,\mathbf{u}\lambda} : \mathbf{v}_1 \otimes \mathbf{v}_1 \right) \\ & \left. + \mathbf{v}_1^T \cdot \mathbf{K}_{T,\mathbf{u}} : \mathbf{v}_1 \otimes \mathbf{v}_2 + \frac{1}{6} \mathbf{v}_1^T \cdot \mathbf{K}_{T,\mathbf{uu}} : \mathbf{v}_1 \otimes \mathbf{v}_1 \otimes \mathbf{v}_1 \right). \end{aligned} \quad (3.13)$$

Structures with $\lambda_1 \neq 0$ are inherently imperfection sensitive [30] because of the decrease of the load for either $\eta > 0$ or $\eta < 0$. Such structures will be excluded

from the following considerations. If $\lambda_1 = 0$, then, at least for an arbitrarily small neighborhood of S , $\lambda(\eta)$ either increases or decreases for both $\eta < 0$ and $\eta > 0$. Restriction to $\lambda_1 = 0$ significantly simplifies further calculations. Moreover, this restriction is necessary for conversion of originally imperfection-sensitive structures into imperfection insensitive ones in the course of sensitivity analysis of the initial postbuckling behavior by means of variation of a suitable design parameter. For conciseness, we will introduce abbreviations in the expressions for λ_2 , λ_3 and λ_4 , where terms containing λ_1 as a factor were dropped. These expressions are given as follows:

$$\lambda_2 = d_1, \quad (3.14)$$

$$\lambda_3 = b_1 \lambda_2 + d_2, \quad (3.15)$$

$$\lambda_4 = a_1 \lambda_2^2 + b_2 \lambda_2 + b_1 \lambda_3 + d_3. \quad (3.16)$$

The full expressions for the terms in (3.14)-(3.16) can be found in Appendix A.

3.2 Symmetry

In many practical applications, structures have geometric symmetry properties and are loaded symmetrically. This results in symmetry of the bifurcation behavior (Figure 3.2). This situation was investigated by Steinboeck et al. [31]. In this work, the basis for the considerations was symmetry of the potential energy function, expressed by

$$V(\mathbf{u}, \lambda) = V(\mathbf{T} \cdot \mathbf{u}, \lambda) \quad (3.17)$$

where $\mathbf{T} \in \mathbb{R}^N \times \mathbb{R}^N$ is an element of a suitable symmetry group. The displacement of the primary path of such a structure lies in the subspace of \mathbb{R}^N that is invariant under \mathbf{T} .

Symmetric load-displacement behavior is characterized by

$$\lambda(\eta) = \lambda(-\eta), \quad \nu(\eta) = \mathbf{T} \cdot \nu(-\eta), \quad \tilde{\mathbf{u}}(\lambda(\eta)) = \mathbf{T} \cdot \tilde{\mathbf{u}}(\lambda(\eta)). \quad (3.18)$$

This results in

$$\lambda_1 = \lambda_3 = \lambda_5 = \dots = 0. \quad (3.19)$$

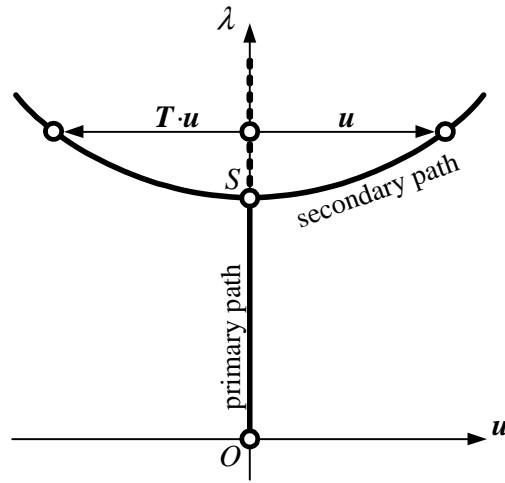


Figure 3.2: Symmetric bifurcation: An element \mathbf{T} of a symmetry group exists which maps the two branches of the secondary path onto each other.

Comparing the conditions for symmetric postbuckling (3.18) with those for imperfection insensitivity (2.18), it becomes clear that symmetry is not necessary for conversion of imperfection sensitive structures into imperfection insensitive ones. Nevertheless, $\lambda_1 \equiv 0$ is necessary which constitutes a restricted form of asymmetry in the sense that at least in an arbitrarily small neighborhood of the stability limit the load either increases or decreases on both branches of the secondary path. [30].

3.3 The coefficients a_1 and a_1^*

The coefficients a_1 and a_1^* , defined in Appendix A, play an important role in this work. In [29], a_1 was denoted as nonlinearity factor. This is due to the fact that for linear stability problems, characterized by $\widetilde{\mathbf{K}}_T = \mathbf{K}_0 + \lambda \mathbf{K}_1$, $a_1 \equiv 0$. However, $a_1 = 0$ does not imply linearity of the primary path.

Once the stability limit is found and \mathbf{v}_1 is calculated, \mathbf{v}_1 can be used to (locally) define a function

$$f(\lambda) := \mathbf{v}_1^T \cdot \widetilde{\mathbf{K}}_T(\lambda) \cdot \mathbf{v}_1. \quad (3.20)$$

Note that in this definition only $\widetilde{\mathbf{K}}_T$ depends on λ whereas \mathbf{v}_1 is constant. a_1 and a_1^* are obtained as

$$a_1 = -\frac{1}{2} \frac{f_{,\lambda\lambda}(\lambda_S)}{f_{,\lambda}(\lambda_S)} \quad (3.21)$$

and

$$a_1^* = -\frac{1}{6} \frac{f_{,\lambda\lambda\lambda}(\lambda_S)}{f_{,\lambda}(\lambda_S)}. \quad (3.22)$$

The evolution of a_1 in the course of sensitivity analysis of the initial postbuckling behavior is determined by the evolution of $f(\lambda)$. The connection between the load-displacement path of the structure and $f(\lambda)$ is sketched in Figure 3.3.

At all bifurcation points where \mathbf{v}_1 is the zero eigenvector of $\widetilde{\mathbf{K}}_T$, $f(\lambda) = 0$. This is, of course, the case at the stability limit. If a second intersection of the primary path and the secondary path exists and if \mathbf{v}_1 is also the eigenvector referring to this bifurcation point, $f(\lambda) = 0$ will also hold for this point. Such a situation was found to be the case for the two-degree-of-freedom systems presented in Section 8.1. Figure 3.3 refers to such a situation.

At the stability limit, the stiffness matrix is positive semidefinite. Thus, $f_{,\lambda}(\lambda_S) < 0$. Consequently, the sign of a_1 depends only on the curvature of $f(\lambda)$ at the stability limit. At hilltop buckling (see Figure 3.3(a)), the vertical tangent, as a consequence of the local maximum of the load, together with a negative curvature of $f(\lambda)$ implies $a_1 = -\infty$. Formally, (3.21) and (3.22) have to be calculated as limits from the left. In a situation as shown in Figure 3.3(b), the curvature of $f(\lambda)$ at λ_S and consequently a_1 , is still negative. After the sign transition, either in form of a point of inflection or of a planar point of $f(\lambda)$ at λ_S , characterized by $a_1 = 0$, the curvature of $f(\lambda)$ eventually becomes positive (see Figure 3.3(c)),

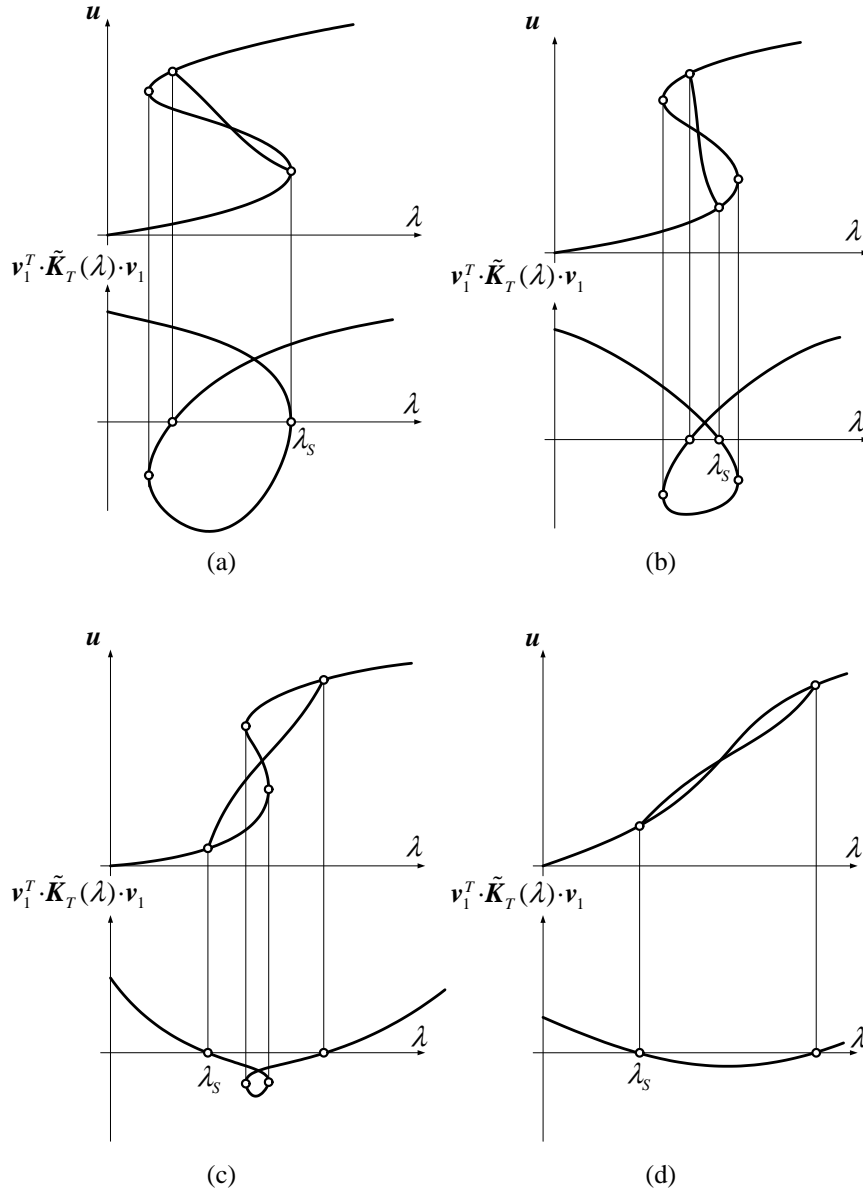


Figure 3.3: Sensitivity analysis of a simple structure, load-displacement path and $\mathbf{v}_1^T \cdot \tilde{\mathbf{K}}_T(\lambda) \cdot \mathbf{v}_1$ (a) at the start with hilltop buckling, (b) before conversion from imperfection sensitivity into imperfection insensitivity (c) after conversion into imperfection insensitivity (d) after change from a non-monotonic to a monotonically increasing primary path.

implying $a_1 > 0$. The curve becomes flatter as the load along the primary path becomes monotonous in consequence of the increased stiffness of the structure. Typically, the decrease in the curvature with increasing κ is stronger than the decrease in the slope of $f(\lambda)$, leading to $a_1 \rightarrow 0$ (see Figure 3.3(d)).

The function (3.20) can be used in a computer program to find a_1 also for general examples. The restriction in the preceding considerations concerning the eigenvector \mathbf{v}_1 at the second bifurcation point is not necessary to calculate a_1 using (3.21) at the stability limit. If only a_1 and a_1^* are needed, it suffices to find the stability limit and \mathbf{v}_1 and then calculate samples of (3.20). These scalar values can easily be stored and used for numerical differentiation. Thus, there is no need to solve an eigenproblem or store large global tangent stiffness matrices.

Chapter 4

Special modes of buckling and postbuckling

4.1 Hilltop buckling

Hilltop buckling is characterized by the coincidence of a bifurcation point with a snap-through point on the load-displacement path, i.e. $S = D$, as depicted in Figure 4.1. In this figure, the primary path is marked as I and the secondary path as II.

Mathematically, hilltop buckling is characterized by a defect of the tangent stiff-

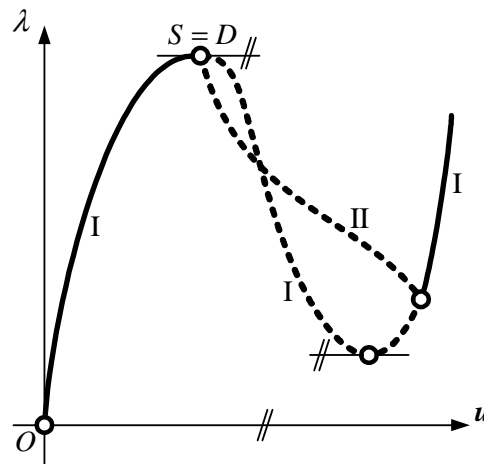


Figure 4.1: Load-displacement path for the case of hilltop buckling.

ness matrix \mathbf{K}_T of at least 2, where one eigenvector, denoted as \mathbf{v}_1 , is orthogonal to the load vector whereas the other one, $\mathbf{d}\tilde{\mathbf{u}}$, is not. This situation was studied e.g. by Fujii and Noguchi [8].

Hilltop buckling is always imperfection sensitive. To prove this, analysis tools must be used which do not *a priori* rule out the possibility of imperfection insensitivity. This requirement restricts the use of Koiter's postbuckling analysis where the displacements describing the secondary path are considered as relative to the ones representing the primary path which is described by $\tilde{\mathbf{u}}(\lambda)$. For hilltop buckling, it is impossible to find even an arbitrarily small neighborhood of the critical load $\lambda_S = \lambda(\eta = 0)$ such that in this neighborhood $\tilde{\mathbf{u}}(\lambda)$ is well defined for all values of λ .

The initial postbuckling behavior at a turning point is described similarly as in Koiter's postbuckling analysis, using, however, absolute instead of relative displacements. The starting point is again the out-of-balance force $\mathbf{G}(\mathbf{u}, \lambda)$. As before, a series expansion is used to describe the secondary path in parameter form:

$$\hat{\lambda}(\eta) = \hat{\lambda}_S + \hat{\lambda}_1\eta + \hat{\lambda}_2\eta^2 + \hat{\lambda}_3\eta^3 + O(\eta^4), \quad (4.1)$$

$$\mathbf{w}(\eta) = \mathbf{w}_0 + \mathbf{w}_1\eta + \mathbf{w}_2\eta^2 + \mathbf{w}_3\eta^3 + O(\eta^4), \quad (4.2)$$

where $(\mathbf{w}_0, \hat{\lambda}_S)$ defines the critical point, characterized by $\eta = 0$. Now, the domain of $\mathbf{G}(\mathbf{u}, \lambda)$ can be restricted to the path described by (4.1) and (4.2),

$$\hat{\mathbf{G}}(\eta) = \mathbf{G}(\mathbf{w}(\eta), \hat{\lambda}(\eta)), \quad (4.3)$$

and, by analogy to Koiter's postbuckling analysis, a Taylor series can be formulated for $\hat{\mathbf{G}}(\eta)$. For the given purpose, an expansion up to quadratic terms suffices:

$$\hat{\mathbf{G}}(\eta) = \hat{\mathbf{G}}_0 + \hat{\mathbf{G}}_1\eta + \hat{\mathbf{G}}_2\eta^2 + O(\eta^3) = \mathbf{0}. \quad (4.4)$$

In (4.4),

$$\hat{\mathbf{G}}_0 = \mathbf{0} \quad \text{by definition,} \quad (4.5)$$

$$\hat{\mathbf{G}}_1 = \hat{\mathbf{G}}_{,\eta} = \left(\hat{\mathbf{G}}_{,\mathbf{u}} \cdot \mathbf{w}_{,\eta} - \hat{\lambda}_{,\eta} \bar{\mathbf{P}} \right)_S = \widetilde{\mathbf{K}}_T \cdot \mathbf{w}_1 - \hat{\lambda}_1 \bar{\mathbf{P}}, \quad (4.6)$$

$$\begin{aligned} \hat{\mathbf{G}}_2 &= \frac{1}{2} \hat{\mathbf{G}}_{,\eta\eta} = \frac{1}{2} \left(\hat{\mathbf{G}}_{,\mathbf{uu}} : \mathbf{w}_{,\eta} \otimes \mathbf{w}_{,\eta} \right. \\ &\quad \left. + \hat{\mathbf{G}}_{,\mathbf{u}} \cdot \mathbf{w}_{,\eta\eta} + \hat{\mathbf{G}}_{,\lambda\lambda} (\hat{\lambda}_{,\eta})^2 + \hat{\mathbf{G}}_{,\lambda} \hat{\lambda}_{,\eta\eta} \right)_S \\ &= \mathbf{K}_{T,\mathbf{u}} : \mathbf{w}_1 \otimes \mathbf{w}_1 + \widetilde{\mathbf{K}}_T \cdot \mathbf{w}_2 - \hat{\lambda}_2 \bar{\mathbf{P}}. \end{aligned} \quad (4.7)$$

Equation (4.6) contains two unknowns, $\hat{\lambda}_1$ and \mathbf{w}_1 , and thus has no unique solution for a general buckling point. This is why in Koiter's postbuckling analysis, displacements relative to the primary path, in form of the shift $\nu(\eta)$ to $\tilde{\mathbf{u}}(\lambda)$, were used. For the special case of hilltop buckling, however, there are two eigenvectors corresponding to the eigenvalue 0 of the stiffness matrix $\widetilde{\mathbf{K}}_T$. These eigenvectors represent the two modes of loss of stability. The eigenvector corresponding to the snap-through mode is denoted as $d\tilde{\mathbf{u}}$. This vector is not perpendicular to the load vector (contrary to the eigenvector corresponding to the bifurcation mode). We can multiply (4.6) and (4.7) from the left by $d\tilde{\mathbf{u}}^T$, thus eliminating the terms containing $\widetilde{\mathbf{K}}_T$. This allows successive calculation of the unknowns. As follows from (4.6),

$$d\tilde{\mathbf{u}}^T \cdot (\widetilde{\mathbf{K}}_T \cdot \mathbf{w}_1 - \hat{\lambda}_1 \bar{\mathbf{P}}) = -\hat{\lambda}_1 (d\tilde{\mathbf{u}}^T \cdot \bar{\mathbf{P}}) = 0. \quad (4.8)$$

By definition, $d\tilde{\mathbf{u}}^T \cdot \bar{\mathbf{P}} \neq 0$, which implies

$$\hat{\lambda}_1 = 0 \quad (4.9)$$

for hilltop buckling. Inserting (4.9) into (4.6), shows that \mathbf{w}_1 can be chosen arbitrarily from the nullspace of $\widetilde{\mathbf{K}}_T$. A reasonable choice is $\mathbf{w}_1 = \mathbf{v}_1$, i.e. the eigenvector of $\widetilde{\mathbf{K}}_T$ corresponding to the bifurcation buckling mode. By analogy, (4.7) gives

$$\begin{aligned} &d\tilde{\mathbf{u}}^T \cdot \left(\frac{1}{2} \mathbf{K}_{T,\mathbf{u}} : \mathbf{w}_1 \otimes \mathbf{w}_1 + \mathbf{K}_T \cdot \mathbf{w}_2 - \hat{\lambda}_2 \bar{\mathbf{P}} \right) \\ &= \frac{1}{2} d\tilde{\mathbf{u}}^T \cdot \mathbf{K}_{T,\mathbf{u}} : \mathbf{w}_1 \otimes \mathbf{w}_1 - \hat{\lambda}_2 d\tilde{\mathbf{u}}^T \cdot \bar{\mathbf{P}} = 0, \end{aligned} \quad (4.10)$$

allowing calculation of $\hat{\lambda}_2$ from (4.10) as

$$\hat{\lambda}_2 = \frac{1}{2(\mathbf{d}\tilde{\mathbf{u}}^T \cdot \bar{\mathbf{P}})} \mathbf{d}\tilde{\mathbf{u}}^T \cdot \mathbf{K}_{T,\mathbf{u}} : \mathbf{w}_1 \otimes \mathbf{w}_1 = \frac{1}{2(\mathbf{d}\tilde{\mathbf{u}}^T \cdot \bar{\mathbf{P}})} \mathbf{w}_1^T \cdot \mathbf{K}_{T,\mathbf{u}} : \mathbf{d}\tilde{\mathbf{u}} \otimes \mathbf{w}_1, \quad (4.11)$$

noting that $\mathbf{K}_{T,\mathbf{u}}$ is the third derivative of the potential energy function, which allows re-ordering of multiplications with the vectors in (4.11). $\mathbf{d}\tilde{\mathbf{u}}$ is an infinitesimal displacement increment of the primary path, satisfying the equation

$$\tilde{\mathbf{K}}_T \cdot \mathbf{d}\tilde{\mathbf{u}} = d\lambda \bar{\mathbf{P}}. \quad (4.12)$$

The vector $\mathbf{d}\tilde{\mathbf{u}}$ becomes an eigenvector of $\tilde{\mathbf{K}}_T$ at a snap-through point where $d\lambda = 0$. To determine the sign of $\mathbf{d}\tilde{\mathbf{u}}$ uniquely, it is stipulated that $d\lambda > 0$ for the prebuckling domain. Then

- $(\mathbf{d}\tilde{\mathbf{u}}^T \cdot \bar{\mathbf{P}})_s > 0$ can be easily shown: By definition, $\mathbf{d}\tilde{\mathbf{u}}^T \cdot \bar{\mathbf{P}} \neq 0$ at the snap-through point. Premultiplication of (4.12) with $\mathbf{d}\tilde{\mathbf{u}}^T$ and division by $d\lambda$ gives

$$\frac{\mathbf{d}\tilde{\mathbf{u}}^T \cdot \tilde{\mathbf{K}}_T \cdot \mathbf{d}\tilde{\mathbf{u}}}{d\lambda} = \mathbf{d}\tilde{\mathbf{u}}^T \cdot \bar{\mathbf{P}}. \quad (4.13)$$

The left-hand side of (4.13) is always positive before the critical point as a consequence of the positive definiteness of $\tilde{\mathbf{K}}_T$. As the sign of $\mathbf{d}\tilde{\mathbf{u}}^T \cdot \bar{\mathbf{P}}$ does not jump, $\mathbf{d}\tilde{\mathbf{u}}^T \cdot \bar{\mathbf{P}}$ is non-zero at the critical point by definition and has only positive values before this point, thus $(\mathbf{d}\tilde{\mathbf{u}}^T \cdot \bar{\mathbf{P}})_s > 0$.

- $\mathbf{w}_1^T \cdot \mathbf{K}_{T,\mathbf{u}} : \mathbf{d}\tilde{\mathbf{u}} \otimes \mathbf{w}_1$ has the same sign as $\mathbf{w}_1^T \cdot \mathbf{K}_{T,\mathbf{u}} : \tilde{\mathbf{u}}_{,\lambda} \otimes \mathbf{w}_1 = \mathbf{v}_1^T \cdot \tilde{\mathbf{K}}_{T,\lambda} \cdot \mathbf{v}_1$, but is bounded, since $\mathbf{d}\tilde{\mathbf{u}}$ has the same orientation (sign) as $\tilde{\mathbf{u}}_{,\lambda}$ whereas its norm can be chosen such that $\|\mathbf{d}\tilde{\mathbf{u}}\| < \infty$.
- The sign of the expression $\mathbf{v}_1^T \cdot \tilde{\mathbf{K}}_{T,\lambda} \cdot \mathbf{v}_1$ is always negative in a sufficiently close neighborhood of the critical point. This becomes clear if this expression is viewed as the derivative of $\mathbf{v}_1^T \cdot \tilde{\mathbf{K}}_T(\lambda) \cdot \mathbf{v}_1$, see also Section 3.3.

Finally, (4.11) yields

$$\hat{\lambda}_2 = \frac{1}{\underbrace{2(\mathbf{d}\tilde{\mathbf{u}}^T \cdot \bar{\mathbf{P}})}_{> 0}} \underbrace{\mathbf{w}_1^T \cdot \mathbf{K}_{T,\mathbf{u}} : \mathbf{d}\tilde{\mathbf{u}} \otimes \mathbf{w}_1}_{< 0} < 0 \quad (4.14)$$

Since (4.14) proves that the slope of the secondary path locally around the hilltop buckling point is negative, the condition for imperfection insensitivity in (2.18) is not fulfilled, rendering the structure imperfection sensitive.

When it comes to choosing a suitable normalization for \mathbf{v}_1 , the possibility of the occurrence of hilltop buckling must be checked. Following from

$$\|\tilde{\mathbf{u}}_{,\lambda}\|_2 \rightarrow \infty \quad \Rightarrow \quad \|\tilde{\mathbf{K}}_{T,\lambda}\|_2 \rightarrow \infty, \quad (4.15)$$

we get

$$\mathbf{v}_1^T \cdot \tilde{\mathbf{K}}_{T,\lambda} \cdot \mathbf{v}_1 = -1 \quad \Rightarrow \quad \|\mathbf{v}_1\|_2 \rightarrow 0 \quad (4.16)$$

at hilltop buckling. As the Euclidean norm of \mathbf{v}_1 influences all the other terms in Koiter's postbuckling analysis, this leads to

$$\lambda_j \rightarrow 0, \quad \|\mathbf{v}_j\|_2 \rightarrow 0. \quad (4.17)$$

Figuratively speaking, the parametrization of the secondary path close to hilltop buckling is very slow. Points with large values of the path parameter are still very close to the stability limit. The result is that for a situation where imperfection sensitivity is most pronounced, reflected by a steep decrease of the load along the secondary path, the load coefficients λ_i tend to zero. This may be misleading, if the degree of imperfection sensitivity is assessed by means of λ_i . A remedy is to use the normalization condition $\|\mathbf{v}_1\|_2 = 1$. Nevertheless, for theoretical derivations, it is reasonable to use the condition (3.9).

4.2 Zero-stiffness postbuckling

Zero-stiffness postbuckling may occur as a special form of postbuckling behavior. Its characteristic feature is a strictly horizontal postbuckling path emanating from a linear or nonlinear primary path at the critical point, as illustrated in Figure 4.2. This allows the structure to take on an arbitrary displacement along the postbuckling path without a change of the external load. Thus, each point on a zero-stiffness postbuckling path can be viewed as a neutral state of equilibrium. Tarnai [34] has pioneered research on zero-stiffness postbuckling, including presentation of two simple examples. According to Tarnai, zero-stiffness structures

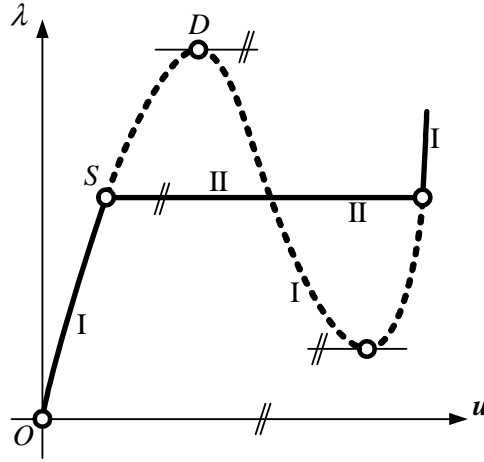


Figure 4.2: Load-displacement path in the case of zero-stiffness postbuckling.

represent a special kind of mechanism in which internal forces are present but are continuously re-arranged during the motion along the equilibrium path. Schranz et al. [29] presented a numerical example which was further elaborated by Steinboeck et al. [32]. Schenk et al. [28] discussed tensegrity structures exhibiting zero-stiffness postbuckling paths.

In the context of Koiter's postbuckling analysis, zero-stiffness postbuckling is defined by

$$\lambda_i = 0 \quad \forall i \in \mathbb{N}. \quad (4.18)$$

The potential energy along the secondary path is constant. Zero-stiffness postbuckling marks the onset of imperfection insensitivity in the course of sensitivity analysis of the initial postbuckling path. It is a particularly favorable form of transition from imperfection sensitivity to insensitivity because all coefficients λ_i with even subscripts change their signs from negative to positive, as was shown numerically.

Zero-stiffness postbuckling represents a special case of postbuckling behavior for which the criteria for imperfection insensitivity, given as (2.18) and (2.19), respectively, do not agree. It is classified imperfection sensitive according to (2.18) but imperfection insensitive with regard to (2.19). Jia et al. [13] have shown that zero-stiffness postbuckling is imperfection insensitive in the follow-

ing sense: for imperfections preventing the investigated structure from bifurcation buckling, the load-displacement path is characterized by a monotonically increasing load in the neighborhood of the bifurcation point of the corresponding perfect structure. Moreover, by investigating the potential energy of this structure, Jia et al. [13] have shown that zero-stiffness postbuckling is imperfection insensitive.

Equation (4.18) would require checking infinitely many terms to be sure that a structure indeed exhibits zero-stiffness postbuckling. This is neither possible nor necessary, as was shown in [19]. A necessary condition is buckling from a membrane stress state. Derivation of a necessary and sufficient condition for such a stress state is the topic of Chapter 6. If, for bifurcation buckling from a membrane stress state,

$$\lambda_1 = \lambda_2 = \lambda_3 = \lambda_4 = 0, \quad (4.19)$$

zero-stiffness postbuckling will occur. An example is given in Section 8.1. It will be shown in Section 8.3 that (4.19) is not sufficient if bifurcation buckling occurs from a general stress state.

Chapter 5

The consistently linearized eigenvalue problem

5.1 Definition

For finite dimensional systems, Helnwein [11, 12] introduced the so-called consistently linearized eigenproblem. His motivation was to obtain estimates for the buckling load without tracing the primary path in the vicinity of the stability limit and, thus, having to solve the fully nonlinear eigenvalue problem which is numerically demanding because of the singularity of $\tilde{\mathbf{K}}_T$ [4].

The main motivation to deal with the consistently linearized eigenproblem in this work is its role in various classification approaches as presented e.g. in [21, 32]. Solutions of the consistently linearized eigenvalue problem are used to gain additional information about structures indicating a specific postbuckling behavior. It plays a pivotal role in the deduction of equations necessary for the classification given in Chapter 6. The connection with Koiter's postbuckling analysis becomes obvious through the appearance of a_1 and a_1^* in this analysis as well as in the mathematical formulation of the consistently linearized eigenvalue problem. This formulation reads as

$$\left[\tilde{\mathbf{K}}_T(\lambda) + (\lambda^* - \lambda) \tilde{\mathbf{K}}_{T,\lambda}(\lambda) \right] \cdot \mathbf{v}^* = \mathbf{0}. \quad (5.1)$$

This eigenvalue problem is solved for every value of λ . With $\tilde{\mathbf{K}}_T(\lambda) \in \mathbb{R}^{N \times N}$, (5.1) in general has N solution pairs $(\lambda_j^*(\lambda), \mathbf{v}_j^*(\lambda))$. The index 1 will be assigned to the solution pair that fulfills $\lambda_1^*(\lambda_S) = \lambda_S$, $\mathbf{v}_1^*(\lambda_S) = \mathbf{v}_1$. Because of the singu-

larity of $\widetilde{\mathbf{K}}_T(\lambda_S)$, such a solution pair always exists. In general, $\widetilde{\mathbf{K}}_T$ and $\widetilde{\mathbf{K}}_{T,\lambda}$ are symmetric, real, and regular almost everywhere. Under these conditions, (5.1) can be rewritten as

$$-\left(\widetilde{\mathbf{K}}_{T,\lambda}(\lambda)\right)^{-1} \left[\widetilde{\mathbf{K}}_T(\lambda) - \lambda \widetilde{\mathbf{K}}_{T,\lambda}(\lambda)\right] \cdot \mathbf{v}^* = \lambda^* \mathbf{v}^*, \quad (5.2)$$

constituting an ordinary eigenvalue problem. As a consequence, the N solution pairs are always real. Furthermore, a basis of the \mathbb{R}^N , consisting of pairwise orthogonal eigenvectors \mathbf{v}_j^* , exists. The indefiniteness of $\widetilde{\mathbf{K}}_{T,\lambda}$ does not play a role here.

In the following, it will be assumed, that N solution pairs exist. It is noted that this is not the case for linear stability problems. In their most simple form with 2 degrees of freedom, their tangent stiffness matrix can be written as

$$\widetilde{\mathbf{K}}_T(\lambda) = \begin{pmatrix} a - b\lambda & 0 \\ 0 & c \end{pmatrix}. \quad (5.3)$$

The eigenproblem then is

$$\left[\begin{pmatrix} a - b\lambda & 0 \\ 0 & c \end{pmatrix} + (\lambda^* - \lambda) \begin{pmatrix} -b & 0 \\ 0 & 0 \end{pmatrix} \right] \cdot \mathbf{v}^* = \mathbf{0}. \quad (5.4)$$

From the first line, the solution $\lambda_1^* = a/b$ with the eigenvector $\mathbf{v}_1^* = [1 \ 0]^T$ can be calculated. A second eigenpair does not exist.

5.2 Properties of eigenvalues and eigenvectors

Specializing (5.1) for the first solution pair gives

$$\left[\widetilde{\mathbf{K}}_T(\lambda) + (\lambda_1^* - \lambda) \widetilde{\mathbf{K}}_{T,\lambda}(\lambda)\right] \cdot \mathbf{v}_1^* = \mathbf{0}. \quad (5.5)$$

In the following, the arguments will not be written explicitly. The first derivative of (5.5) with respect to λ results in

$$\left[\lambda_{1,\lambda}^* \widetilde{\mathbf{K}}_{T,\lambda} + (\lambda_1^* - \lambda) \widetilde{\mathbf{K}}_{T,\lambda\lambda}\right] \cdot \mathbf{v}_1^* + \left[\widetilde{\mathbf{K}}_T + (\lambda_1^* - \lambda) \widetilde{\mathbf{K}}_{T,\lambda}\right] \cdot \mathbf{v}_{1,\lambda}^* = \mathbf{0}. \quad (5.6)$$

Premultiplication of (5.6) with \mathbf{v}_1^{*T} gives

$$\lambda_{1,\lambda}^* = -(\lambda_1^* - \lambda) \frac{\mathbf{v}_1^{*T} \cdot \widetilde{\mathbf{K}}_{T,\lambda\lambda} \cdot \mathbf{v}_1^*}{\mathbf{v}_1^{*T} \cdot \widetilde{\mathbf{K}}_{T,\lambda} \cdot \mathbf{v}_1^*}. \quad (5.7)$$

Because all matrices are symmetric,

$$\mathbf{v}_1^{*T} \cdot [\widetilde{\mathbf{K}}_T + (\lambda_1^* - \lambda)\widetilde{\mathbf{K}}_{T,\lambda}] = [\widetilde{\mathbf{K}}_T + (\lambda_1^* - \lambda)\widetilde{\mathbf{K}}_{T,\lambda}] \cdot \mathbf{v}_1^* = 0. \quad (5.8)$$

The second derivative of (5.5) with respect to λ results in

$$\begin{aligned} & [\lambda_{1,\lambda\lambda}^* \widetilde{\mathbf{K}}_{T,\lambda} + (2\lambda_{1,\lambda}^* - 1)\widetilde{\mathbf{K}}_{T,\lambda\lambda} + (\lambda_1^* - \lambda)\widetilde{\mathbf{K}}_{T,\lambda\lambda\lambda}] \cdot \mathbf{v}_1^* \\ & + 2[\lambda_{1,\lambda}^* \widetilde{\mathbf{K}}_{T,\lambda} + (\lambda_1^* - \lambda)\widetilde{\mathbf{K}}_{T,\lambda\lambda}] \cdot \mathbf{v}_{1,\lambda}^* \\ & + [\widetilde{\mathbf{K}}_T + (\lambda_1^* - \lambda)\widetilde{\mathbf{K}}_{T,\lambda}] \cdot \mathbf{v}_{1,\lambda\lambda}^* = \mathbf{0}. \end{aligned} \quad (5.9)$$

The third derivative of (5.5) with respect to λ gives

$$\begin{aligned} & [\lambda_{1,\lambda\lambda\lambda}^* \widetilde{\mathbf{K}}_{T,\lambda} + 3\lambda_{1,\lambda\lambda}^* \widetilde{\mathbf{K}}_{T,\lambda\lambda} + (3\lambda_{1,\lambda}^* - 2)\widetilde{\mathbf{K}}_{T,\lambda\lambda\lambda} + (\lambda_1^* - \lambda)\widetilde{\mathbf{K}}_{T,\lambda\lambda\lambda\lambda}] \cdot \mathbf{v}_1^* \\ & + 3[\lambda_{1,\lambda\lambda}^* \widetilde{\mathbf{K}}_{T,\lambda} + (2\lambda_{1,\lambda}^* - 1)\widetilde{\mathbf{K}}_{T,\lambda\lambda} + (\lambda_1^* - \lambda)\widetilde{\mathbf{K}}_{T,\lambda\lambda\lambda}] \cdot \mathbf{v}_{1,\lambda}^* \\ & + 3[\lambda_{1,\lambda}^* \widetilde{\mathbf{K}}_{T,\lambda} + (\lambda_1^* - \lambda)\widetilde{\mathbf{K}}_{T,\lambda\lambda}] \cdot \mathbf{v}_{1,\lambda\lambda}^* \\ & + [\widetilde{\mathbf{K}}_T + (\lambda_1^* - \lambda)\widetilde{\mathbf{K}}_{T,\lambda}] \cdot \mathbf{v}_{1,\lambda\lambda\lambda}^* = \mathbf{0}. \end{aligned} \quad (5.10)$$

Special orthogonalities of the eigenvectors of the consistently linearized eigenproblem follow from its mathematical structure. Premultiplying (5.5) by \mathbf{v}_j^{*T} gives

$$\mathbf{v}_j^{*T} \cdot [\widetilde{\mathbf{K}}_T + (\lambda_1^* - \lambda)\widetilde{\mathbf{K}}_{T,\lambda}] \cdot \mathbf{v}_1^* = 0. \quad (5.11)$$

Specializing (5.1) for the j -th solution pair, premultiplying the resulting relation by \mathbf{v}_1^{*T} and making use of the symmetry of $\widetilde{\mathbf{K}}_T$ and $\widetilde{\mathbf{K}}_{T,\lambda}$ yields

$$\mathbf{v}_j^{*T} \cdot [\widetilde{\mathbf{K}}_T + (\lambda_j^* - \lambda)\widetilde{\mathbf{K}}_{T,\lambda}] \cdot \mathbf{v}_1^* = 0. \quad (5.12)$$

Subtraction of (5.12) from (5.11) gives

$$\mathbf{v}_j^{*T} \cdot [(\lambda_1^* - \lambda_j^*)\widetilde{\mathbf{K}}_{T,\lambda}] \cdot \mathbf{v}_1^* = 0. \quad (5.13)$$

With $\lambda_1^* \neq \lambda_j^*$, which holds for distinct eigenvalues, (5.13) results in

$$\mathbf{v}_j^{*T} \cdot \widetilde{\mathbf{K}}_{T,\lambda} \cdot \mathbf{v}_1^* = 0 \stackrel{(5.5)}{\implies} \mathbf{v}_j^{*T} \cdot \widetilde{\mathbf{K}}_T \cdot \mathbf{v}_1^* = 0. \quad (5.14)$$

For a basis of the eigenvectors of (5.1), $\mathbf{v}_{1,\lambda}^*$ can be written as

$$\mathbf{v}_{1,\lambda}^* = \sum_{j=1}^N c_{1j} \mathbf{v}_j^*. \quad (5.15)$$

Using (5.15) and (5.14) in (5.6) gives

$$(\lambda_1^* - \lambda) \mathbf{v}_j^{*T} \cdot \widetilde{\mathbf{K}}_{T,\lambda\lambda} \cdot \mathbf{v}_1^* + \sum_{k=2}^N \mathbf{v}_j^{*T} \cdot [\widetilde{\mathbf{K}}_T + (\lambda_1^* - \lambda) \widetilde{\mathbf{K}}_{T,\lambda}] \cdot c_{1k} \mathbf{v}_k^* = 0. \quad (5.16)$$

If we assume that the λ_j^* are pairwise distinct, (5.14) holds if \mathbf{v}_1^* is replaced by \mathbf{v}_k^* . This simplifies (5.16) and allows calculation of c_{1j} :

$$(\lambda_1^* - \lambda) \mathbf{v}_j^{*T} \cdot \widetilde{\mathbf{K}}_{T,\lambda\lambda} \cdot \mathbf{v}_1^* + \mathbf{v}_j^{*T} \cdot [\widetilde{\mathbf{K}}_T + (\lambda_1^* - \lambda) \widetilde{\mathbf{K}}_{T,\lambda}] \cdot c_{1j} \mathbf{v}_j^* = 0. \quad (5.17)$$

Using

$$\mathbf{v}_j^{*T} \cdot [\widetilde{\mathbf{K}}_T + (\lambda_j^* - \lambda) \widetilde{\mathbf{K}}_{T,\lambda}] \cdot \mathbf{v}_j^* = 0 \quad (5.18)$$

which implies

$$\mathbf{v}_j^{*T} \cdot \widetilde{\mathbf{K}}_T \cdot \mathbf{v}_j^* = -(\lambda_j^* - \lambda) \mathbf{v}_j^{*T} \cdot \widetilde{\mathbf{K}}_{T,\lambda} \cdot \mathbf{v}_j^*, \quad (5.19)$$

gives

$$c_{1j} = -\frac{(\lambda_1^* - \lambda)}{(\lambda_1^* - \lambda_j^*)} \cdot \frac{\mathbf{v}_j^{*T} \cdot \widetilde{\mathbf{K}}_{T,\lambda\lambda} \cdot \mathbf{v}_1^*}{\mathbf{v}_j^{*T} \cdot \widetilde{\mathbf{K}}_{T,\lambda} \cdot \mathbf{v}_j^*}. \quad (5.20)$$

\mathbf{v}_1^* has to be normalized in order to fully define $\mathbf{v}_{1,\lambda}^*$. Note that c_{1j} depends linearly on the norm of \mathbf{v}_1^* . Using the condition

$$\mathbf{v}_1^{*T} \cdot \widetilde{\mathbf{K}}_{T,\lambda} \cdot \mathbf{v}_1^* = -1, \quad (5.21)$$

c_{11} can be calculated by differentiating (5.21) and using the orthogonality relations (5.14):

$$\begin{aligned} 2\mathbf{v}_1^{*T} \cdot \widetilde{\mathbf{K}}_{T,\lambda} \cdot \mathbf{v}_{1,\lambda}^* + \mathbf{v}_1^{*T} \cdot \widetilde{\mathbf{K}}_{T,\lambda\lambda} \cdot \mathbf{v}_1^* \\ = 2\mathbf{v}_1^{*T} \cdot \widetilde{\mathbf{K}}_{T,\lambda} \cdot c_{11} \mathbf{v}_1^* + \mathbf{v}_1^{*T} \cdot \widetilde{\mathbf{K}}_{T,\lambda\lambda} \cdot \mathbf{v}_1^* = 0, \end{aligned} \quad (5.22)$$

$$\Rightarrow c_{11} = -\frac{1}{2} \frac{\mathbf{v}_1^{*T} \cdot \widetilde{\mathbf{K}}_{T,\lambda\lambda} \cdot \mathbf{v}_1^*}{\mathbf{v}_1^{*T} \cdot \widetilde{\mathbf{K}}_{T,\lambda} \cdot \mathbf{v}_1^*} \stackrel{(5.21)}{=} \frac{1}{2} \mathbf{v}_1^{*T} \cdot \widetilde{\mathbf{K}}_{T,\lambda\lambda} \cdot \mathbf{v}_1^*. \quad (5.23)$$

At the stability limit $\mathbf{v}_1^* = \mathbf{v}_1$. Hence

$$c_{11} = a_1. \quad (5.24)$$

Thus, a representation for $\mathbf{v}_{1,\lambda}^*$ can be written as

$$\begin{aligned}\mathbf{v}_{1,\lambda}^* &= c_{11}\mathbf{v}_1^* + \sum_{j=2}^N c_{1j}\mathbf{v}_j^* \\ &= \frac{1}{2}(\mathbf{v}_1^{*T} \cdot \widetilde{\mathbf{K}}_{T,\lambda\lambda} \cdot \mathbf{v}_1^*)\mathbf{v}_1^* - \sum_{j=2}^N \frac{(\lambda_1^* - \lambda)}{(\lambda_1^* - \lambda_j^*)} \frac{\mathbf{v}_j^{*T} \cdot \widetilde{\mathbf{K}}_{T,\lambda\lambda} \cdot \mathbf{v}_1^*}{\mathbf{v}_j^{*T} \cdot \widetilde{\mathbf{K}}_{T,\lambda} \cdot \mathbf{v}_j^*} \mathbf{v}_j^*.\end{aligned}\quad (5.25)$$

$\mathbf{v}_{1,\lambda\lambda}^*$ is calculated directly, using (5.25):

$$\mathbf{v}_{1,\lambda\lambda}^* = c_{11,\lambda}\mathbf{v}_1^* + c_{11}\mathbf{v}_{1,\lambda}^* + \sum_{j=2}^N (c_{1j,\lambda}\mathbf{v}_j^* + c_{1j}\mathbf{v}_{j,\lambda}^*).\quad (5.26)$$

For $\mathbf{v}_{j,\lambda}^*$, a similar representation as in (5.25) can be introduced:

$$\mathbf{v}_{j,\lambda}^* = \sum_{k=1}^N c_{kj}\mathbf{v}_k^*.\quad (5.27)$$

Inserting (5.25) and (5.27) into (5.26) gives

$$\mathbf{v}_{1,\lambda\lambda}^* = \left(c_{11}^2 + c_{11,\lambda} + \sum_{j=2}^N c_{1j}c_{j1} \right) \mathbf{v}_1^* + \sum_{j=2}^N \left((c_{1j}c_{11} + c_{1j,\lambda}) \mathbf{v}_j^* + c_{1j} \sum_{k=2}^N c_{jk}\mathbf{v}_k^* \right).\quad (5.28)$$

The definitions for c_{11} and c_{1j} can be found in (5.23) and (5.20), respectively.

The other coefficients appearing in (5.28) are defined as

$$c_{jj} = -\frac{1}{2} \frac{\mathbf{v}_j^{*T} \cdot \widetilde{\mathbf{K}}_{T,\lambda\lambda} \cdot \mathbf{v}_j^*}{\mathbf{v}_j^{*T} \cdot \widetilde{\mathbf{K}}_{T,\lambda} \cdot \mathbf{v}_j^*},\quad (5.29)$$

$$c_{jk} = -\frac{(\lambda_j^* - \lambda)}{(\lambda_j^* - \lambda_k^*)} \frac{\mathbf{v}_k^{*T} \cdot \widetilde{\mathbf{K}}_{T,\lambda\lambda} \cdot \mathbf{v}_j^*}{\mathbf{v}_k^{*T} \cdot \widetilde{\mathbf{K}}_{T,\lambda} \cdot \mathbf{v}_k^*},\quad (5.30)$$

$$c_{11,\lambda} = -\frac{1}{2} \frac{2\mathbf{v}_1^{*T} \cdot \widetilde{\mathbf{K}}_{T,\lambda\lambda} \cdot \mathbf{v}_{1,\lambda}^* + \mathbf{v}_1^{*T} \cdot \widetilde{\mathbf{K}}_{T,\lambda\lambda\lambda} \cdot \mathbf{v}_1^*}{\mathbf{v}_1^{*T} \cdot \widetilde{\mathbf{K}}_{T,\lambda} \cdot \mathbf{v}_1^*},\quad (5.31)$$

$$\begin{aligned}
 c_{1j,\lambda} = & -\frac{(\lambda_{1,\lambda}^* - 1)(\mathbf{v}_j^{*T} \cdot \widetilde{\mathbf{K}}_{T,\lambda\lambda} \cdot \mathbf{v}_1^*) + (\lambda_1^* - \lambda)(\mathbf{v}_{j,\lambda}^{*T} \cdot \widetilde{\mathbf{K}}_{T,\lambda\lambda} \cdot \mathbf{v}_1^*)}{(\lambda_1^* - \lambda_j^*)(\mathbf{v}_j^{*T} \cdot \widetilde{\mathbf{K}}_{T,\lambda} \cdot \mathbf{v}_j^*)} \\
 & - \frac{(\lambda_1^* - \lambda)(\mathbf{v}_j^{*T} \cdot \widetilde{\mathbf{K}}_{T,\lambda\lambda} \cdot \mathbf{v}_1^* + \mathbf{v}_j^{*T} \cdot \widetilde{\mathbf{K}}_{T,\lambda\lambda} \cdot \mathbf{v}_{1,\lambda}^*)}{(\lambda_1^* - \lambda_j^*)(\mathbf{v}_j^{*T} \cdot \widetilde{\mathbf{K}}_{T,\lambda} \cdot \mathbf{v}_j^*)} \\
 & + \frac{(\lambda_1^* - \lambda)(\mathbf{v}_j^{*T} \cdot \widetilde{\mathbf{K}}_{T,\lambda\lambda} \cdot \mathbf{v}_1^*) \left((\lambda_{1,\lambda}^* - \lambda_{j,\lambda}^*)(\mathbf{v}_1^{*T} \cdot \widetilde{\mathbf{K}}_{T,\lambda} \cdot \mathbf{v}_j^*) + (\lambda_1^* - \lambda_j^*)(\mathbf{v}_{j,\lambda}^{*T} \cdot \widetilde{\mathbf{K}}_{T,\lambda} \cdot \mathbf{v}_j^*) \right)}{(\lambda_1^* - \lambda_j^*)^2 (\mathbf{v}_j^{*T} \cdot \widetilde{\mathbf{K}}_{T,\lambda} \cdot \mathbf{v}_j^*)^2} \\
 & + \frac{(\lambda_1^* - \lambda)(\mathbf{v}_j^{*T} \cdot \widetilde{\mathbf{K}}_{T,\lambda\lambda} \cdot \mathbf{v}_1^*) \left(\mathbf{v}_j^{*T} \cdot \widetilde{\mathbf{K}}_{T,\lambda\lambda} \cdot \mathbf{v}_j^* + \mathbf{v}_j^{*T} \cdot \widetilde{\mathbf{K}}_{T,\lambda} \cdot \mathbf{v}_{j,\lambda}^* \right)}{(\lambda_1^* - \lambda_j^*)^2 (\mathbf{v}_j^{*T} \cdot \widetilde{\mathbf{K}}_{T,\lambda} \cdot \mathbf{v}_j^*)^2}. \quad (5.32)
 \end{aligned}$$

For calculation of (5.31), use of the constancy of the denominator of the expression for c_{11} (see (5.21)) was made. The derivatives of \mathbf{v}_1^* with respect to λ can now be specialized for the stability limit, for which

$$\lambda_1^* = \lambda, \quad \lambda_{1,\lambda}^* = 0, \quad \mathbf{v}_1^* = \mathbf{v}_1. \quad (5.33)$$

This leads to

$$c_{11} = a_1, \quad (5.34)$$

$$c_{1j} = 0, \quad j = 2, \dots, N, \quad (5.35)$$

$$c_{11,\lambda} = 2a_1^2 + 3a_1^*. \quad (5.36)$$

This gives

$$\mathbf{v}_{1,\lambda}^* = a_1 \mathbf{v}_1 \quad (5.37)$$

and

$$\mathbf{v}_{1,\lambda\lambda}^* = 3(a_1^2 + a_1^*)\mathbf{v}_1 + \sum_{j=2}^N \frac{\mathbf{v}_j^* \cdot \widetilde{\mathbf{K}}_{T,\lambda\lambda} \cdot \mathbf{v}_1}{(\lambda_1^* - \lambda_j^*)(\mathbf{v}_j^* \cdot \widetilde{\mathbf{K}}_{T,\lambda} \cdot \mathbf{v}_j^*)} \mathbf{v}_j^*. \quad (5.38)$$

Calculation of the derivatives of λ_1^* provides information about the function $\lambda_1^*(\lambda)$. $\lambda_{1,\lambda}^*$, given in (5.7), can now be specialized for the stability limit:

$$\lambda_{1,\lambda}^* = -(\lambda_1^* - \lambda) \frac{\mathbf{v}_1^{*T} \cdot \widetilde{\mathbf{K}}_{T,\lambda\lambda} \cdot \mathbf{v}_1^*}{\mathbf{v}_1^{*T} \cdot \widetilde{\mathbf{K}}_{T,\lambda} \cdot \mathbf{v}_1^*} \stackrel{\text{stab. limit}}{=} 0. \quad (5.39)$$

Premultiplication of higher-order derivatives of the consistently linearized eigenproblem allows calculation of $\lambda_{1,\lambda\lambda}^*$ and $\lambda_{1,\lambda\lambda\lambda}^*$ and specialization of the obtained

relations for the stability limit:

$$\begin{aligned} \lambda_{1,\lambda\lambda}^* &= -2\lambda_{1,\lambda}^* \frac{\mathbf{v}_1^{*T} \cdot \widetilde{\mathbf{K}}_{T,\lambda} \cdot \mathbf{v}_{1,\lambda}^*}{\mathbf{v}_1^{*T} \cdot \widetilde{\mathbf{K}}_{T,\lambda} \cdot \mathbf{v}_1^*} - (\lambda_1^* - \lambda) \frac{\mathbf{v}_1^{*T} \cdot \widetilde{\mathbf{K}}_{T,\lambda\lambda} \cdot \mathbf{v}_{1,\lambda}^*}{\mathbf{v}_1^{*T} \cdot \widetilde{\mathbf{K}}_{T,\lambda} \cdot \mathbf{v}_1^*} \\ &\quad - (2\lambda_{1,\lambda}^* - 1) \frac{\mathbf{v}_1^{*T} \cdot \widetilde{\mathbf{K}}_{T,\lambda\lambda} \cdot \mathbf{v}_1^*}{\mathbf{v}_1^{*T} \cdot \widetilde{\mathbf{K}}_{T,\lambda} \cdot \mathbf{v}_1^*} - (\lambda_1^* - \lambda) \frac{\mathbf{v}_1^{*T} \cdot \widetilde{\mathbf{K}}_{T,\lambda\lambda\lambda} \cdot \mathbf{v}_{1,\lambda}^*}{\mathbf{v}_1^{*T} \cdot \widetilde{\mathbf{K}}_{T,\lambda} \cdot \mathbf{v}_1^*} \\ &\stackrel{\text{stab. limit}}{=} -2a_1. \end{aligned} \quad (5.40)$$

$$\begin{aligned} \lambda_{1,\lambda\lambda\lambda}^* &= -\frac{1}{\mathbf{v}_1^{*T} \cdot \widetilde{\mathbf{K}}_{T,\lambda} \cdot \mathbf{v}_1^*} \left(3\lambda_{1,\lambda\lambda}^* \mathbf{v}_1^{*T} \cdot \widetilde{\mathbf{K}}_{T,\lambda\lambda} \cdot \mathbf{v}_1^* + (3\lambda_{1,\lambda}^* - 2) \mathbf{v}_1^{*T} \cdot \widetilde{\mathbf{K}}_{T,\lambda\lambda\lambda} \cdot \mathbf{v}_1^* \right. \\ &\quad + (\lambda_1^* - \lambda) \mathbf{v}_1^{*T} \cdot \widetilde{\mathbf{K}}_{T,\lambda\lambda\lambda} \cdot \mathbf{v}_1^* \\ &\quad + 3[\lambda_{1,\lambda\lambda}^* \mathbf{v}_1^{*T} \cdot \widetilde{\mathbf{K}}_{T,\lambda} \cdot \mathbf{v}_{1,\lambda}^* + (2\lambda_{1,\lambda}^* - 1) \mathbf{v}_1^{*T} \cdot \widetilde{\mathbf{K}}_{T,\lambda\lambda} \cdot \mathbf{v}_{1,\lambda}^* + (\lambda_1^* - \lambda) \mathbf{v}_1^{*T} \cdot \widetilde{\mathbf{K}}_{T,\lambda\lambda\lambda} \cdot \mathbf{v}_{1,\lambda}^*] \\ &\quad \left. + 3[\lambda_{1,\lambda}^* \mathbf{v}_1^{*T} \cdot \widetilde{\mathbf{K}}_{T,\lambda} \cdot \mathbf{v}_{1,\lambda\lambda}^* + (\lambda_1^* - \lambda) \mathbf{v}_1^{*T} \cdot \widetilde{\mathbf{K}}_{T,\lambda\lambda} \cdot \mathbf{v}_{1,\lambda\lambda}^*] \right) \\ &\stackrel{\text{stab. limit}}{=} -12(a_1^2 + a_1^*). \end{aligned} \quad (5.41)$$

The preceding considerations allow examination of the eigenvalue curve $\lambda_1^*(\lambda)$. At the stability limit ($\lambda_1^* = \lambda$), this curve has a horizontal tangent ($\lambda_{1,\lambda}^* = 0$) and its curvature equals $-2a_1$, as follows from specialization of the general expression for the curvature at the stability limit

$$\kappa = \frac{\lambda_{1,\lambda\lambda}^*}{(1 + \lambda_{1,\lambda}^{*2})^{\frac{3}{2}}} \stackrel{\text{stab. limit}}{=} \lambda_{1,\lambda\lambda}^* = -2a_1. \quad (5.42)$$

The derivative of the curvature κ with respect to λ is given as

$$\begin{aligned} \kappa_{,\lambda} &= \frac{\lambda_{1,\lambda\lambda\lambda}^* (1 + \lambda_{1,\lambda}^{*2})^{\frac{3}{2}} - 3\lambda_{1,\lambda}^* \lambda_{1,\lambda\lambda}^{*2} (1 + \lambda_{1,\lambda}^{*2})^{\frac{1}{2}}}{(1 + \lambda_{1,\lambda}^{*2})^3} \stackrel{\text{stab. limit}}{=} \lambda_{1,\lambda\lambda\lambda}^* \\ &= -12(a_1^2 + a_1^*). \end{aligned} \quad (5.43)$$

The second equal sign in (5.43) holds at all points with $\lambda_{1,\lambda}^* = 0$ and, consequently, at the stability limit. If $a_1^* + a_1^2 = 0$ at the stability limit, the curvature of the eigenvalue curve has a local extremum.

Chapter 6

Classification of elastic structures regarding sensitivity analysis of their initial postbuckling behavior

Buckling may occur from a general stress state or a membrane stress state which may be viewed as a constraint imposed on a general stress state. This suggests the existence of constraints in the frame of sensitivity analysis of the initial postbuckling behavior. An example for such a constraint is (4.19) which, for the special case of bifurcation from a membrane stress state, implies zero-stiffness postbuckling. For bifurcation buckling from a general stress state, however, (4.19) does not impose a restriction on the coefficients λ_i , $i > 4$. Hence, it is important to know whether bifurcation buckling occurs from a general or a membrane stress state.

In the following, a necessary and sufficient condition for bifurcation buckling from a membrane stress state will be presented. It was derived by Mang and verified numerically by the author of this dissertation [15].

6.1 A necessary and sufficient condition for bifurcation buckling from a membrane stress state

The first derivative of (5.5) with respect to λ is obtained as (see (5.6))

$$\left[\lambda_{1,\lambda}^* \tilde{\mathbf{K}}_{T,\lambda} + (\lambda_1^* - \lambda) \tilde{\mathbf{K}}_{T,\lambda\lambda} \right] \cdot \mathbf{v}_1^* + \left[\tilde{\mathbf{K}}_T + (\lambda_1^* - \lambda) \tilde{\mathbf{K}}_{T,\lambda} \right] \cdot \mathbf{v}_{1,\lambda}^* = \mathbf{0}. \quad (6.1)$$

With the help of (5.5) and (5.25), (6.1) can be rewritten as

$$\left[\frac{\lambda_{1,\lambda}^*}{\lambda_1^* - \lambda} \tilde{\mathbf{K}}_{T,\lambda} + \tilde{\mathbf{K}}_{T,\lambda\lambda} \right] \cdot \mathbf{v}_1^* - \left[\tilde{\mathbf{K}}_T + (\lambda_1^* - \lambda) \tilde{\mathbf{K}}_{T,\lambda} \right] \cdot \sum_{j=2}^N \frac{\mathbf{v}_j^{*T} \cdot \tilde{\mathbf{K}}_{T,\lambda\lambda} \cdot \mathbf{v}_1}{(\lambda_1^* - \lambda_j^*)(\mathbf{v}_j^{*T} \cdot \tilde{\mathbf{K}}_{T,\lambda} \cdot \mathbf{v}_j^*)} \mathbf{v}_j^* = \mathbf{0}. \quad (6.2)$$

Specialization of (6.2) for the stability limit where (see (5.33))

$$\lambda_1^* - \lambda = 0, \quad \lambda_{1,\lambda}^* = 0, \quad \mathbf{v}_1^* = \mathbf{v}_1, \quad (6.3)$$

resulting in

$$\frac{\lambda_{1,\lambda}^*}{\lambda_1^* - \lambda} = \frac{0}{0} = \frac{\lambda_{1,\lambda\lambda}^*}{\lambda_{1,\lambda}^* - 1} = -\lambda_{1,\lambda\lambda}^*. \quad (6.4)$$

yields

$$\left[-\lambda_{1,\lambda\lambda}^* \tilde{\mathbf{K}}_{T,\lambda} + \tilde{\mathbf{K}}_{T,\lambda\lambda} \right] \cdot \mathbf{v}_1 - \tilde{\mathbf{K}}_T \cdot \left(\sum_{j=2}^N \frac{\mathbf{v}_j^{*T} \cdot \tilde{\mathbf{K}}_{T,\lambda\lambda} \cdot \mathbf{v}_1}{(\lambda_1^* - \lambda_j^*)(\mathbf{v}_j^{*T} \cdot \tilde{\mathbf{K}}_{T,\lambda} \cdot \mathbf{v}_j^*)} \mathbf{v}_j^* \right) = \mathbf{0}. \quad (6.5)$$

Interpreting

$$\mathbf{v}_{1,\lambda\lambda}^* = 3(a_1^2 + a_1^*)\mathbf{v}_1 + \sum_{j=2}^N \frac{\mathbf{v}_j^* \cdot \tilde{\mathbf{K}}_{T,\lambda\lambda} \cdot \mathbf{v}_1}{(\lambda_1^* - \lambda_j^*)(\mathbf{v}_j^* \cdot \tilde{\mathbf{K}}_{T,\lambda} \cdot \mathbf{v}_j^*)} \mathbf{v}_j^* \quad (6.6)$$

(see (5.38)) formally as the vector acceleration of a moving particle at the point on the vector curve $\mathbf{v}_1^*(\lambda)$ (see Figure 6.1) that represents the stability limit (point S with $\lambda = \lambda_S$),

$$\left(\mathbf{v}_{1,\lambda\lambda}^* \right)_\parallel = 3(a_1^2 + a_1^*)\mathbf{v}_1 \quad (6.7)$$

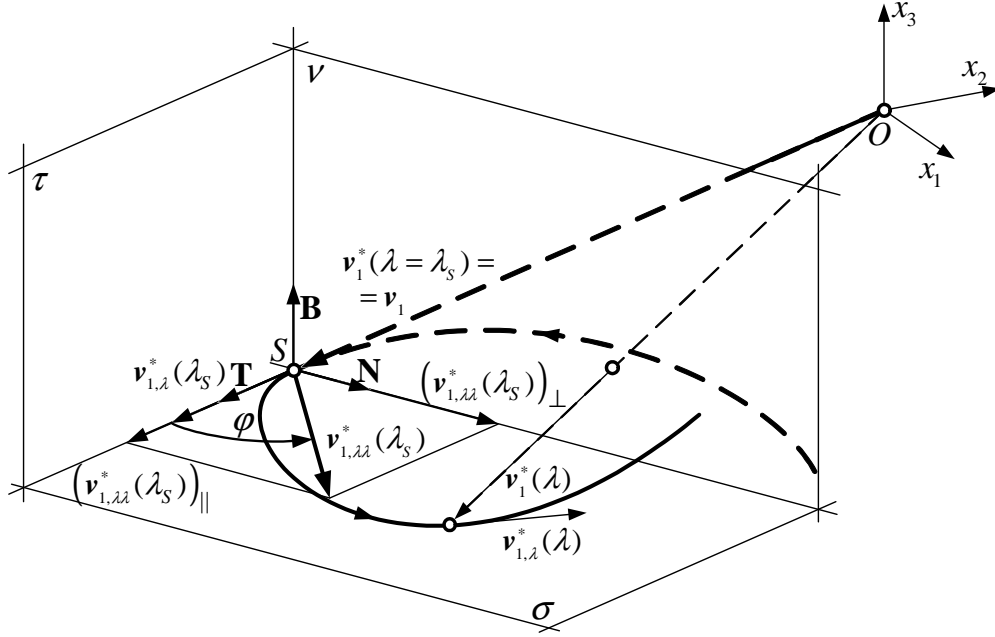


Figure 6.1: Bifurcation from a general stress state: sketch of $\mathbf{v}_1^*(\lambda)$ in the vicinity of the stability limit S for the special case of $\mathbf{u} \in \mathbb{R}^3$ (σ : osculating plane, v : normal plane, τ : rectifying plane; \mathbf{T} : tangent vector, \mathbf{N} : normal vector, \mathbf{B} : binormal vector; $|\mathbf{T}| = |\mathbf{N}| = |\mathbf{B}| = 1$).

is the tangential acceleration and

$$(\mathbf{v}_{1,\lambda\lambda}^*)_{\perp} = \sum_{j=2}^N \frac{\mathbf{v}_j^{*T} \cdot \widetilde{\mathbf{K}}_{T,\lambda\lambda} \cdot \mathbf{v}_1}{(\lambda_1^* - \lambda_j^*)(\mathbf{v}_j^{*T} \cdot \widetilde{\mathbf{K}}_{T,\lambda} \cdot \mathbf{v}_j^*)} \mathbf{v}_j^* \quad (6.8)$$

is the normal acceleration of the particle at this point. For bifurcation buckling from a membrane stress state, the aforementioned constraint is characterized by the disintegration of (6.5) into

$$\widetilde{\mathbf{K}}_{T,\lambda\lambda} \cdot \mathbf{v}_1 = \lambda_{1,\lambda\lambda}^* \widetilde{\mathbf{K}}_{T,\lambda} \cdot \mathbf{v}_1 \quad (6.9)$$

and

$$\widetilde{\mathbf{K}}_T \cdot \left(\sum_{j=2}^N \frac{\mathbf{v}_j^{*T} \cdot \widetilde{\mathbf{K}}_{T,\lambda\lambda} \cdot \mathbf{v}_1}{(\lambda_1^* - \lambda_j^*)(\mathbf{v}_j^{*T} \cdot \widetilde{\mathbf{K}}_{T,\lambda} \cdot \mathbf{v}_j^*)} \mathbf{v}_j^* \right) = \mathbf{0}. \quad (6.10)$$

Premultiplication of (6.9) by \mathbf{v}_j^{*T} , $j \neq 1$, and consideration of the orthogonality condition (5.14.1) gives

$$\mathbf{v}_j^T \cdot \widetilde{\mathbf{K}}_{T,\lambda\lambda} \cdot \mathbf{v}_1^* = 0 \quad \forall j \in \{2, 3, \dots, N\} \quad (6.11)$$

which shows that (6.10) is satisfied. Premultiplication of (6.9) by \mathbf{v}_1^T and consideration of (5.21) results in

$$\lambda_{1,\lambda}^* = -\mathbf{v}_1^T \cdot \widetilde{\mathbf{K}}_{T,\lambda\lambda} \cdot \mathbf{v}_1. \quad (6.12)$$

Equation (6.12) would also have been obtained by premultiplication of (6.1) by \mathbf{v}_1^{*T} and consideration of (2.10) and (5.21), i.e. without disintegration of (5.6) to (6.9) and (6.10). The character of (6.9) as a constraint condition becomes apparent if (6.12) is inserted into (6.9) which gives

$$\left[\widetilde{\mathbf{K}}_{T,\lambda\lambda} + (\mathbf{v}_1^T \cdot \widetilde{\mathbf{K}}_{T,\lambda\lambda} \cdot \mathbf{v}_1) \widetilde{\mathbf{K}}_{T,\lambda} \right] \cdot \mathbf{v}_1 = \mathbf{0}. \quad (6.13)$$

Substitution of (6.11) into (6.8) yields

$$\left(\mathbf{v}_{1,\lambda}^* \right)_\perp = \mathbf{0}, \quad (6.14)$$

resulting in

$$\mathbf{v}_{1,\lambda}^*(\lambda_S) = \left(\mathbf{v}_{1,\lambda}^*(\lambda_S) \right)_\parallel = 3(a_1^2 + a_1^*)\mathbf{v}_1 \quad (6.15)$$

(see Figure 6.2). At point S, the vector curve shown in Figure 6.2 does not only intersect the osculatory and the normal plane but also the rectifying plane. Figure 6.2 shows that the length and the direction of \mathbf{v}_1^{*T} depend on λ . For the special case that only the length of \mathbf{v}_1^* depends on λ , i.e.

$$c_{1j} = 0 \quad \forall \lambda \quad \stackrel{(5.20)}{\implies} \quad \mathbf{v}_j^T \cdot \widetilde{\mathbf{K}}_{T,\lambda\lambda} \cdot \mathbf{v}_1^* = 0 \quad \forall j \in \{2, 3, \dots, N\}, \quad (6.16)$$

$$\mathbf{v}_{1,\lambda}^* = c_{11}\mathbf{v}_1^*. \quad (6.17)$$

If neither the length nor the direction of \mathbf{v}_1^* depends on λ ,

$$\mathbf{v}_{1,\lambda}^* = \mathbf{0} \quad \forall \lambda \quad (6.18)$$

which requires

$$\widetilde{\mathbf{K}}_{T,\lambda\lambda} = \mathbf{0} \quad \implies \quad \widetilde{\mathbf{K}}_T = \mathbf{K}_0 + \lambda\mathbf{K}_1 \quad (6.19)$$

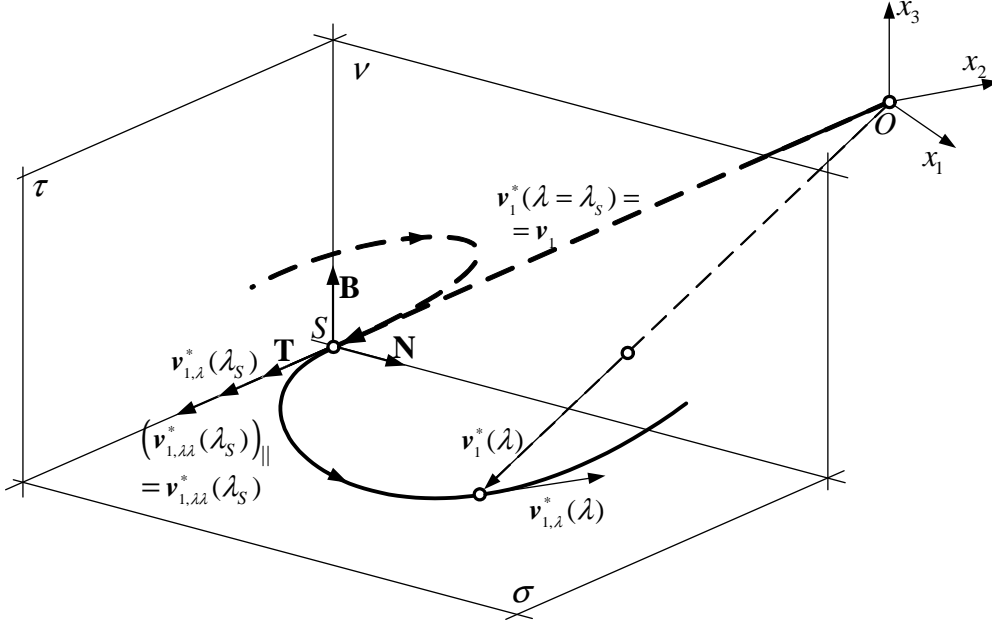


Figure 6.2: Bifurcation from a membrane stress state: sketch of $\mathbf{v}_1^*(\lambda)$ in the vicinity of the stability limit S for the special case of $\mathbf{u} \in \mathbb{R}^3$ (σ : osculating plane, ν : normal plane, τ : rectifying plane; \mathbf{T} : tangent vector, \mathbf{N} : normal vector, \mathbf{B} : binormal vector; $|\mathbf{T}| = |\mathbf{N}| = |\mathbf{B}| = 1$).

where \mathbf{K}_0 and \mathbf{K}_1 are constant matrices defining a linear stability problem (see (2.20)).

The first and the second derivative of (2.5) are obtained as

$$\widetilde{\mathbf{K}}_{T,\lambda} \cdot \mathbf{u}_{,\lambda} + \widetilde{\mathbf{K}}_T \cdot \mathbf{u}_{,\lambda\lambda} = \mathbf{0} \quad (6.20)$$

and

$$\widetilde{\mathbf{K}}_{T,\lambda\lambda} \cdot \mathbf{u}_{,\lambda} + 2\widetilde{\mathbf{K}}_{T,\lambda} \cdot \mathbf{u}_{,\lambda\lambda} + \widetilde{\mathbf{K}}_T \cdot \mathbf{u}_{,\lambda\lambda\lambda} = \mathbf{0}, \quad (6.21)$$

respectively. Premultiplication of (2.5), (6.20), and (6.21) by \mathbf{v}_1^T and consideration of (2.10) result in the following relations for the stability limit:

$$\mathbf{v}_1^T \cdot \bar{\mathbf{P}} = 0, \quad (6.22)$$

$$\mathbf{v}_1^T \cdot \widetilde{\mathbf{K}}_{T,\lambda} \cdot \mathbf{u}_{,\lambda} = 0, \quad (6.23)$$

$$\mathbf{v}_1^T \cdot \widetilde{\mathbf{K}}_{T,\lambda\lambda} \cdot \mathbf{u}_{,\lambda} + 2\mathbf{v}_1^T \cdot \widetilde{\mathbf{K}}_{T,\lambda} \cdot \mathbf{u}_{,\lambda\lambda} = 0. \quad (6.24)$$

Substitution of (6.9) into the expression for the first term in (6.24) and consideration of (6.23) gives

$$\mathbf{v}_1^T \cdot \widetilde{\mathbf{K}}_{T,\lambda\lambda} \cdot \mathbf{u}_{,\lambda} = \lambda_{1,\lambda\lambda}^* \mathbf{v}_1^T \cdot \widetilde{\mathbf{K}}_{T,\lambda} \cdot \mathbf{u}_{,\lambda} = 0. \quad (6.25)$$

Substitution of (6.25) into (6.24) yields

$$\mathbf{v}_1^T \cdot \widetilde{\mathbf{K}}_{T,\lambda} \cdot \mathbf{u}_{,\lambda\lambda} = 0. \quad (6.26)$$

Hence, disintegration of (6.1) entails disintegration of (6.24) as a characteristic feature of bifurcation buckling from a membrane stress state. For

$$\widetilde{\mathbf{K}}_{T,\lambda\lambda} = \mathbf{0} \quad \text{or} \quad \mathbf{u}_{,\lambda\lambda} = \mathbf{0}, \quad (6.27)$$

this disintegration is trivial.

Elimination of $\mathbf{v}_1^T \cdot \widetilde{\mathbf{K}}_{T,\lambda}$ in (6.26) with the help of (6.9) results in

$$\frac{1}{\lambda_{1,\lambda\lambda}^*} \mathbf{v}_1^T \cdot \widetilde{\mathbf{K}}_{T,\lambda\lambda} \cdot \mathbf{u}_{,\lambda\lambda} = 0. \quad (6.28)$$

If and only if

$$\lambda_{1,\lambda\lambda}^* = 0, \quad (6.29)$$

then, following from (6.9),

$$\widetilde{\mathbf{K}}_{T,\lambda\lambda} \cdot \mathbf{v}_1 = \mathbf{0}. \quad (6.30)$$

Hence,

$$\mathbf{v}_1^T \cdot \widetilde{\mathbf{K}}_{T,\lambda\lambda} \cdot \mathbf{u}_{,\lambda\lambda} = 0 \quad (6.31)$$

is a necessary condition for bifurcation buckling from a membrane stress state.

In order to prove that (6.31) is also a sufficient condition for buckling from a membrane stress state, $\mathbf{u}_{,\lambda\lambda}$ is expressed as a linear combination of the eigenvectors of (5.1),

$$\mathbf{u}_{,\lambda\lambda} = c_1 \mathbf{v}_1 + c_2 \mathbf{v}_2^* + \cdots + c_N \mathbf{v}_N^*, \quad (6.32)$$

with [37]

$$c_i = -\mathbf{v}_i^{*T} \cdot \widetilde{\mathbf{K}}_{T,\lambda} \cdot \mathbf{u}_{,\lambda\lambda}, \quad \mathbf{v}_i^{*T} \cdot \widetilde{\mathbf{K}}_{T,\lambda} \cdot \mathbf{v}_i^* = -1 \quad \forall i \in \{1, 2, \dots, N\}. \quad (6.33)$$

Substitution of (6.33) into (6.31) gives

$$\begin{aligned} \mathbf{v}_1^T \cdot \widetilde{\mathbf{K}}_{T,\lambda\lambda} \cdot \mathbf{u}_{,\lambda} &= c_1 \left(\mathbf{v}_1^T \cdot \widetilde{\mathbf{K}}_{T,\lambda\lambda} \cdot \mathbf{v}_1 \right) + c_2 \left(\mathbf{v}_1^T \cdot \widetilde{\mathbf{K}}_{T,\lambda\lambda} \cdot \mathbf{v}_2^* \right) + \dots \\ &\quad \dots + c_N \left(\mathbf{v}_1^T \cdot \widetilde{\mathbf{K}}_{T,\lambda\lambda} \cdot \mathbf{v}_N^* \right) = 0. \end{aligned} \quad (6.34)$$

Substitution of

$$c_1 = -\mathbf{v}_1^T \cdot \widetilde{\mathbf{K}}_{T,\lambda} \cdot \mathbf{u}_{,\lambda}, \quad (6.35)$$

which follows from (6.33.1), into (6.24), yields

$$\mathbf{v}_1^T \cdot \widetilde{\mathbf{K}}_{T,\lambda\lambda} \cdot \mathbf{u}_{,\lambda} - 2c_1 = 0. \quad (6.36)$$

Expressing also $\mathbf{u}_{,\lambda}$ as a linear combination of the eigenvectors of (5.1) results in

$$\mathbf{u}_{,\lambda} = b_1 \mathbf{v}_1 + b_2 \mathbf{v}_2^* + \dots + b_N \mathbf{v}_N^* \quad (6.37)$$

with [37]

$$b_i = -\mathbf{v}_i^{*T} \cdot \widetilde{\mathbf{K}}_{T,\lambda} \cdot \mathbf{u}_{,\lambda}, \quad \mathbf{v}_i^{*T} \cdot \widetilde{\mathbf{K}}_{T,\lambda} \cdot \mathbf{v}_i^* = -1 \quad \forall i \in \{1, 2, \dots, N\}. \quad (6.38)$$

Satisfaction of (6.23) requires

$$b_1 = 0. \quad (6.39)$$

Substitution of (6.37) into (6.36) and consideration of (6.39) gives

$$b_2 \left(\mathbf{v}_1^T \cdot \widetilde{\mathbf{K}}_{T,\lambda\lambda} \cdot \mathbf{v}_2^* \right) + \dots + b_N \left(\mathbf{v}_1^T \cdot \widetilde{\mathbf{K}}_{T,\lambda\lambda} \cdot \mathbf{v}_N^* \right) - 2c_1 = 0. \quad (6.40)$$

Expressing c_1 in (6.40) with the help of (6.34) in terms of c_2, \dots, c_N , yields

$$\begin{aligned} &\left[b_2 \left(\mathbf{v}_1^T \cdot \widetilde{\mathbf{K}}_{T,\lambda\lambda} \cdot \mathbf{v}_1 \right) + 2c_2 \right] \left(\mathbf{v}_1^T \cdot \widetilde{\mathbf{K}}_{T,\lambda\lambda} \cdot \mathbf{v}_2^* \right) + \dots + \\ &\quad + \left[b_N \left(\mathbf{v}_1^T \cdot \widetilde{\mathbf{K}}_{T,\lambda\lambda} \cdot \mathbf{v}_1 \right) + 2c_N \right] \left(\mathbf{v}_1^T \cdot \widetilde{\mathbf{K}}_{T,\lambda\lambda} \cdot \mathbf{v}_N^* \right) = 0. \end{aligned} \quad (6.41)$$

Equation (6.41) is satisfied if and only if the orthogonality condition

$$\mathbf{v}_1^T \cdot \widetilde{\mathbf{K}}_{T,\lambda\lambda} \cdot \mathbf{v}_j^* = 0 \quad \forall j \in \{2, 3, \dots, N\} \quad (6.42)$$

holds. This orthogonality condition (see (6.11)) follows from (6.13) which was used for derivation of the condition for bifurcation buckling from a membrane stress state (see (6.31)). Hence, (6.31) is a necessary and sufficient condition for bifurcation buckling from a membrane stress state.

This condition applies to the following four cases:

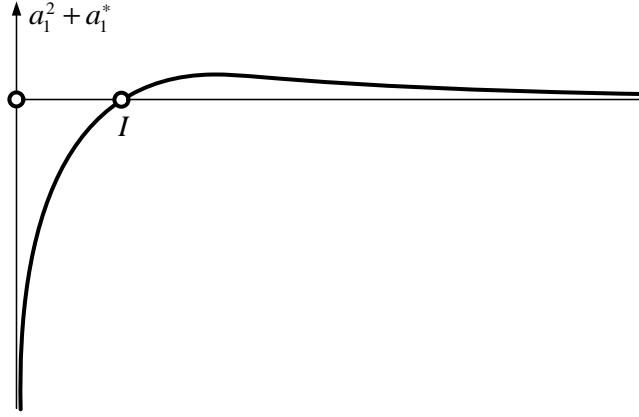
- (a) $\widetilde{\mathbf{K}}_{T,\lambda\lambda} \neq \mathbf{0}$, $\mathbf{u}_{,\lambda\lambda} \neq \mathbf{0}$, nonlinear stability problem, nonlinear prebuckling paths,
- (b) $\widetilde{\mathbf{K}}_{T,\lambda\lambda} \neq \mathbf{0}$, $\mathbf{u}_{,\lambda\lambda} = \mathbf{0}$, nonlinear stability problem, linear prebuckling paths,
- (c) $\widetilde{\mathbf{K}}_{T,\lambda\lambda} = \mathbf{0}$, $\mathbf{u}_{,\lambda\lambda} \neq \mathbf{0}$, linear stability problem, nonlinear prebuckling paths,
- (d) $\widetilde{\mathbf{K}}_{T,\lambda\lambda} = \mathbf{0}$, $\mathbf{u}_{,\lambda\lambda} = \mathbf{0}$, linear stability problem, linear prebuckling paths.

Case (a) shows that the existence of a membrane stress state does not rule out the possibility of a nonlinear stability problem with bifurcation buckling from nonlinear prebuckling paths. A classical example for this case is the *von Mises* truss [5] for which (6.31) will be verified in Section 8.2. The cases (b) and (c) demonstrate that linear stability problems and linear prebuckling paths are not mutually conditional [33].

6.2 Bifurcation buckling from a membrane stress state as a special case in the frame of sensitivity analysis of bifurcation buckling from a general stress state

If, in the frame of sensitivity analysis of bifurcation buckling, a general stress state for a specific value of the design parameter becomes a membrane stress state, bifurcation buckling from such a stress state will occur as a special case of bifurcation buckling from a general stress state. To deal with such a situation requires investigation of specific features of sensitivity analysis of bifurcation buckling both from a general and a membrane stress state.

The starting point for the following considerations is the expression for the cosine of the angle φ enclosed by the directions of $\boldsymbol{\nu}_{1,\lambda\lambda}^*$ and $\boldsymbol{\nu}_1$ which is collinear


 Figure 6.3: $a_1^2 + a_1^*$ as a function of the design parameter κ .

with $(\mathbf{v}_{1,\lambda\lambda}^*)_{\parallel}$ (see Figure 6.1). With the help of (6.6), $\cos \varphi$ is obtained as

$$\cos \varphi = \frac{\mathbf{v}_1^T \cdot \mathbf{v}_{1,\lambda\lambda}^*}{|\mathbf{v}_1| |\mathbf{v}_{1,\lambda\lambda}^*|} = \frac{3(a_1^2 + a_1^*)}{\sqrt{9(a_1^2 + a_1^*)^2 + \sum_{j=2}^N \left(\frac{\mathbf{v}_j^{*T} \cdot \tilde{\mathbf{K}}_{T,\lambda\lambda} \cdot \mathbf{v}_1}{(\lambda_1^* - \lambda_j^*)(\mathbf{v}_j^{*T} \cdot \tilde{\mathbf{K}}_{T,\lambda} \cdot \mathbf{v}_j^*)} \right)^2} \frac{\mathbf{v}_j^{*T} \cdot \mathbf{v}_j^*}{\mathbf{v}_1^T \cdot \mathbf{v}_1}}. \quad (6.43)$$

It is emphasized that the vector curve $\mathbf{v}_1^*(\lambda)$ in Figure 6.1 refers to a specific value of κ . For each value of κ such a vector curve exists. Figure 6.3 shows a typical qualitative shape of the function $a_1^2 + a_1^*$ in the numerator of 6.43 in the frame of sensitivity analysis of bifurcation buckling. $a_1(\kappa = \kappa_0) = a_1^*(\kappa = \kappa_0) = -\infty$ refers to hilltop buckling which is characterized by the coincidence of the bifurcation point with a snap-through point [20]. κ_0 is the value of the design parameter at hilltop buckling which is chosen as the starting point of sensitivity analysis. The second term under the square root in the denominator of (6.43) represents the influence of non-membrane (non-axial) deformations on bifurcation buckling. For hilltop buckling, both terms in the denominator of (6.43) become infinite.

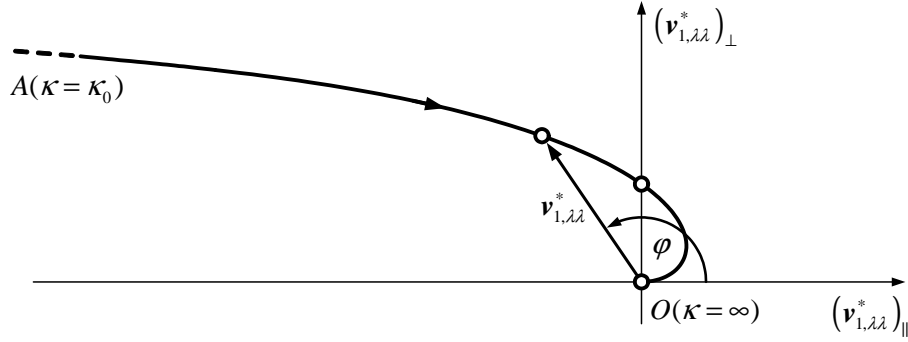


Figure 6.4: Sensitivity analysis of bifurcation buckling from a general stress state. ($A(\kappa = \kappa_0)$: starting point, $O(\kappa = \infty)$: end point ($a_1^2 = a_1^* = 0$ trivially)).

Hence,

$$\frac{\sum_{j=2}^N \left(\frac{\mathbf{v}_j^{*T} \cdot \tilde{\mathbf{K}}_{T,\lambda\lambda} \cdot \mathbf{v}_1}{(\lambda_1^* - \lambda_j^*)(\mathbf{v}_j^{*T} \cdot \tilde{\mathbf{K}}_{T,\lambda} \cdot \mathbf{v}_j^*)} \right)^2 \frac{\mathbf{v}_j^{*T} \cdot \mathbf{v}_j^*}{\mathbf{v}_1^T \cdot \mathbf{v}_1}}{9(a_1^2 + a_1^*)^2} = \tan^2 \varphi = \frac{\infty}{\infty}. \quad (6.44)$$

It can be shown that this indefinite expression is equal to zero. Thus,

$$\tan^2 \varphi = 0 \implies \cos \varphi = -1, \quad (6.45)$$

with the negative sign in (6.45.2) following from

$$a_1^2 + a_1^* = -\infty \quad (6.46)$$

(see Figure 6.3). For $a_1^2 + a_1^* = 0$, $\kappa = \infty$ (see point I in Figure 6.3), the second term under the square root in the denominator of (6.43) is not equal to zero. Hence, substitution of $a_1^2 + a_1^* = 0$ into (6.43) gives

$$\cos \varphi = 0 \implies \mathbf{v}_{1,\lambda\lambda}^* = (\mathbf{v}_{1,\lambda\lambda}^*)_{\perp}. \quad (6.47)$$

For the physically meaningless borderline case of $\kappa = \infty$,

$$a_1^2 + a_1^* = 0 \quad (6.48)$$

(see Figure 6.3). Moreover, the second term under the square root in the denominator of (6.43) also becomes zero. Hence,

$$\frac{\sum_{j=2}^N \left(\frac{\mathbf{v}_j^{*T} \cdot \tilde{\mathbf{K}}_{T,\lambda\lambda} \cdot \mathbf{v}_1}{(\lambda_1^* - \lambda_j^*)(\mathbf{v}_j^{*T} \cdot \tilde{\mathbf{K}}_{T,\lambda} \cdot \mathbf{v}_j^*)} \right)^2 \frac{\mathbf{v}_j^{*T} \cdot \mathbf{v}_j^*}{\mathbf{v}_1^T \cdot \mathbf{v}_1}}{9(a_1^2 + a_1^*)^2} = \tan^2 \varphi = \frac{0}{0}. \quad (6.49)$$

As κ tends to infinity, the numerator of (6.49) can be shown to tend to zero more strongly than the denominator. Hence,

$$\tan^2 \varphi = 0 \implies \cos \varphi = 1, \quad (6.50)$$

with the positive sign of (6.50.2) following from $a_1^2 + a_1^* \rightarrow 0+$. Figure 6.4 illustrates the vector function $\mathbf{v}_{1,\lambda\lambda}^*(\lambda_s(\kappa), \kappa)$ in the frame of sensitivity analysis of bifurcation buckling from a general stress state.

For sensitivity analysis for the special case of bifurcation buckling from a membrane stress state, because of (6.14) the vector curve $\mathbf{v}_{1,\lambda\lambda}^*(\lambda_s(\kappa), \kappa)$ degenerates to a straight line coinciding with the abscissa of the system of reference in Figure 6.4.

An interesting difference between the general and the special case exists for

$$\left(\mathbf{v}_{1,\lambda\lambda}^* \right)_{\parallel} = \mathbf{0} \xrightarrow{(6.7)} a_1^2 + a_1^* = 0. \quad (6.51)$$

For the general case,

$$a_1 > 0, \quad a_1^* < 0, \quad (6.52)$$

whereas for the special case

$$a_1 \leq 0, \quad a_1^* \leq 0. \quad (6.53)$$

The only point on the vector curve $\mathbf{v}_{1,\lambda\lambda}^*(\lambda_s(\kappa), \kappa)$ in Figure 6.4 for which $\left(\mathbf{v}_{1,\lambda\lambda}^* \right)_{\perp} = \mathbf{0}$ is the origin of the system of reference, representing the physically meaningless end point of this curve in the frame of sensitivity analysis of bifurcation buckling from a general stress state. Hence, bifurcation buckling from a membrane stress state is not contained as a special case of bifurcation buckling from a general stress state.

It is contained, however, in the form of point O in Figure 6.5 which illustrates

the vector function $\mathbf{v}_{1,\lambda\lambda}^*(\lambda_s(\Delta\kappa), \Delta\kappa)$ in the frame of sensitivity analysis of bifurcation buckling from a general stress state. $\Delta\kappa$ represents e.g. the deviation from the geometric shape of a structure for which, for a particular load case, only axial forces occur, as is the case for a thrust-line arch. Hence, for point O in Figure 6.5, $\Delta\kappa = 0$. For this point,

$$\left(\mathbf{v}_{1,\lambda\lambda}^*\right)_{\parallel} = \mathbf{0}, \quad \left(\mathbf{v}_{1,\lambda\lambda}^*\right)_{\perp} = \mathbf{0}, \quad (6.54)$$

which requires (see (6.7) and (6.8))

$$a_1^2 + a_1^* = 0, \quad \mathbf{v}_j^{*T} \cdot \tilde{\mathbf{K}}_{T,\lambda\lambda} \cdot \mathbf{v}_1 = 0 \quad \forall j \in \{2, 3, \dots, N\}. \quad (6.55)$$

The Equations (6.55) are satisfied if and only if

$$\tilde{\mathbf{K}}_{T,\lambda\lambda} \cdot \mathbf{v}_1 = \mathbf{0} \xRightarrow{(A.1)} a_1 = 0 \xRightarrow{(5.37)} \mathbf{v}_{1,\lambda}^* = \mathbf{0}, \quad (6.56)$$

$$\tilde{\mathbf{K}}_{T,\lambda\lambda} \cdot \mathbf{v}_1 = \mathbf{0} \xRightarrow{(A.2)} a_1^* = 0, \quad (6.57)$$

resulting in

$$\mathbf{v}_{1,\lambda\lambda\lambda}^* \sim \mathbf{v}_1. \quad (6.58)$$

Usually, $\mathbf{v}_{1,\lambda}^* = \mathbf{0}$ indicates a singular point on the vector curve $\mathbf{v}_1^*(\lambda)$ [37]. In the given case, however, because of $\mathbf{v}_{1,\lambda}^*(\lambda = \lambda_s) = \mathbf{0}$ and $\mathbf{v}_{1,\lambda\lambda}^*(\lambda = \lambda_s) = \mathbf{0}$, point S on a sketch of $\mathbf{v}_1^*(\lambda)$, similar to the one shown in Figure 6.1 and, hence, not shown

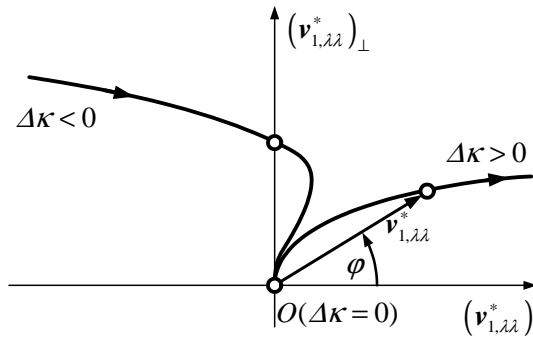


Figure 6.5: Sensitivity analysis of bifurcation buckling from a general stress state containing bifurcation buckling from a membrane stress state as a special case.

herein, is a regular point, representing a planar point on the path. Since (6.56.1) satisfies (6.13), point O in Figure 6.5 refers to the special case of buckling from a membrane stress state. At this point, the vector curve $\boldsymbol{\nu}_{1,\lambda\lambda}^*(\lambda_s(\Delta\kappa), \Delta\kappa)$ has a singular point in form of a cusp of second kind with a vertical tangent. This is the consequence of a minimum of both $a_1(\kappa)$ and $a_1^*(\kappa)$ at point O .

Chapter 7

Implementation of the theoretical concepts in a computer program

7.1 Layout of the computer program

In order to verify the theoretical findings, a computer program for sensitivity analysis of the initial postbuckling behavior was developed. It is based on Koiter's initial postbuckling analysis and can solve the consistently linearized eigenvalue problem.

Such a program must allow

- the input of model data of the structure,
- nonlinear finite element analysis,
- calculation of the primary path,
- branch switching to the secondary path,
- calculation of derivatives of the tangent stiffness matrix along the primary path,
- calculation of directional derivatives of the tangent stiffness matrix for arbitrary directions, and
- post processing of data to obtain series expansions for the secondary path.

For programming, basically three software tools were used. The first one is the finite element software FEAP which offers a wide range of available element types, in particular, advanced shell elements. The second one is MATLAB, a high-level programming language as well as a programming environment. The third software tool is the interface MATFEAP which allows the exchange of data between FEAP and MATLAB.

A detailed description of a basic version of FEAP can be found in [38] and further information is available in [35]. FEAP was chosen because of a wide range of available element types, in particular, advanced shell elements, and the availability of the source code, allowing small modifications which are necessary for the data exchange via the interface to MATLAB.

MATFEAP, available online from David Bindel's website [1], allows to start a finite element calculation in FEAP from MATLAB, to issue FEAP macro commands from within MATLAB, and to read or set variables in FEAP, e.g. displacements, the residual and the tangent stiffness matrix.

In MATLAB, mathematical programming is significantly simplified as compared to low level programming languages. Its strength is the simple and efficient handling of vector and matrix arrays as well as a wide variety of available mathematical features including solvers for systems of linear equations and for linear eigenvalue problems which were used in this work.

The input of the model data is based on the input format of FEAP which uses input files. When FEAP is started through MATLAB, the model data are processed and then FEAP is set to the so-called interactive mode, awaiting macro commands. The interface MATFEAP allows to start FEAP with input files containing parameters which can be set in MATLAB.

The elements used in the numerical studies are a four-node shell element with five degrees of freedom at each node (three displacement degrees of freedom and two degrees of freedom defining the rotation of a director vector) and a beam element with two nodes with six degrees of freedom each (displacements of the nodes and rotations of the cross section, referred to global coordinates). FEAP allows to add additional stiffness to certain degrees of freedom at given nodes. This is used to model linear springs attached to the structure.

The arc-length algorithm, required for calculation of the nonlinear load-displace-

ment path, was programmed completely in MATLAB. A detailed description of the algorithm is given in Subsection 7.3.2.

Pinpointing, representing the iterative process to locate the stability limit, was steered by the MATLAB program, using the arc-length method. As a measure for the stability of the equilibrium, an estimate for the lowest eigenvalue of $\widetilde{\mathbf{K}}_T$ was chosen. It is provided by the MATLAB function `eigs` which uses subspace iteration. The determinant, often used for determination of loss of stability in theoretical considerations, cannot be used for numerical work because its computation is costly in case of large matrices. The determinant of such matrices may be too large for the employed floating point arithmetic unless one is close enough to the stability limit. The step-length for the arc-length method was chosen by applying the secant method to the lowest eigenvalue as a function of the arc-length on the primary path. Let $\mu(n)$ denote the lowest eigenvalue of $\widetilde{\mathbf{K}}_T$ in the n -th step and $\bar{L}(n)$ be the arc-length in this step, then

$$\bar{L}(n+1) = \bar{L}(n) \left(\frac{1}{\frac{\mu(n-1)}{\mu(n)} - 1} \right) \quad (7.1)$$

gives a value for the arc-length in the following step. To start the iteration, two values of μ must be known. Hence, one initial step has to be made with an arbitrary arc-length. In order to keep the algorithm stable, a maximum arc-length was set by assigning

$$\bar{L}(n+1) \leftarrow \max(\bar{L}(n+1), \bar{L}_{\max}). \quad (7.2)$$

Since only a few structures were analyzed and determination of the complete secondary path was only necessary for verification purposes, there was no need for implementation of an advanced strategy for branch switching. With the stability limit $(\mathbf{u}_S, \lambda_S)$ and the estimate $(\mathbf{u}_S + \varepsilon \mathbf{v}_1, \lambda_S)$, the two necessary starting points for the same arc-length algorithm as was used for the primary path are available. The magnitude of ε , which was tuned manually, is crucial. If ε is chosen too small, calculation of $\mathbf{u}_{,l}$ fails because of the bad condition of $\widetilde{\mathbf{K}}_T$, and if it is too large, the residual at $(\mathbf{u}_S + \varepsilon \mathbf{v}_1, \lambda_S)$ is large, but the algorithm needs a nearly converged starting point.

For the academic examples analyzed in this work, restricted to less than a few thousand degrees of freedom, it is possible to store displacement data for the whole equilibrium path as well as a sample of the stiffness matrix around the stability limit for post-processing.

7.2 Post-processing

For verification purposes, the coefficients a_1 and a_1^* were computed in two ways, either directly using the function $f(\lambda)$ defined in Section 3.3 or by calculating $\lambda_1^*(\lambda)$ at five points around the stability limit and using the relations (5.40) and (5.41) from the consistently linearized eigenproblem. For direct calculation using $f(\lambda)$ and the finite difference algorithm presented in Subsection 7.3.1, five evaluations of $\tilde{\mathbf{K}}_T$ in the vicinity of the stability limit are necessary. Calculation via the consistently linearized eigenproblem requires five values of $\lambda_1^*(\lambda)$ in the vicinity of the stability limit. The eigenproblem is solved with the help of a MATLAB function which uses subspace iteration. For the solution of the eigenproblem, a central differential quotient is used to calculate $\tilde{\mathbf{K}}_{T,\lambda}$, which makes two additional evaluations of $\tilde{\mathbf{K}}_T$ in the vicinity of the stability limit necessary. The directional derivative of first order with respect to \mathbf{v}_1 is defined as

$$\left. \frac{d\mathbf{K}_T(\mathbf{u})}{d\mathbf{v}_1} \right|_{\mathbf{u}=\mathbf{u}_C} := \left. \frac{d\mathbf{K}_T(\mathbf{u}_C + \varepsilon \mathbf{v}_1)}{d\varepsilon} \right|_{\varepsilon=0} = \mathbf{K}_{T,\mathbf{u}} \cdot \mathbf{v}_1. \quad (7.3)$$

Since \mathbf{v}_1 was already calculated during the pinpointing process, \mathbf{K}_T can be sampled at five points around the stability limit in the direction of \mathbf{v}_1 . These points are then used in the finite difference algorithm. Higher-order directional derivatives of \mathbf{K}_T in the direction of \mathbf{v}_1 are used to compute $\mathbf{v}_1 \cdot \mathbf{K}_{T,\mathbf{uu}} \cdot \mathbf{v}_1$, $\mathbf{v}_1 \cdot \mathbf{K}_{T,\mathbf{uuu}} : \mathbf{v}_1 \otimes \mathbf{v}_1$, and $\mathbf{v}_1 \cdot \mathbf{K}_{T,\mathbf{uuuu}} : \mathbf{v}_1 \otimes \mathbf{v}_1 \otimes \mathbf{v}_1$. Only symmetric structures were analyzed numerically. Thus, $\lambda_1 = \lambda_3 = \lambda_5 = \dots = 0$. Considering the comparably low computational cost, λ_1 was calculated for verification purposes.

In order to calculate \mathbf{v}_4 and λ_4 , another directional derivative is necessary, even if λ_1 and λ_3 are set equal to zero. The term $\mathbf{v}_2^T \cdot \mathbf{K}_{T,\mathbf{u}} \cdot \mathbf{v}_2$ appears in the equation

for ν_4 . Consequently, it is necessary for the calculation of d_3 (see (A.8)) and, thus, for λ_4 (see (3.16)). Hence, \mathbf{K}_T has to be sampled at five points around the stability limit in the direction of ν_2 .

7.3 Technical details of the implementation

7.3.1 Finite differences

Koiter's postbuckling analysis requires evaluation of higher-order differential quotients. Herein, they were approximated by means of finite differences based on function values at five interpolation nodes. The approximations have the form

$$f^{(n)}(x_3) \approx \sum_{k=1}^5 c_{kn} f(x_k). \quad (7.4)$$

The task is to find c_{kn} for a given set of x_k which may be non-equidistant. This can be done by using Taylor series expansions of $f(x)$ around x_3 :

$$f(x_1) = \sum_{k=0}^4 \frac{1}{k!} f^{(k)}(x_3)(x_3 - x_1)^k + O((x_3 - x_1)^5), \quad (7.5)$$

$$f(x_2) = \sum_{k=0}^4 \frac{1}{k!} f^{(k)}(x_3)(x_3 - x_2)^k + O((x_3 - x_2)^5), \quad (7.6)$$

$$f(x_3) = f(x_3), \quad (7.7)$$

$$f(x_4) = \sum_{k=0}^4 \frac{1}{k!} f^{(k)}(x_3)(x_3 - x_4)^k + O((x_3 - x_4)^5), \quad (7.8)$$

$$f(x_5) = \sum_{k=0}^4 \frac{1}{k!} f^{(k)}(x_3)(x_3 - x_5)^k + O((x_3 - x_5)^5). \quad (7.9)$$

Insertion of these expansions into (7.4), ordering by powers of x_k , and comparison of coefficients allows efficient calculation of the coefficients c_{kn} in form of a

linear system of equations:

$$\begin{pmatrix} 1 & 1 & 1 & 1 & 1 \\ (x_3 - x_1) & (x_3 - x_2) & 0 & (x_3 - x_4) & (x_3 - x_1) \\ (x_3 - x_1)^2 & (x_3 - x_2)^2 & 0 & (x_3 - x_4)^2 & (x_3 - x_1)^2 \\ (x_3 - x_1)^3 & (x_3 - x_2)^3 & 0 & (x_3 - x_4)^3 & (x_3 - x_1)^3 \\ (x_3 - x_1)^4 & (x_3 - x_2)^4 & 0 & (x_3 - x_4)^4 & (x_3 - x_1)^4 \end{pmatrix} \cdot \begin{pmatrix} c_{11} & c_{12} & c_{13} & c_{14} \\ c_{21} & c_{22} & c_{23} & c_{24} \\ c_{31} & c_{32} & c_{33} & c_{34} \\ c_{41} & c_{42} & c_{43} & c_{44} \\ c_{51} & c_{52} & c_{53} & c_{54} \end{pmatrix} = \begin{pmatrix} 0 & 0 & 0 & 0 \\ 1 & 0 & 0 & 0 \\ 0 & 2 & 0 & 0 \\ 0 & 0 & 6 & 0 \\ 0 & 0 & 0 & 24 \end{pmatrix}. \quad (7.10)$$

The error of the approximation is given by

$$e_n = \sum_{k=1}^5 c_{kn} \mathcal{O}((x_3 - x_k)^5). \quad (7.11)$$

As a consequence of (7.10), the coefficients c_{nk} are of the form

$$c_{kn} = \frac{1}{\mathcal{O}((x_3 - x_k)^n)}. \quad (7.12)$$

This results in the following order of the error:

$$e_n = \sum_{k=1}^5 \mathcal{O}((x_3 - x_k)^{5-n}). \quad (7.13)$$

This means that the highest order of differentiation that can be approximated by this method is four. This is just enough to calculate λ_4 in Koiter's postbuckling analysis. In the MATLAB program, (7.10) was solved column-wise, depending on the required order of differentiation.

7.3.2 Arc-length algorithm

In the analysis of geometrically nonlinear structures, computation of equilibrium paths past the stability limit, especially for the case of hilltop buckling, requires

strategies that are more advanced than the Newton-Raphson method. An arc-length algorithm, introduced by Crisfield [7], was used. His work was based on a solution procedure proposed by Riks [26]. An overview over arc-length and other control methods can be found in [27].

The basic idea of an arc-length algorithm is to restrict the arc-length of each increment in the load-displacement space. In the algorithm applied in this work, the equilibrium iteration within each increment consists of several steps. The first one is called the predictor step whereas the others are referred to as corrector steps.

For this Subsection, vectors in the load-displacement space will be denoted by \mathbf{t} :

$$\mathbf{t} := \begin{pmatrix} \mathbf{u} \\ \lambda \end{pmatrix}. \quad (7.14)$$

In many applications, the numerical values in the load-direction are much larger than those in the displacement-directions. In order to reduce this large disparity which may lead to numerical problems, scalar products are computed as

$$\mathbf{t}^T \cdot \mathbf{t} = \mathbf{u}^T \cdot \mathbf{u} + \psi^2 \lambda^2 \quad (7.15)$$

with $\psi \in (0, 1)$. In the following, the position vectors of points in the load-displacement space will be indicated by a single subscript, e.g. $\mathbf{t}_A = (\mathbf{u}_A, \lambda_A)^T$; vectors connecting such points have two subscripts identifying these points, e.g. \mathbf{t}_{AB} .

The equilibrium iteration withing each increment starts at an equilibrium point Z . In the first increment, this represents the unloaded position. The target is to find an equilibrium solution, the distance of which from Z , measured in the norm induced by the scalar product defined in (7.15), is equal to the arbitrarily chosen value \bar{L} . The tangential direction at Z is given as

$$\mathbf{t}^P = \begin{pmatrix} \tilde{\mathbf{u}}_{,\lambda}(\lambda_Z) \\ 1 \end{pmatrix}. \quad (7.16)$$

The first iteration step is characterized by the length \bar{L} in the direction of \mathbf{t}^P . For this purpose, a multiplier for \mathbf{t}^P is calculated, subject to

$$\Delta\lambda_P = \frac{\bar{L}}{\sqrt{\mathbf{u}_\lambda^T \cdot \mathbf{u}_\lambda + \psi^2}}. \quad (7.17)$$

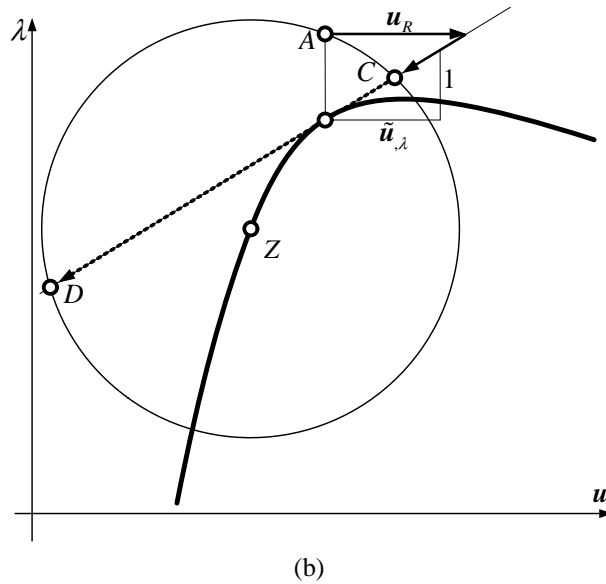
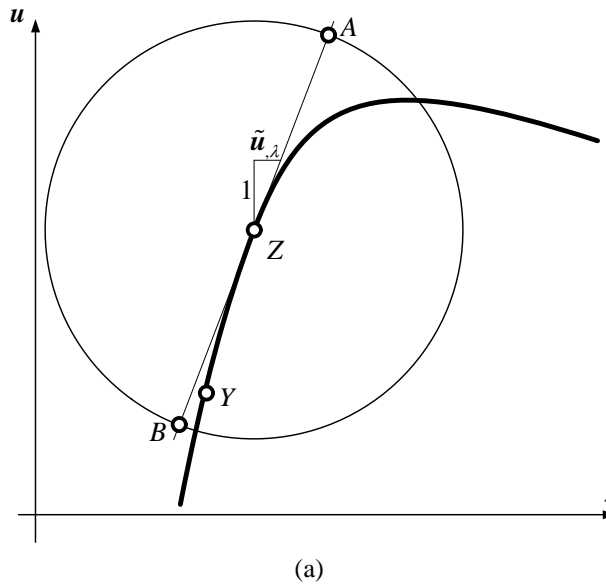


Figure 7.1: (a) possible solutions A and B of the predictor step, starting from the last converged solution Z ; (b) possible solutions C and D of the corrector step, starting from the solution A of the preceding step.

The two intersections of the tangent to the equilibrium path with the circle around Z , denoted as A and B (see Figure 7.1(a)), are obtained as

$$\mathbf{t}_{A,B} = \mathbf{t}^Z \pm \Delta\lambda_P \mathbf{t}^P. \quad (7.18)$$

The sign in (7.18) is chosen according to the following rule: The correct direction is the one which encloses an acute angle with the last increment \mathbf{t}_{YZ} where Y is the last converged solution before Z . For the first increment, only one equilibrium solution is known. In this case the plus sign is chosen.

Without loss of generality, let A be the result from the predictor step. After this step, several corrector steps follow. They are repeated until an equilibrium solution is reached within a specified tolerance, measured in terms of the norm of the residual. Each corrector step consists of two parts, the first of which is defined as

$$\mathbf{t}^R = \begin{pmatrix} \mathbf{u}_R \\ 0 \end{pmatrix} \quad (7.19)$$

where \mathbf{u}_R solves

$$\mathbf{K}_T(\mathbf{u}_A) \cdot \mathbf{u}_R = \mathbf{G}(\mathbf{u}_A, \lambda_A). \quad (7.20)$$

A correction that is restricted to the direction of \mathbf{t}^R corresponds with the Newton-Raphson-method. The second part of the corrector step is given as $\Delta\lambda_{cor} \mathbf{t}^Q$, with

$$\mathbf{t}^Q = \begin{pmatrix} \mathbf{u}_Q \\ 1 \end{pmatrix}, \quad (7.21)$$

where \mathbf{u}_Q is calculated from

$$\mathbf{K}_T(\mathbf{u}_A) \cdot \mathbf{u}_Q = \bar{\mathbf{P}}. \quad (7.22)$$

$\Delta\lambda_{cor}$ must be calculated such that the arc length of the step is \bar{L} . The two solutions are the points C and D in Figure 7.1(b). The quadratic equation for $\Delta\lambda_{cor}$, given as

$$(\mathbf{t}_{ZA} + \mathbf{t}_R + \Delta\lambda_{cor} \mathbf{t}^Q)^T \cdot (\mathbf{t}_{ZA} + \mathbf{t}_R + \Delta\lambda_{cor} \mathbf{t}^Q) = \bar{L}, \quad (7.23)$$

has the two solutions $(\Delta\lambda_{cor})_{1,2}$. This gives

$$\mathbf{t}_{C,D} = \mathbf{t}_A + \mathbf{t}_R + (\Delta\lambda_{cor})_{1,2} \mathbf{t}^Q. \quad (7.24)$$

The point which is closer to A is chosen as the result from the corrector step. Therefore,

$$\mathbf{t}_{ZA}^T \cdot (\mathbf{t}_{ZA} + \mathbf{t}_R + \Delta\lambda_{cor}\mathbf{t}^Q) \quad (7.25)$$

should be maximized. It is sufficient to check only the term in (7.25) which depends on $\Delta\lambda_{cor}$. Hence,

$$\mathbf{t}_{ZA}^T \cdot ((\Delta\lambda_{cor})_1\mathbf{t}^Q) > \mathbf{t}_{ZA}^T \cdot ((\Delta\lambda_{cor})_2\mathbf{t}^Q), \quad (7.26)$$

is checked. If it is satisfied, $(\Delta\lambda_{cor})_1$ is chosen as the result of the corrector step.

If this is not the case, $(\Delta\lambda_{cor})_2$ represents the result of the corrector step.

For iterative pinpointing, it may be necessary to change the direction on the equilibrium path, i.e. to go backwards once the stability limit was passed. In this case, it is sufficient to invert the condition for the choice of the correct point in the predictor step whereas the corrector steps remain unchanged.

Chapter 8

Numerical investigation

8.1 Two-bar system

Figure 8.1 shows a planar, static, conservative system with two degrees of freedom. Unlike the following examples, this structure was not analyzed by the FEM but investigated analytically, using the computer algebra system Maple. The description of this system closely follows [32]. Both rigid bars, 1 and 2, have the same length L , and in the non-buckled state they are in-line. The bars are linked at one end and supported by turning-and-sliding joints at their other ends. A horizontal linear elastic spring of stiffness k and a vertical linear elastic spring of stiffness κk are attached to turning-and-sliding joints. A spring of stiffness μk pulls the two bars back into their in-line position. The system is loaded

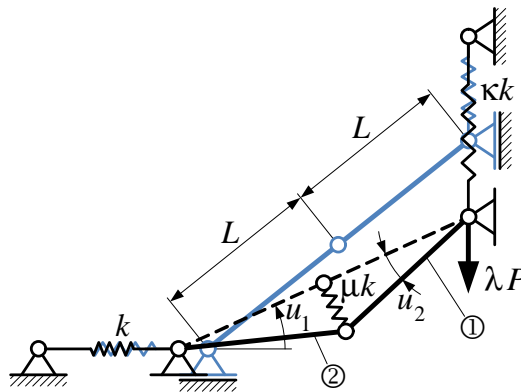


Figure 8.1: Pin-jointed two-bar system.

by a vertical load λP at the vertical turning-and-sliding joint, which results in the reference load vector $\bar{\mathbf{P}} = (P, 0)^T$. The two displacement coordinates are the angles u_1 and u_2 , summarized in the vector $\mathbf{u} = (u_1, u_2)^T$. In order to write the out-of-balance force \mathbf{G} for the structure as defined in (2.2), other coordinates would have to be chosen. In fact, the angle u_1 would have to be replaced by the vertical position of the upper turning-and-sliding joint. This would only require a simple coordinate transformation. For convenience, however, the angle u_1 was chosen as a coordinate. The unloaded position, delineated in blue, is defined by $\mathbf{u} = (u_{10}, 0)^T$. This system was first investigated in [29] and later on in [32]. The potential energy expression follows as

$$\begin{aligned} V(\mathbf{u}, \lambda) = & 2\kappa k L^2 (\sin(u_{10}) - \sin(u_1) \cos(u_2))^2 + \frac{\mu\kappa}{2} L^2 \sin^2(u_2) \\ & + 2k L^2 (\cos(u_{10}) - \cos(u_1) \cos(u_2))^2 - \lambda P 2L (\sin(u_{10}) - \sin(u_1) \cos(u_2)). \end{aligned} \quad (8.1)$$

The equilibrium equations $V_{u_1} = 0$ and $V_{u_2} = 0$ are satisfied for the primary path where

$$u_2 = 0 \quad (8.2)$$

and

$$\lambda = \frac{2Lk}{P} ((1 - \kappa) \sin(u_1) - \cos(u_{10}) \tan(u_1) + \kappa \sin(u_{10})), \quad (8.3)$$

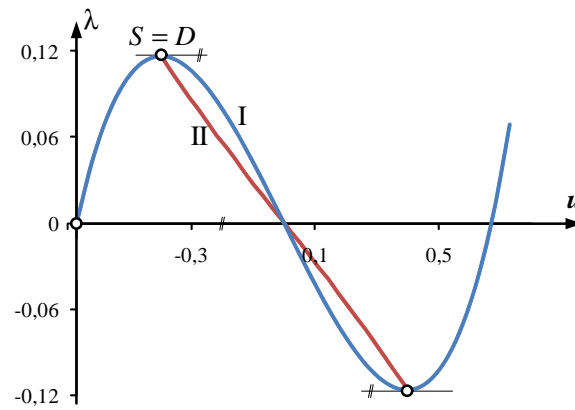
and for the secondary path with

$$u_2 = \pm \arccos\left(\frac{4}{4 - \mu} \frac{\cos(u_{10})}{\cos(u_1)}\right) \quad (8.4)$$

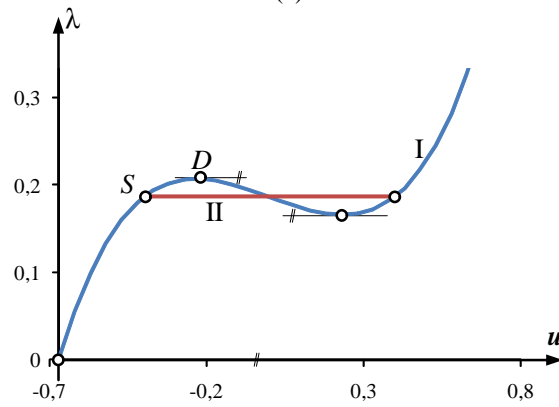
and

$$\lambda = \frac{2Lk}{P} \left(\frac{\mu - 4\kappa}{4 - \mu} \cos(u_{10}) \tan(u_1) + \kappa \sin(u_{10}) \right). \quad (8.5)$$

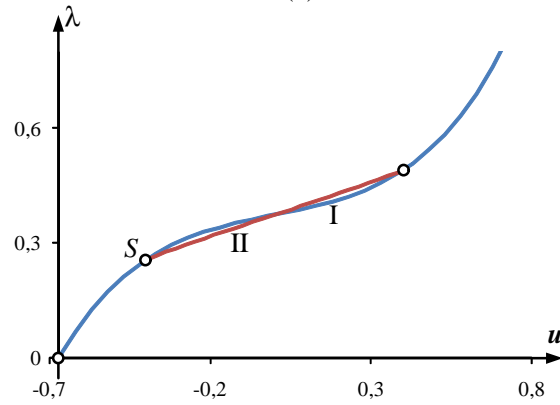
Since a perfect system is assumed, the sign of u_2 is indeterminate, i.e. it is not known into which direction the two bars will buckle. The tangent-stiffness



(a)



(b)



(c)

Figure 8.2: Selected results from sensitivity analysis of the initial postbuckling behavior of the pin-jointed two-bar system shown in Figure 8.1: projections of load-displacement paths onto the plane $u_2 = 0$ for (a) hilltop buckling, (b) zero-stiffness postbuckling, (c) imperfection insensitivity.

matrix is obtained as

$$\mathbf{K}_T = 4kL^2 \begin{pmatrix} \kappa(1 + \sin(u_{10})\sin(u_1) - 2\sin^2(u_1)) & & & & \\ +1 + \cos(u_{10})\cos(u_1) - 2\cos^2(u_1) & & 0 & & \\ & -\lambda \frac{P}{2kL} \sin(u_1) & & & \\ & & 0 & \kappa(\sin(u_{10})\sin(u_1) - \sin^2(u_1)) & \\ & & & + \cos(u_{10})\cos(u_1) - \cos^2(u_1) & \\ & & & & -\lambda \frac{P}{2kL} \sin(u_1) \end{pmatrix}. \quad (8.6)$$

$u_{10} \in (-\pi/2, \pi/2)$, $\mu \in \mathbb{R}^+$ and $\kappa \in \mathbb{R}^+$ are parameters that can be varied in order to achieve qualitative changes of the system. However, in the following only κ is varied. The remaining two parameters were chosen as $\mu = 3/5$ and $u_{10} = 0.67026$ such that hilltop buckling occurs for $\kappa = 0$, representing the starting point for sensitivity analysis of the initial postbuckling behavior. The projection of the load-displacement path for hilltop buckling is shown in Figure 8.2(a).

If $\eta = u_2$, the relevant coefficients of the series expansion (3.2) follow as

$$\begin{aligned} \lambda_1 &= 0, & \lambda_2 &= \frac{kL}{P} \frac{(\kappa - \mu/4)}{\sqrt{1 - \frac{\cos^2(u_{10})}{(1 - \mu/4)^2}}}, \\ \lambda_3 &= 0, & \lambda_4 &= -\frac{\lambda_2}{12} \frac{1 - 4\frac{\cos^2(u_{10})}{(1 - \mu/4)^2}}{1 - \frac{\cos^2(u_{10})}{(1 - \mu/4)^2}}. \end{aligned} \quad (8.7)$$

Thus, λ_2 is proportional to λ_4 . For $\kappa = 0$ (hilltop buckling), the perfect system is imperfection sensitive ($\lambda_2 < 0$) and λ_5 exceeds the ultimate load of any imperfect system. Increasing the parameter κ , i.e. the stiffness of the vertical spring, improves the postbuckling behavior insofar as λ_2 becomes positive, see Figure 8.3. The system is imperfection insensitive for $\kappa \geq \mu/4$. Figure 8.2(b) refers to $\kappa = \mu/4$, for which zero-stiffness postbuckling occurs. As κ is further increased, the primary path becomes monotonically increasing. This situation is shown in Figure 8.2(c). A comparison of Figures 8.2(a), 8.2(b), and 8.2(c) shows that the

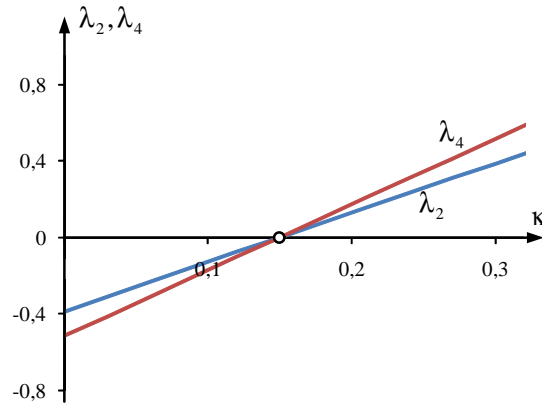


Figure 8.3: Coefficients λ_2 and λ_4 of Koiter's initial postbuckling analysis, both increasing linearly and crossing 0 at the same value of κ .

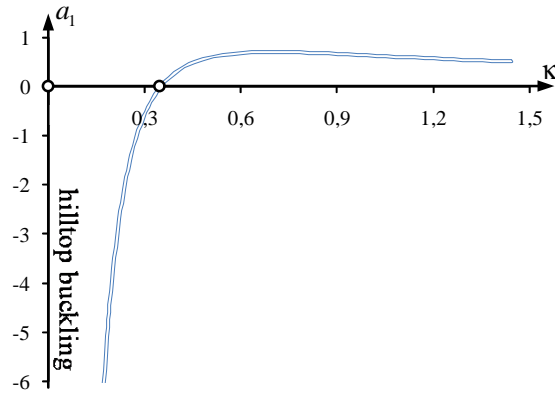


Figure 8.4: Coefficient $a_1(\kappa)$ exhibiting the predicted behavior (see Section 3.3).

bifurcation point S is increasing less strongly with increasing κ than the snap-through point D . Hence, the two points are diverging from each other.

Figure 8.4 shows a_1 as a function of the design parameter κ . It conforms with the theoretical considerations in Section 3.3.

8.2 Von Mises truss

Figure 8.5 shows a *von Mises* truss supplemented by a vertical spring with a spring constant κk where $k = 1\text{N/cm}$ and $\kappa \in \mathbb{R}$ is a scaling parameter. Actually,

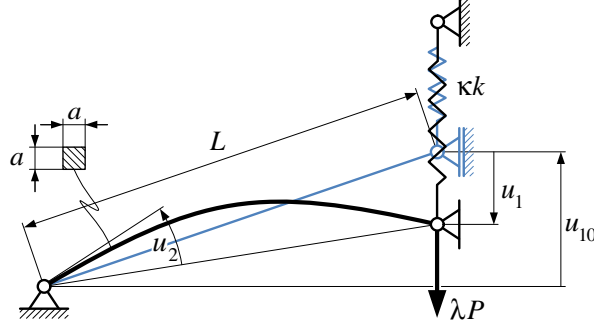
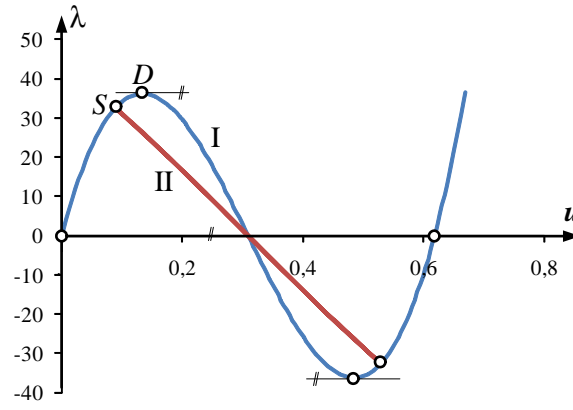
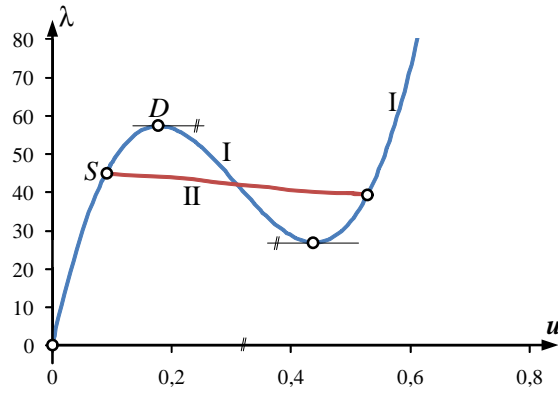


Figure 8.5: Von Mises truss with an elastic vertical spring attached to the load point.

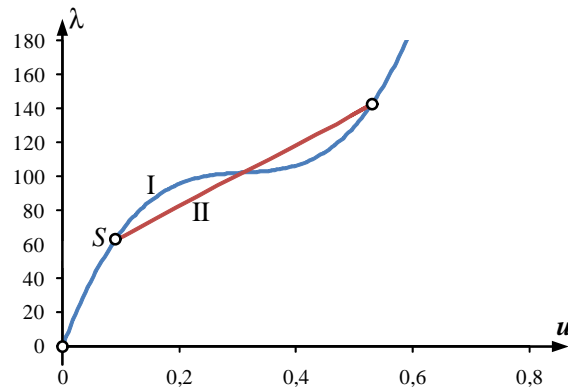
only one half of the truss is analyzed in order to avoid a multiple bifurcation point which is not in the scope of the present work. The undeformed length of the bar, L , is 100cm , the initial position of the load point, u_{10} , is 30.9cm . The side length of the quadratic cross section, a , is 17cm , the elastic modulus, E , is $2.8 \times 10^{11}\text{kN/cm}^2$. The reference load vector, $\bar{\mathbf{P}}$, is $(P, 0)^T$ with the vertical reference load $P = 1\text{N}$. In the unbuckled configuration the bar is straight. A detailed analytical treatment of a similar structure can be found in [32] and [29] where the only difference is that the side length of the cross section was chosen such that hilltop buckling occurs for $\kappa = 0$. This was avoided here because of numerical instabilities at hilltop buckling in Koiter's initial postbuckling analysis when using the FEM. The structure was discretized using 30 FEAP beam elements for finite displacements. For $\kappa = 0$, the bifurcation point S is relatively close to the snap-through point D (Figure 8.6(a)), the structure is imperfection sensitive. Stiffening the vertical spring by increasing κ improves the postbuckling behavior, expressed by a linear increase of $\lambda_2(\kappa)$ (Figure 8.7(a)). Figure 8.6(b) refers to the situation characterized by $\lambda_2 = 0$. Because of $\lambda_4 < 0$, zero-stiffness postbuckling does not occur. As κ is further increased, the primary path eventually becomes monotonically increasing (Figure 8.6(c)). Figure 8.8 shows a_1 and a_1^* as functions of κ . The functions $b_2(\kappa)$ and $d_3(\kappa)$ are shown exemplarily in Figure 8.9. Figure 8.10 serves the purpose of verification of the condition for



(a)

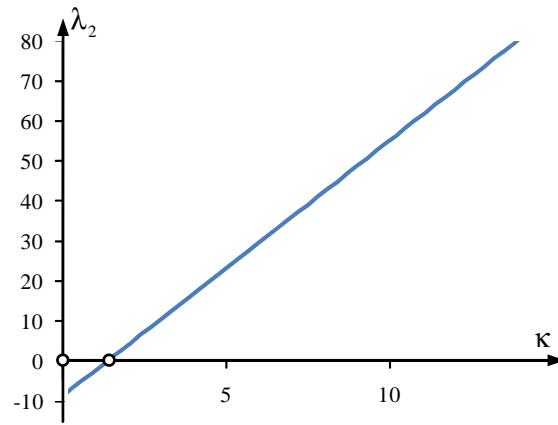


(b)

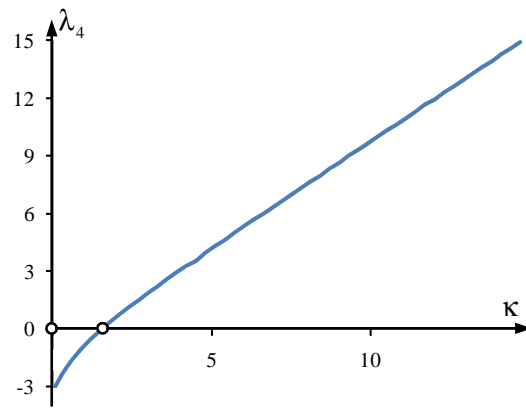


(c)

Figure 8.6: λ as a function of the vertical displacement of the load point, for three different values of the top spring stiffness c : (a) $c = 0$, $\lambda_2 < 0$, (b) $c = 5.55$, $\lambda \approx 0$, $\lambda_4 < 0$, (c) $c = 12$, $\lambda_2 > 0$, $\lambda_4 > 0$.



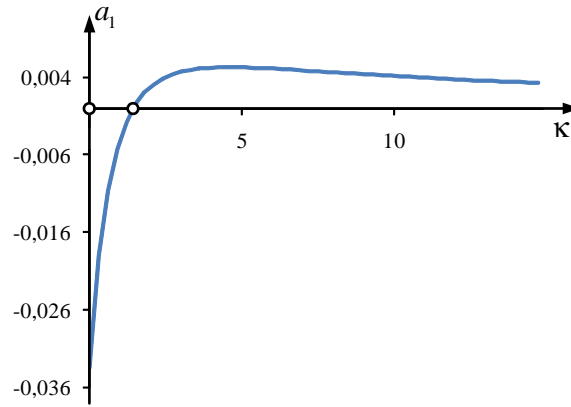
(a)



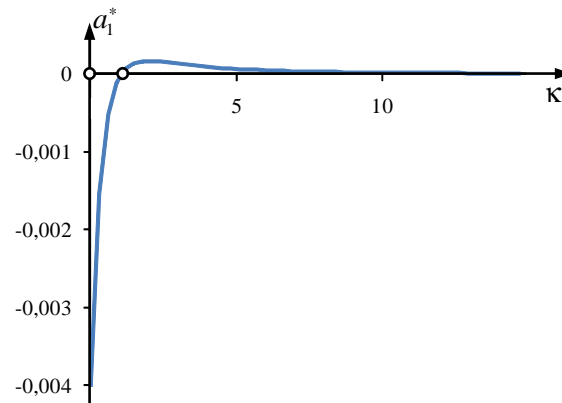
(b)

Figure 8.7: Coefficients λ_2 and λ_4 of Koiter's initial postbuckling analysis. Both coefficients are monotonic functions of κ . Although their zeros are close, zero-stiffness postbuckling does not occur.

bifurcation buckling from a membrane stress state (see (6.31)).

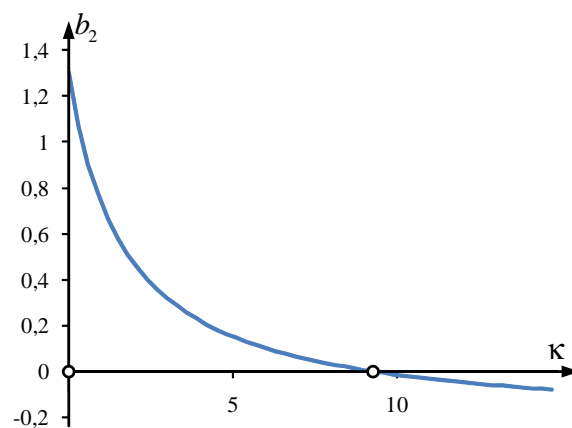


(a)

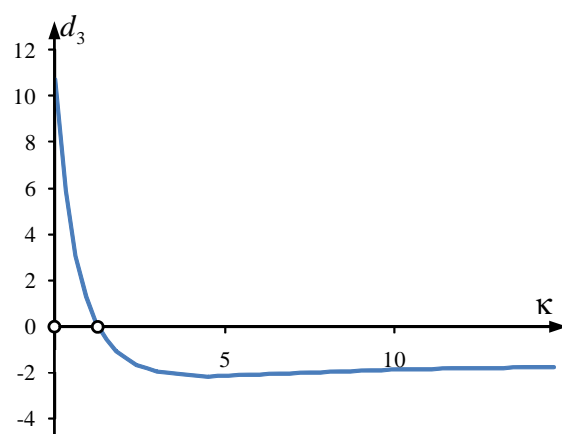


(b)

Figure 8.8: a_1 and a_1^* as functions of κ , starting with negative values because the bifurcation point is relatively close to the snap-through point, and converging to 0 as $\kappa \rightarrow \infty$.



(a)



(b)

Figure 8.9: Coefficients b_2 and d_3 required for computation of λ_4 as functions of κ .

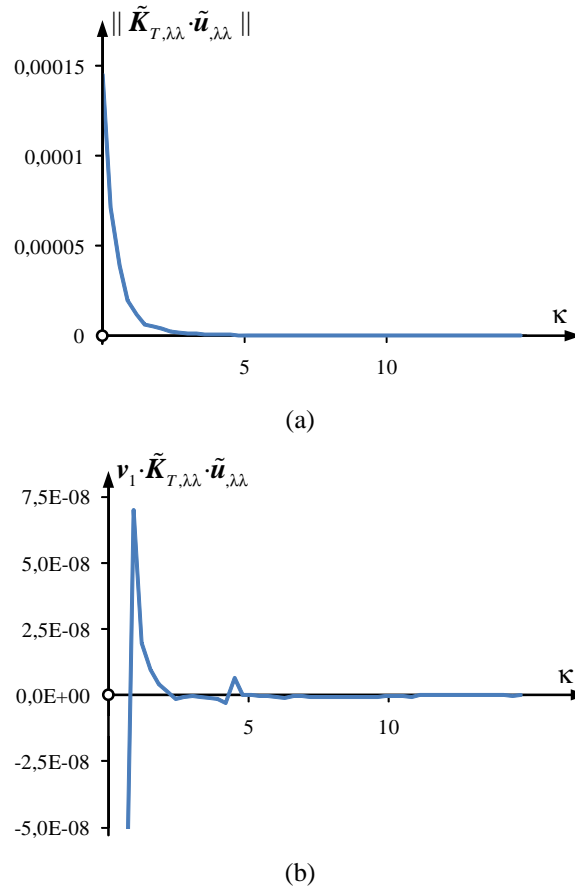


Figure 8.10: Verification of the condition for bifurcation buckling from a pre-buckling membrane stress state (see (6.31)): While the norm of $\tilde{\mathbf{K}}_{T,\lambda\lambda} \cdot \tilde{\mathbf{u}}_{,\lambda\lambda}$ is relatively smooth and clearly non-zero, $\nu_1 \cdot \tilde{\mathbf{K}}_{T,\lambda\lambda} \cdot \tilde{\mathbf{u}}_{,\lambda\lambda}$ is zero apart from “numerical noise”.

8.3 Shallow cylindrical shell

Stability analysis of elastic shells and sensitivity analysis of the initial postbuckling path of such structures are challenging topics that have attracted great interest of researchers [4, 9, 25, 36]. An example belonging to this category of structures is the shallow cylindrical shell illustrated in Figure 8.11 [29]. The length of the longitudinal sides, l , is 508cm , the length of the free edges, b , is 506.45cm , the elevation of the load point, h , is 12.7cm , the only non-zero component $P = 0.527\text{kN}$ of the reference load vector $\bar{\mathbf{P}}$ is a vertical load at the load point, as shown in Figure 8.11. The material parameters E and ν are given as

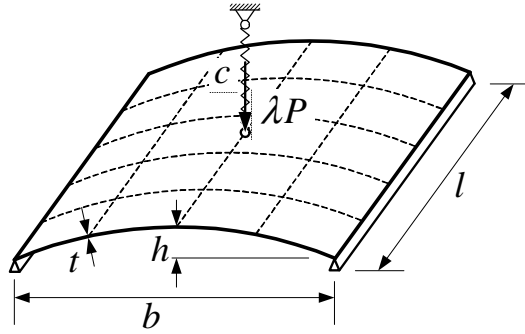


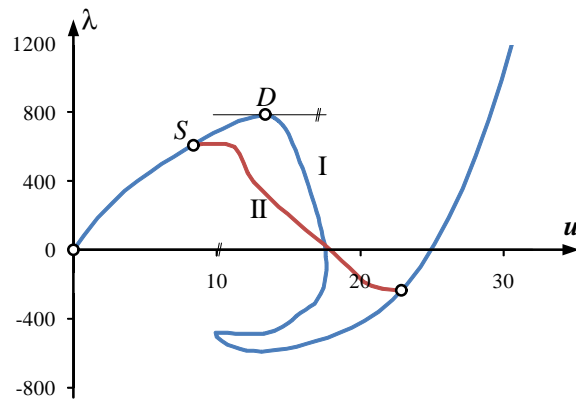
Figure 8.11: Shallow cylindrical shell with an elastic spring attached to the load point.

3102.75 kN/cm^2 and 0.3 , respectively. The shell thickness t and the stiffness of a vertical spring attached to the load point, respectively, were chosen as design parameters in [29].

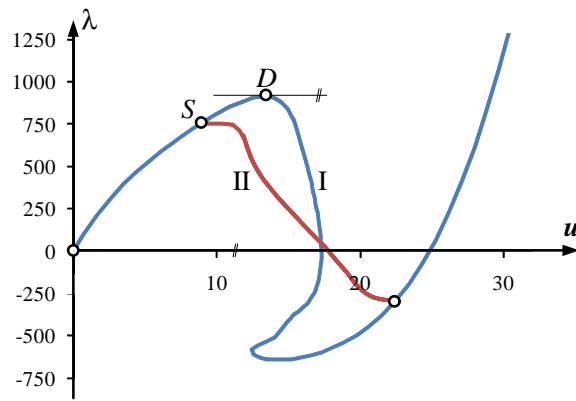
In this work, the thickness of the shell is selected as the design parameter κ , whereas the spring stiffness is chosen such that two different special cases occur. The first one, with $c = 0.72 \text{ kN/m}$, is the limit case for no conversion from imperfection sensitivity into imperfection insensitivity. As κ is increasing, λ_2 is increasing, reaching a maximum value of 0 for $\kappa \approx 5.7$. Thereafter, λ_2 is decreasing until hilltop buckling is eventually reached for $\kappa \approx 8.0$. Load-displacement paths for these three values of κ are shown in Figure 8.12. This example illustrates that $\lambda_2(\kappa)$ may be a non-monotonic function of κ (see Figure 8.13(a)) and that stiffening of the structure leading to an increase of the buckling load may result in a deterioration of the postbuckling behavior, characterized by the increase of the steepness of the slope of the projection of the secondary path onto the $\lambda - \mathbf{u}$ plane.

In contrast to the two previous examples, in the present example the bifurcation point S converges to the snap-through point D (see Figure 8.12). The reason for this convergence is that, unlike the increase of the stiffness of the attached elastic spring in these two examples, the increase of the thickness of the shell has no influence on the boundary conditions.

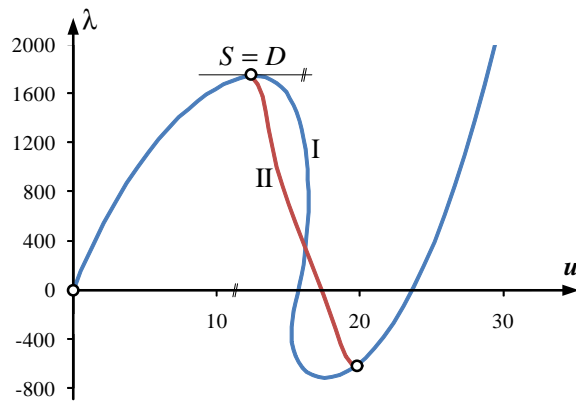
For the second case, the spring stiffness is chosen as $c = 2.704 \text{ kN/m}$. For this case, λ_2 and λ_4 are plotted as functions of the shell thickness in Figure 8.14. Al-



(a)

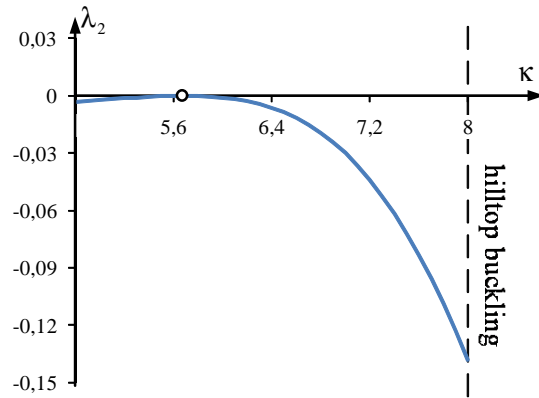


(b)

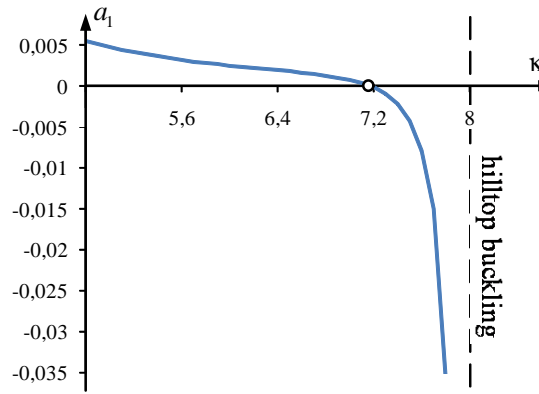


(c)

Figure 8.12: λ as a function of the vertical displacement of the load point, for three different values of t , (a) $t = 5.3$, $\lambda_2 < 0$, (b) $t = 5.7$, $\lambda_2 \approx 0$, (c) $t = 8$, hilltop buckling.



(a)



(b)

Figure 8.13: (a) λ_2 as a function of the shell thickness, starting from a very thin shell, ending at hilltop buckling; maximum value for $\kappa \approx 5.8$, (b) a_1 as a function of the shell thickness.

though both functions vanish for the same value of the design parameter, zero-stiffness does not occur because buckling does not occur from a membrane stress state.

In contrast to Figures 8.3 and 8.7(a), referring to bifurcation buckling from a membrane stress state, Figures 8.13(a) and 8.14 exhibit non-monotonic functions $\lambda_2(\kappa)$. As will be shown in the following, the difference between $\lambda_2(\kappa)$ for bifurcation buckling from a general state of stress and from a membrane stress state is that for the former non-monotony of $\lambda_2(\kappa)$ is possible whereas it is impossible for the latter.

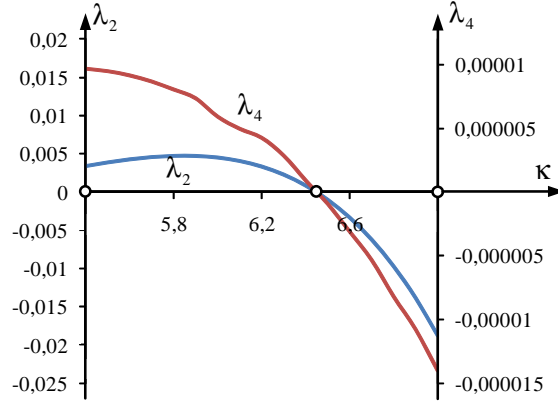


Figure 8.14: λ_2 and λ_4 as functions of the shell thickness for a spring stiffness $c = 2.704 \text{ kN/m}$.

Derivation of (3.16) with respect to the design parameter κ yields

$$\lambda_{4,\kappa} = a_{1,\kappa}\lambda_2^2 + 2a_1\lambda_2\lambda_{2,\kappa} + b_{2,\kappa}\lambda_2 + b_2\lambda_{2,\kappa} + (b_1\lambda_3 + d_3)_{,\kappa} \quad (8.8)$$

Solving the ‘quadratic equation’ (8.8) for λ_2 results in

$$\lambda_2 = -\frac{2a_1\lambda_{2,\kappa} + b_{2,\kappa}}{2a_{1,\kappa}} \pm \frac{\sqrt{(2a_1\lambda_{2,\kappa} + b_{2,\kappa})^2 - 4a_{1,\kappa}[(b_1\lambda_3 + d_3)_{,\kappa}]}}{2a_{1,\kappa}} \quad (8.9)$$

The sign before the second term on the right-hand side of (8.9) follows from knowledge of the value of λ_2 . Since λ_2 is a real quantity, the discriminant of (8.9) cannot be negative, i.e.

$$D = (2a_1\lambda_{2,\kappa} + b_{2,\kappa})^2 - 4a_{1,\kappa}[(b_1\lambda_3 + d_3)_{,\kappa}] \geq 0. \quad (8.10)$$

D can be rewritten as

$$D = 4\lambda_{2,\kappa}(a_1^2\lambda_{2,\kappa} + a_1b_{2,\kappa} - a_{1,\kappa}b_2) + [b_{2,\kappa}^2 - 4a_{1,\kappa}(b_1\lambda_3 + d_3)_{,\kappa}]. \quad (8.11)$$

Following from (8.10) and (8.11),

$$4\lambda_{2,\kappa}(a_1^2\lambda_{2,\kappa} + a_1b_{2,\kappa} - a_{1,\kappa}b_2) \geq -[b_{2,\kappa}^2 - 4a_{1,\kappa}(b_1\lambda_3 + d_3)_{,\kappa}]. \quad (8.12)$$

For sensitivity analysis of the initial postbuckling behavior of elastic structures which buckle from a general stress state,

$$b_{2,\kappa}^2 - 4a_{1,\kappa}(b_1\lambda_3 + d_3)_{,\kappa} \geq 0, \quad (8.13)$$

as was confirmed numerically by the example analyzed in Section 8.4. Since (8.12) is satisfied for (8.13) and $\lambda_{2,\kappa} = 0$, $\lambda_2(\kappa)$ may be a non-monotonic function (see Figures 8.13(a) and 8.14).

For sensitivity analysis of the initial postbuckling behavior of elastic structures which buckle from a membrane stress state, the expression in (8.13) is not restricted to non-negative values. For

$$b_{2,\kappa}^2 - 4a_{1,\kappa}(b_1\lambda_3 + d_3 - \lambda_4)_{,\kappa} < 0, \quad (8.14)$$

according to (8.12),

$$4\lambda_{2,\kappa}(a_1^2\lambda_{2,\kappa} + a_1b_{2,\kappa} - a_{1,\kappa}b_2) > 0 \implies \lambda_{2,\kappa} \neq 0. \quad (8.15)$$

In contrast to the situation for bifurcation buckling from a general stress state, satisfaction of (8.13) together with

$$4\lambda_{2,\kappa}(a_1^2\lambda_{2,\kappa} + a_1b_{2,\kappa} - a_{1,\kappa}b_2) = 0 \quad (8.16)$$

is restricted to

$$\lambda_{2,\kappa} \neq 0 \quad a_1^2\lambda_{2,\kappa} + a_1b_{2,\kappa} - a_{1,\kappa}b_2 = 0. \quad (8.17)$$

Hence, $\lambda_2(\kappa)$ must be a monotonic function.

8.4 Parabolic arch

A parametrized family of two-hinged arches, subjected to a uniformly distributed load p , was investigated by the FEM [18]. The design parameter $\Delta\kappa$ refers to the deviation of the geometric form of the axis of the arch from a quadratic parabola for which $\Delta\kappa = 0$, representing a thrust-line arch. The geometric form of the axis of the arch is given as

$$x \in [0, l], \quad y = \frac{4h}{l^2}x(l-x) + \Delta\kappa \sin\left(\frac{l-x}{l}\pi\right). \quad (8.18)$$

For the numerical sensitivity analysis, l and h were chosen as $6m$ and $2.4m$, respectively. The side length of the constant quadratic cross-section was chosen

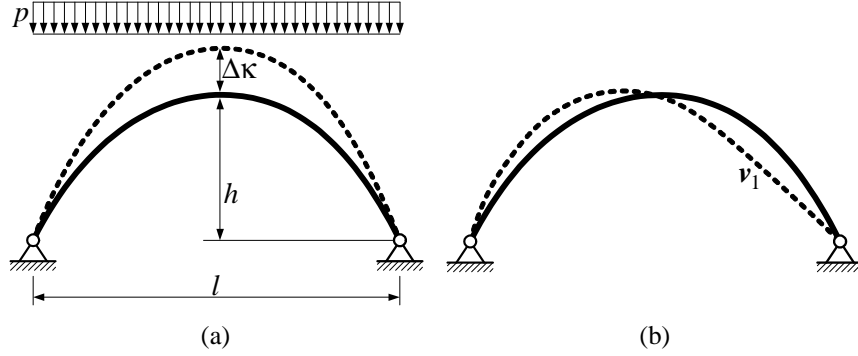


Figure 8.15: (a) arch axes according to (8.18) (solid line: thrust-line arch, dashed line: modified configuration), (b) axis of the thrust-line arch (solid line) and buckling mode (dashed line).

as $0.07m$. The modulus of elasticity was assumed as $2.1 \times 10^{11} N/m^2$. For the chosen configuration of the arches, symmetric bifurcation with an antisymmetric buckling mode is relevant. Figure 8.15(b) contains the buckling mode for the special case of a thrust-line arch.

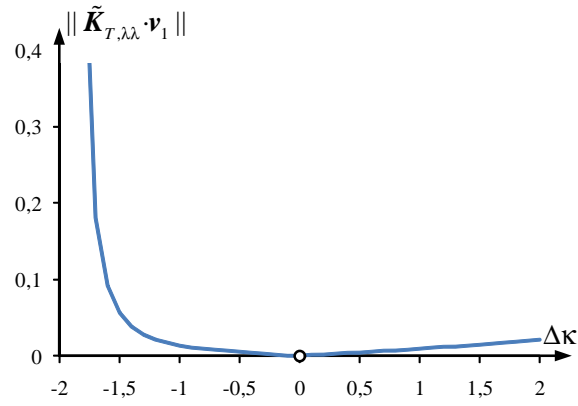
Figures 8.16(a), (b) show the Euclidean norms $\|\tilde{\mathbf{K}}_{T,\lambda\lambda} \cdot \boldsymbol{\nu}_1\|_2$ and $\|\tilde{\mathbf{K}}_{T,\lambda\lambda\lambda} \cdot \boldsymbol{\nu}_1\|_2$ as functions of the design parameter $\Delta\kappa$. For the special case of a thrust-line arch ($\Delta\kappa = 0$),

$$\|\tilde{\mathbf{K}}_{T,\lambda\lambda} \cdot \boldsymbol{\nu}_1\|_2 = 0, \quad \|\tilde{\mathbf{K}}_{T,\lambda\lambda\lambda} \cdot \boldsymbol{\nu}_1\|_2 = 0. \quad (8.19)$$

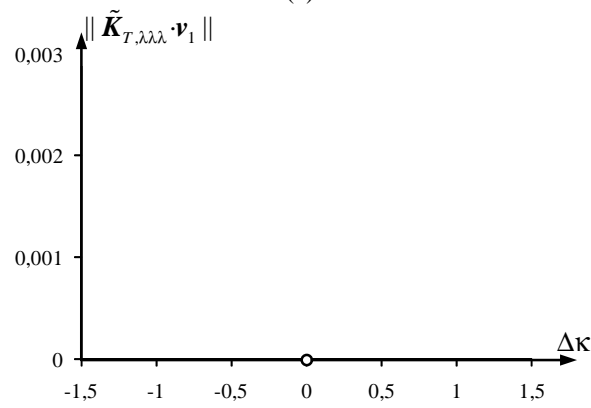
This implies the vanishing of a_1 and a_1^* , which is illustrated in Figure 8.17. These results confirm (6.56) and (6.57). Substitution of $a_1 = a_{2,\kappa} = 0$ (see Figure 8.17(a)) into (8.12) gives

$$0 > -b_{2,\kappa}^2. \quad (8.20)$$

At the same time, (8.17.2) is satisfied. The numerical investigation resulted in $\lambda_{2,\kappa} > 0$ which confirms (8.17.1).

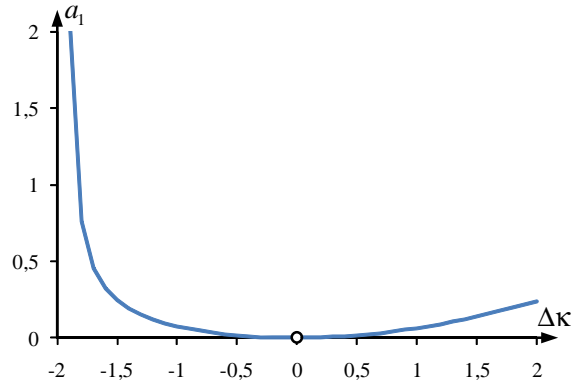


(a)

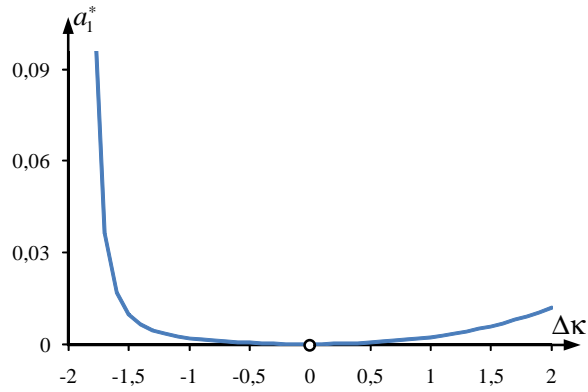


(b)

Figure 8.16: Sensitivity analysis of bifurcation buckling of a family of two-hinged arches: (a) $\|\tilde{\mathbf{K}}_{T,\lambda\lambda} \cdot \mathbf{v}_1\|_2$, (b) $\|\tilde{\mathbf{K}}_{T,\lambda\lambda\lambda} \cdot \mathbf{v}_1\|_2$ as functions of $\Delta\kappa$ representing the deviation from a thrust-line arch.



(a)



(b)

Figure 8.17: a_1 and a_1^* as functions of κ . For the special case of a membrane stress state, $\widetilde{\mathbf{K}}_{T,\lambda\lambda} \cdot \boldsymbol{\nu}_1 = \mathbf{0}$ and $\widetilde{\mathbf{K}}_{T,\lambda\lambda\lambda} \cdot \boldsymbol{\nu}_1 = \mathbf{0}$ (see Figure 8.16), resulting in the vanishing of a_1 and a_1^* .

Chapter 9

Conclusions

Sensitivity analysis of the initial postbuckling behavior of elastic structures aims at the conversion of imperfection-sensitive structures into imperfection-insensitive ones by means of minor design changes. The answer to the question of how to achieve this aim depends on the considered structure and its loading. Hence, a general answer is impossible. The motivation for this work was the search for design principles either allowing such a conversion or ensuring imperfection insensitivity right from the beginning. For this purpose, Koiter's postbuckling analysis was used together with information obtained from the consistently linearized eigenvalue problem. Theoretical analysis as well as numerical studies were performed in a research project¹ that framed the work for this thesis. Notwithstanding that there are still open questions, many pertinent problems were solved.

One of them was the role of symmetry in sensitivity analysis of the initial postbuckling behavior. It turned out that, contrary to earlier assertions, symmetry is not necessary for conversion from imperfection-sensitive into imperfection-insensitive structures. Nevertheless, the necessary condition $\lambda_1 = 0$ represents a restriction on the degree of asymmetry of the initial postbuckling behavior.

A proof was given for the inherent imperfection sensitivity of hilltop buckling. This proof is important insofar, as its result suggests to avoid hilltop buckling even if it results in a maximum of the critical load in the feasible range of design

¹‘Imperfection sensitivity: an unfavorable mechanical diagnosis of the initial postbuckling behavior of structures, calling for an effective design therapy’, funded by the Austrian Academy of Sciences.

parameters. The proof uses a similar series expansion as in Koiter's postbuckling analysis and makes explicit use of the positive semi-definiteness of $\tilde{\mathbf{K}}_T$ at the stability limit.

Scientific work with zero-stiffness postbuckling was primarily of academic interest, as this special form of postbuckling is restricted to rather simple structures. Interest in structures exhibiting this form of postbuckling behavior is of more recent date. A necessary condition for zero-stiffness postbuckling is buckling from a membrane stress state. Insofar as in the frame of sensitivity analysis of the initial postbuckling behavior of elastic structures all coefficients λ_{2k} change their sign from negative to positive, zero-stiffness postbuckling may be considered as the most favorable form of transition to imperfection insensitivity.

The conception of a membrane stress state as a constraint imposed on a general stress state may also serve as an explanation for the restriction of $\lambda_2(\kappa)$ to a monotonic function in the frame of sensitivity analysis of the initial postbuckling behavior for the special case of bifurcation buckling from a membrane stress state.

The presented theory was implemented in a computer program for structural analysis by the FEM. For symmetric structures, the series expansions of Koiter's postbuckling analysis were computed up to fourth order. The numerical results were validated thoroughly because numerical errors are inevitable, arising primarily through higher-order numerical differentiation and badly conditioned equation systems in the immediate neighborhood of the stability limit. Although both problems can be controlled by means of suitable algorithms, they cannot be eliminated. Nevertheless, the developed algorithms fulfill their main purpose which is numerical verification of theoretical results.

The thrust of the numerical investigation were sensitivity analyses of the initial postbuckling behavior of elastic structures. In these analyses, special emphasis was laid on symmetry, hilltop buckling, zero-stiffness postbuckling, buckling from a general stress state as well as from a membrane stress state and, last but not least, on buckling from a membrane stress state representing a special case in the frame of sensitivity analysis referring to buckling from a general stress state. It was shown that the addition of tensile members which overcompensate the decrease in the load carried by the original structure in the postbuckling

regime are effective means for converting imperfection-sensitive structures into imperfection-insensitive ones. The increase of the thickness of a structure, on the other hand, is usually not effective for improving the postbuckling behavior. The resulting improvement of the prebuckling behavior of the structure, consisting of a stiffening of the prebuckling load-displacement paths and an increase of the buckling load, is accompanied by a deterioration of the postbuckling behavior. A reduction of bending in the prebuckling domain in consequence of a modification of the original geometric form of the structure will improve the postbuckling behavior.

Appendix A

Coefficients in Koiter's initial postbuckling analysis

$$a_1 = -\frac{1}{2} \frac{\boldsymbol{\nu}_1^T \cdot \widetilde{\mathbf{K}}_{T,\lambda\lambda} \cdot \boldsymbol{\nu}_1}{\boldsymbol{\nu}_1^T \cdot \widetilde{\mathbf{K}}_{T,\lambda} \cdot \boldsymbol{\nu}_1}, \quad (\text{A.1})$$

$$a_1^* = -\frac{1}{6} \frac{\boldsymbol{\nu}_1^T \cdot \widetilde{\mathbf{K}}_{T,\lambda\lambda\lambda} \cdot \boldsymbol{\nu}_1}{\boldsymbol{\nu}_1^T \cdot \widetilde{\mathbf{K}}_{T,\lambda} \cdot \boldsymbol{\nu}_1}, \quad (\text{A.2})$$

$$\hat{a}_1 = -\frac{1}{24} \frac{\boldsymbol{\nu}_1^T \cdot \widetilde{\mathbf{K}}_{T,\lambda\lambda\lambda\lambda} \cdot \boldsymbol{\nu}_1}{\boldsymbol{\nu}_1^T \cdot \widetilde{\mathbf{K}}_{T,\lambda} \cdot \boldsymbol{\nu}_1}, \quad (\text{A.3})$$

$$b_1 = -\frac{1}{\boldsymbol{\nu}_1^T \cdot \widetilde{\mathbf{K}}_{T,\lambda} \cdot \boldsymbol{\nu}_1} \left(\boldsymbol{\nu}_1^T \cdot \widetilde{\mathbf{K}}_{T,\lambda} \cdot \boldsymbol{\nu}_2 + \frac{1}{2} \boldsymbol{\nu}_1^T \cdot \widetilde{\mathbf{K}}_{T,\mathbf{u}\lambda} : \boldsymbol{\nu}_1 \otimes \boldsymbol{\nu}_1 \right), \quad (\text{A.4})$$

$$b_2 = -\frac{1}{\boldsymbol{\nu}_1^T \cdot \widetilde{\mathbf{K}}_{T,\lambda} \cdot \boldsymbol{\nu}_1} \left(\boldsymbol{\nu}_1^T \cdot \widetilde{\mathbf{K}}_{T,\lambda} \cdot \boldsymbol{\nu}_3 + \boldsymbol{\nu}_1^T \cdot \mathbf{K}_{T\mathbf{u}\lambda} : \boldsymbol{\nu}_1 \otimes \boldsymbol{\nu}_2 + \frac{1}{6} \boldsymbol{\nu}_1^T \cdot \mathbf{K}_{T,\mathbf{uu}\lambda} : \boldsymbol{\nu}_1 \otimes \boldsymbol{\nu}_1 \otimes \boldsymbol{\nu}_1 \right), \quad (\text{A.5})$$

$$d_1 = -\frac{1}{\boldsymbol{\nu}_1^T \cdot \widetilde{\mathbf{K}}_{T,\lambda} \cdot \boldsymbol{\nu}_1} \left(\boldsymbol{\nu}_1^T \cdot \mathbf{K}_{T,\mathbf{u}} : \boldsymbol{\nu}_1 \otimes \boldsymbol{\nu}_2 + \frac{1}{6} \boldsymbol{\nu}_1^T \cdot \mathbf{K}_{T,\mathbf{uu}} : \boldsymbol{\nu}_1 \otimes \boldsymbol{\nu}_1 \otimes \boldsymbol{\nu}_1 \right), \quad (\text{A.6})$$

$$\begin{aligned}
d_2 = & -\frac{1}{\boldsymbol{\nu}_1^T \cdot \widetilde{\mathbf{K}}_{T,\lambda} \cdot \boldsymbol{\nu}_1} \left(\boldsymbol{\nu}_1^T \cdot \mathbf{K}_{T,\mathbf{u}} : \boldsymbol{\nu}_1 \otimes \boldsymbol{\nu}_3 + \frac{1}{2} \boldsymbol{\nu}_1^T \cdot \mathbf{K}_{T,\mathbf{u}} : \boldsymbol{\nu}_2 \otimes \boldsymbol{\nu}_2 \right. \\
& \left. + \frac{1}{2} \boldsymbol{\nu}_1^T \cdot \mathbf{K}_{T,\mathbf{uu}} : \boldsymbol{\nu}_1 \otimes \boldsymbol{\nu}_1 \otimes \boldsymbol{\nu}_2 + \frac{1}{24} \boldsymbol{\nu}_1^T \cdot \mathbf{K}_{T,\mathbf{uuu}} :: \boldsymbol{\nu}_1 \otimes \boldsymbol{\nu}_1 \otimes \boldsymbol{\nu}_1 \otimes \boldsymbol{\nu}_1 \right), \tag{A.7}
\end{aligned}$$

$$\begin{aligned}
d_3 = & -\frac{1}{\boldsymbol{\nu}_1^T \cdot \widetilde{\mathbf{K}}_{T,\lambda} \cdot \boldsymbol{\nu}_1} \left(\boldsymbol{\nu}_1^T \cdot \mathbf{K}_{T,\mathbf{u}} : \boldsymbol{\nu}_1 \otimes \boldsymbol{\nu}_4 + \boldsymbol{\nu}_1^T \cdot \mathbf{K}_{T,\mathbf{u}} : \boldsymbol{\nu}_2 \otimes \boldsymbol{\nu}_3 \right. \\
& + \frac{1}{2} \boldsymbol{\nu}_1^T \cdot \mathbf{K}_{T,\mathbf{uu}} : \boldsymbol{\nu}_1 \otimes \boldsymbol{\nu}_1 \otimes \boldsymbol{\nu}_3 + \frac{1}{2} \boldsymbol{\nu}_1^T \cdot \mathbf{K}_{T,\mathbf{uu}} : \boldsymbol{\nu}_1 \otimes \boldsymbol{\nu}_2 \otimes \boldsymbol{\nu}_2 \\
& + \frac{1}{6} \boldsymbol{\nu}_1^T \cdot \mathbf{K}_{T,\mathbf{uuu}} :: \boldsymbol{\nu}_1 \otimes \boldsymbol{\nu}_1 \otimes \boldsymbol{\nu}_1 \otimes \boldsymbol{\nu}_2 \\
& \left. + \frac{1}{120} \boldsymbol{\nu}_1^T \cdot \mathbf{K}_{T,\mathbf{uuuu}} :: \boldsymbol{\nu}_1 \otimes \boldsymbol{\nu}_1 \otimes \boldsymbol{\nu}_1 \otimes \boldsymbol{\nu}_1 \otimes \boldsymbol{\nu}_1 \right). \tag{A.8}
\end{aligned}$$

Bibliography

- [1] D. Bindel. MATFEAP: A MATLAB-FEAP interface. <http://www.cs.cornell.edu/bindel/cims/matfeap/>, December 2010.
- [2] B. Bochenek. Problems of structural optimization for post-buckling behaviour. *Structural and Multidisciplinary Optimization*, 25:423–425, 2003.
- [3] B. Bochenek and J. Kruzelecki. A new concept of optimization for post-buckling behavior. *Engineering Optimization*, 33(4):503–522, 2001.
- [4] B. Brendel, E. Ramm, D.F. Fischer, and F.G. Rammerstorfer. Linear and nonlinear stability analysis of thin cylindrical shells under wind loads. *Journal of Structural Mechanics*, 9:91–113, 1981.
- [5] D.O. Brush and B.O. Almroth. *Buckling of bars, plates and shells*. McGraw-Hill, 1975.
- [6] B. Budiansky. Theory of buckling and post-buckling behavior of elastic structures. In Chia-Shun Yih, editor, *Advances in Applied Mechanics*, volume 14 of *Advances in Applied Mechanics*, pages 1 – 65. Elsevier, 1974.
- [7] M.A. Crisfield. A fast incremental/iterative solution procedure that handles ‘snap-through’. *Computers and Structures*, 13(1-3):55–62, 1981.
- [8] F. Fujii and H. Noguchi. Multiple hill-top branching. In *Proceedings of the 2nd International Conference on Structural Stability and Dynamics*, *World Scientific*, pages 477–482, Singapore, 2002.
- [9] R.H. Gallagher and H.T.Y. Yang. Elastic instability predictions for doubly-curved shells. In *Proceedings of the Second Conference on Matrix Methods in Structural Mechanics*, pages 711–739, Wright-Patterson Air Force Base, Ohio, New Jersey, 1968.

- [10] L.A. Godoy. Sensitivity of post-critical states to changes in design parameters. *International Journal of Solids and Structures*, 33(15):2177–2192, 1996.
- [11] P. Helnwein. *Zur initialen Abschätzbarkeit von Stabilitätsgrenzen auf nichtlinearen Last-Verschiebungspfaden elastischer Strukturen mittels der Methode der Finiten Elemente [in German; On ab initio assessability of stability limits on nonlinear load-displacement paths of elastic structures by means of the finite element method]*. Ph.D. dissertation, Vienna University of Technology, 1997.
- [12] P. Helnwein and H.A. Mang. An asymptotic approach for the evaluation of errors resulting from estimations of stability limits in nonlinear elasticity. *Acta Mechanica*, 125:235–254, 1997.
- [13] X. Jia, G. Hoefinger, and H.A. Mang. Imperfection sensitivity or insensitivity of zero-stiffness postbuckling ... that is the question. In *Proceedings in Applied Mathematics and Mechanics*, 2009.
- [14] W.T. Koiter. On the stability of elastic equilibrium. (Translation of ‘over de stabiliteit van het elastisch evenwicht’, (1945)). Technical report, Polytechnic Institute Delft, H.J. Paris Publisher Amsterdam, NASA TT F-10, 833, 1967.
- [15] H.A. Mang and G. Hoefinger. Bifurcation buckling from a membrane stress state. Submitted for publication, 2010.
- [16] H.A. Mang, G. Hoefinger, and X. Jia. On the interdependency of primary and initial secondary equilibrium paths in sensitivity analysis of elastic structures. *Computer Methods in Applied Mechanics and Engineering*, in press.
- [17] H.A. Mang, G. Hoefinger, and X. Jia. Modes of transition from imperfection sensitivity to imperfection insensitivity. In K. J. Kalinski, editor, *Proceedings in Applied Mathematics and Mechanics*, volume 9, pages 255–256, 2009.
- [18] H.A. Mang, G. Höfinger, and X. Jia. Sensitivity analysis of the postbuckling behavior of elastic structures. In B. H. V Topping, J. M. Adam, F.J. Pallarés, and M.C. Romero, editors, *Computational Technology Reviews*, volume 2, pages 1–22. Saxe-Coburg Publications, 2010.
- [19] H.A. Mang, Gerhard Höfinger, and Xin Jia. On the predictability of zero-stiffness postbuckling. *Zeitschrift für angewandte Mathematik und Mechanik*, 90(10–11):837–846, 2010.

- [20] H.A. Mang, X. Jia, and G. Hoefinger. Hilltop buckling as the Alpha and Omega in sensitivity analysis of the initial postbuckling behavior of elastic structures. *Journal of Civil Engineering and Management*, 15:35–46, 2009.
- [21] H.A. Mang, C. Schranz, and P. Mackenzie-Helnwein. Conversion from imperfection-sensitive into imperfection-insensitive elastic structures I: Theory. *Computer Methods in Applied Mechanics and Engineering*, 195(13-16):1422–1457, 2006.
- [22] Z. Mróz and R.T. Haftka. Design sensitivity analysis of non-linear structures in regular and critical states. *International Journal of Solids and Structures*, 31(15):2071–2098, 1994.
- [23] Z. Mróz and J. Piekarski. Sensitivity analysis and optimal design of non-linear structures. *International Journal for Numerical Methods in Engineering*, 42:1231–1262, 1998.
- [24] M. Ohsaki and K. Ikeda. Imperfection sensitivity analysis of hill-top branching with many symmetric bifurcation points. *International Journal of Solids and Structures*, 43(16):4704–4719, 2006.
- [25] R. Reitinger and E. Ramm. Buckling and imperfection sensitivity in the optimization of shell structures. *Thin Walled Structures*, 23(1-4):159–177, 1995.
- [26] E. Riks. An incremental approach to the solution of snapping and buckling problems. *International Journal of Solids and Structures*, 15(7):529–551, 1979.
- [27] M. Ritto-Correa and D. Camotim. On the arc-length and other quadratic control methods: Establishes, less known and new implementation procedures. *Computers and Structures*, 86(11-12):1353–1368, 2008.
- [28] M. Schenk, S.D. Guest, and J.L. Herder. Zero stiffness tensegrity structures. *International Journal of Solids and Structures*, 44(20):6569–6583, 2007.
- [29] C. Schranz, B. Krenn, and H.A. Mang. Conversion from imperfection-sensitive into imperfection-insensitive elastic structures. II: Numerical investigation. *Computer Methods in Applied Mechanics and Engineering*, 195(13-16):1458–1479, 2006.
- [30] A. Steinboeck, G. Höfinger, X. Jia, and H.A. Mang. Three pending questions in structural stability. *Journal of the International Association for Shell and Spatial Structures*, 50:51–64, 2009.

- [31] A. Steinboeck, X. Jia, G. Hoefinger, and H.A. Mang. Conditions for symmetric, antisymmetric, and zero-stiffness bifurcation in view of imperfection sensitivity and insensitivity. *Computer Methods in Applied Mechanics and Engineering*, 197(45-48):3623–3636, 2008.
- [32] A. Steinboeck, X. Jia, G. Hoefinger, H. Rubin, and H.A. Mang. Remarkable postbuckling paths analyzed by means of the consistently linearized eigenproblem. *International Journal for Numerical Methods in Engineering*, 76(2):156–182, 2008.
- [33] A. Steinboeck and H.A. Mang. Are linear prebuckling paths and linear stability problems mutually conditional? *Computational Mechanics*, 42(3):441–445, 2008.
- [34] T. Tarnai. Zero stiffness elastic structures. *International Journal of Mechanical Sciences*, 45(3):425–431, 2003.
- [35] Robert L. Taylor. FEAP – A Finite Element Analysis Program, Version 7.4 User Manual. Department of Civil and Environmental Engineering, University of California at Berkeley, 2001.
- [36] J.M.T. Thompson and G.M. Lewis. On the optimum design of thin-walled compression members. *Journal of the Mechanics and Physics of Solids*, 20(2):101–109, 1972.
- [37] C. Ray Wylie. *Advanced Engineering Mathematics*. McGraw-Hill, 1975.
- [38] O. C. Zienkiewicz and R. L. Taylor. *The Finite Element Method*, volume 2. McGraw-Hill, London, England, 4th edition, 1994.

Curriculum Vitae

Dipl.-Ing. Gerhard Höfinger

Personal Details

Date of birth:	04. 07. 1982
Place of birth:	Vienna, Austria
Nationality:	Austria
Postal address:	Fuchsröhrenstraße 39/1/5 1110 Wien, Austria

Education and Qualifications

09/1992 – 06/2000	High school BG/BRG Tulln
10/2000 – 05/2001	Military service
10/2001 – 10/2006	Diploma Studies of Technical Mathematics at Vienna University of Technology
10/2005 – 01/2007	Teaching Assistant, Institute for Analysis and Scientific Computing at Vienna University of Technology
01/2007 – 12/2010	Doctoral studies, Institute for Mechanics of Materials and Structures at Vienna University of Technology
02/2007 – 12/2010	Project Assistant, Institute for Mechanics of Materials and Structures at Vienna University of Technology